NOAA Technical Report NESDIS 151

http://doi.org/10.7289/V5/TR-NESDIS-151

Report for
Dedicated JPSS VIIRS Ocean Color Calibration/Validation Cruise
October 2016

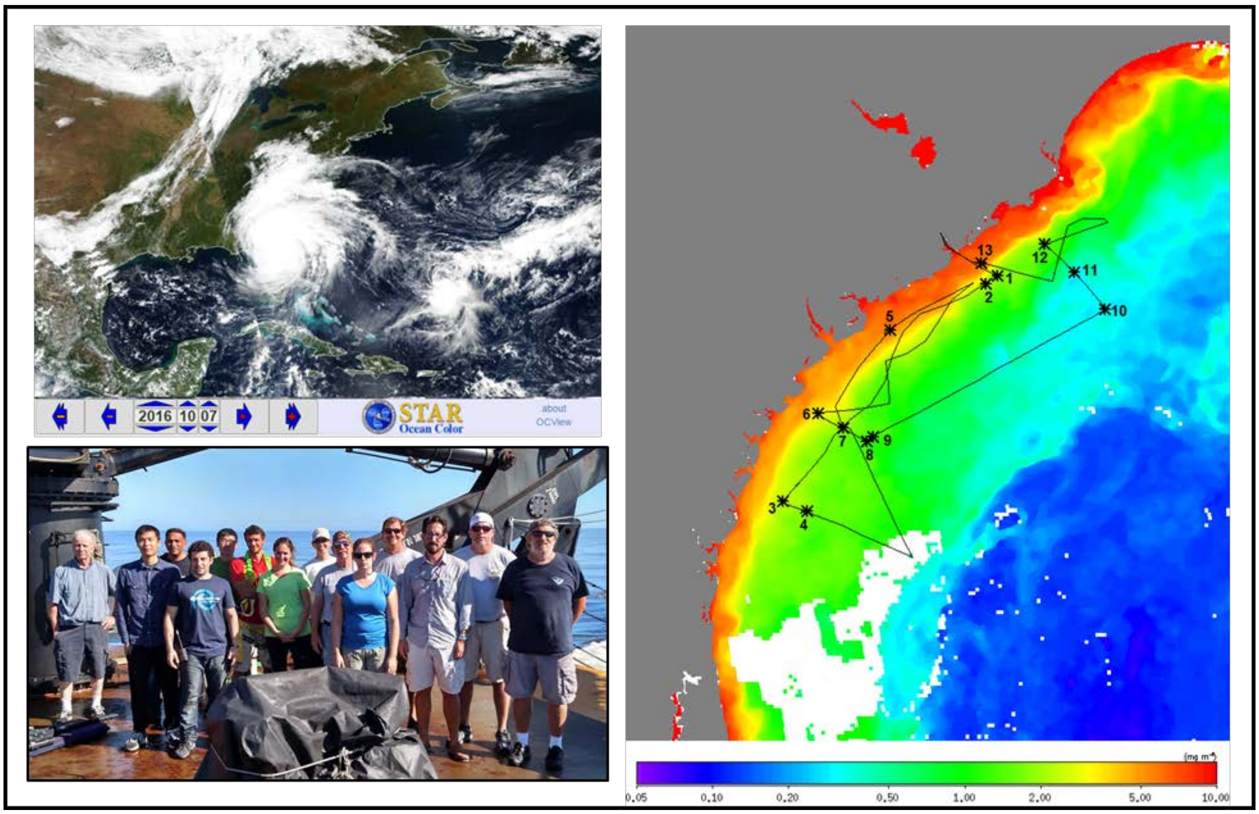

Washington, D.C.
October 2017

US DEPARTMENT OF COMMERCE
National Oceanic and Atmospheric Administration
National Environmental Satellite, Data, and Information Service

NOAA TECHNICAL REPORTS
National Environmental Satellite, Data, and Information Service

The National Environmental Satellite, Data, and Information Service (NESDIS) manages the Nation's civil Earth-observing satellite systems, as well as global national data bases for meteorology, oceanography, geophysics, and solar-terrestrial sciences. From these sources, it develops and disseminates environmental data and information products critical to the protection of life and property, national defense, the national economy, energy development and distribution, global food supplies, and the development of natural resources.

Publication in the NOAA Technical Report series does not preclude later publication in scientific journals in expanded or modified form. The NESDIS series of NOAA Technical Reports is a continuation of the former NESS and EDIS series of NOAA Technical Reports and the NESC and EDS series of Environmental Science Services Administration (ESSA) Technical Reports.

Copies of earlier reports may be available by contacting NESDIS Chief of Staff, NOAA/ NESDIS, 1335 East-West Highway, SSMC1, Silver Spring, MD 20910, (301) 713-3578.

Previous NESDIS Technical Reports on the Dedicated JPSS-VIIRS-Ocean Color Calibration/Validation Cruise Series:

Report #146	November 2014	doi:10.7289/V52B8W0Z
Report #148	December 2015	doi:10.7289/V5/TR-NESDIS-148

*Cover image: (Clockwise from top left): VIIRS SNPP true color image on 7 October 2016 showing Hurricane Matthew approaching Charleston SC region; cruise track and stations overlaid onto VIIRS SNPP chlorophyll-a binned over the time period of the October 2016 cruise; cruise participants on the deck of the NOAA Ship *Nancy Foster*.

NOAA Technical Report NESDIS 151

http://doi.org/10.7289/V5/TR-NESDIS-151

Report for Dedicated JPSS VIIRS Ocean Color Calibration/Validation Cruise October 2016

Edited by Veronica P. Lance[1,2*]
NOAA/NESDIS Center for Satellite Applications and Research (STAR), 5830 University Research Court, College Park, MD 20740, USA
[2]Global Science and Technology, Inc., 7855 Walker Drive, Suite 200, Greenbelt, MD 20770, USA

*Corresponding author: veronica.lance@noaa.gov

Contributing authors:

Michael Ondrusek[1]*, Veronica P. Lance[1,2], Menghua Wang[1], Eric Stengel[1], Charles Kovach[1,2],
[1]NOAA/NESDIS Center for Satellite Applications and Research (STAR), 5830 University Research Court, College Park, MD 20740, USA
[2]Global Science and Technology, Inc., 7855 Walker Drive, Suite 200, Greenbelt, MD 20770, USA
*michael.ondrusek@noaa.gov

And (alphabetical by group lead last name):

Robert Arnone[3]*, Sherwin Ladner[4], Wesley Goode[4]
[3]University of Southern Mississippi, Stennis Space Center, MS 39529, USA
[4]Naval Research Laboratory, Stennis Space Center, MS 39529, USA
*robert.arnone@usm.edu

Alex Gilerson*, Sam Ahmed, Ahmed El-Habashi, Robert Foster and Matteo Ottaviani
City College of the City University of New York, 160 Convent Ave, New York, NY 10031, USA
*gilerson@ccny.cuny.edu

Joaquim I. Goes*, Helga do Rosario Gomes, Kali McKee and Joo Won Kang
Lamont Doherty Earth Observatory at Columbia University, 61 Route 9W, Palisades, NY, 10964, USA
*jig@ldeo.columbia.edu

Chuanmin Hu*, Jennifer Cannizzaro, Shaojie Sun and David English
College of Marine Science, University of South Florida, 140 7th Avenue South, St. Petersburg, FL 33701, USA
*huc@usf.edu

B. Carol Johnson
National Institute of Standards and Technology, Physical Measurement Laboratory,100 Bureau Drive, Stop 8441, Gaithersburg, MD 20899-8441, USA
*carol.johnson@nist.gov

Zhongping Lee*, Laura Zoffoli and Junfang Lin
School for the Environment, University of Massachusetts Boston, 100 Morrissey Blvd, Boston, MA 02125, USA
*zhongping.lee@umb.edu

Nicholas Tufillaro*, Ivan Lalovic, Jasmine Nahorniak and Curtiss O. Davis
College of Earth, Ocean and Atmospheric Sciences, Oregon State University, Corvallis, OR 97331, USA
*nbt@coas.oregonstate.edu

Michael Twardowski* and Nicole Stockley
Harbor Branch Oceanographic Institute, Florida Atlantic University, Fort Pierce, FL 34946, USA
*mtwardowski@fau.edu

Kenneth J. Voss
Department of Physics, University of Miami, Knight Physics Building, Coral Gables, FL 33124, USA
*voss@physics.miami.edu

*Group corresponding contact

Washington, DC
October 2017

US DEPARTMENT OF COMMERCE
Wilbur Ross, Secretary

National Oceanic and Atmospheric Administration
Benjamin Friedman, Performing the duties of Under Secretary of Commerce for Oceans and Atmosphere

National Environmental Satellite, Data, and Information Service
Dr. Stephen Volz, Assistant Administrator

Contents

Preface

The Ocean Color Team at the National Oceanic and Atmospheric Administration (NOAA) Center for Satellite Applications and Research (STAR) is focused on "end-to-end" production of high quality satellite ocean color products. In situ validation of satellite data is essential to produce the high quality, fit-for-purpose remotely sensed ocean color products that are required and expected by all NOAA line offices, as well as by external (both applied and research) users. In addition to serving the needs of its diverse users within the US, NOAA has an ever increasing role in supporting the international ocean color community and is actively engaged in the International Ocean-Colour Coordinating Group (IOCCG). The IOCCG, along with the Committee on Earth Observation Satellites (CEOS) Ocean Colour Radiometry Virtual Constellation (OCR-VC), is developing the International Network for Sensor Inter-comparison and Uncertainty assessment for Ocean Color Radiometry (INSITU-OCR). The INSITU-OCR has identified, amongst other issues, the crucial need for sustained in situ observations for product validation, with long-term measurement programs established and maintained beyond any individual mission.

NOAA/STAR scientists have been collecting in situ data throughout all of the ocean color satellite missions. Since the launch in fall 2011 of the Visible Infrared Imaging Radiometer Suite (VIIRS) aboard the Suomi National Polar-orbiting Partnership (SNPP) platform, part of the US Joint Polar Satellite System (JPSS) program, the NOAA/STAR Ocean Color Team has been making in situ measurements routinely in support of validation and algorithm development activities. To date, three Dedicated JPSS VIIRS Ocean Color Calibration/Validation (Cal/Val) Cruises have been conducted, all off the US East Coast aboard the NOAA Ship *Nancy Foster* and supported by: 1) NOAA Office of Marine and Aviation Operations (OMAO) for ship time, 2) the JPSS program for funding many of the participating groups and 3) NOAA/NESDIS/STAR. The first cruise was during November 2014 as detailed in NESDIS Technical Report #146 [Ondrusek et al., 2015]. The second was in December 2015, detailed in Report #148 [Ondrusek et al., 2016]. This report covers the third dedicated VIIRS Cal/Val cruise in October 2016.

These annual dedicated ocean color validation field campaigns provide in situ measurements needed to produce the best quality, fit-for-purpose ocean color remote sensing data and data products for NOAA applications and for users beyond NOAA. These observations support validation activities for the current JPSS VIIRS sensor on SNPP, which is now the primary source for NOAA operational remotely sensed ocean color data products. Future cruises will support VIIRS on JPSS-1, planned for launch in 2017 and future JPSS missions (i.e., JPSS-2 and beyond) as well as non-NOAA US (e.g., National Aeronautics and Space Administration (NASA) and United States Geological Survey (USGS)) and international ocean color related satellite missions (e.g., the Ocean and Land Colour Instrument (OLCI) aboard Sentinel-3 of the European Union's Copernicus mission and the Second Generation Global Imager (SGLI) aboard Global Climate Observation Mission-Climate (GCOM-C) mission from the Japan Aerospace Exploration Agency). Through the NOAA mission of science, service and stewardship, and in collaboration with the international ocean community, we aim to provide ocean satellite data products that improve our understanding of global and coastal ocean and inland water optical, biological, and biogeochemical properties and that support applications to benefit society.

Menghua Wang
Chief, Marine Ecosystems & Climate Branch; VIIRS Ocean Color Cal/Val Team Lead
Paul DiGiacomo
Chief, Satellite Oceanography & Climatology Division; NOAA Representative to the IOCCG; OCR-VC Co-Chair

List of Figures

List of Tables

List of Equations

NOAA Technical Report NESDIS 151
Report for
Dedicated JPSS VIIRS Ocean Color Calibration/Validation Cruise
October 2016

1. Overview and Summary of Purpose, Project, Principal Investigators and Participants

The overall aim of the annual NOAA Dedicated Joint Polar Satellite System (JPSS) Visible Infrared Imaging Radiometer Suite (VIIRS) Ocean Color Calibration/Validation (Cal/Val) Cruises [Ondrusek et al., 2016; Ondrusek et al., 2015] is to support improvements in the extent and accuracy of satellite remotely sensed ocean color parameters in the near surface ocean. The primary objective of these cruises is to collect high quality in situ optical and related biogeochemical data for purpose of validating satellite ocean color radiometry and derived products from VIIRS on SNPP [Wang et al., 2017; Wang et al., 2014; Wang et al., 2013] and the follow-on JPSS missions. The second objective is to quantify the confidence intervals of optical measurement protocols. The third objective is to characterize the optical signatures of a variety of water masses (i.e., coastal, near-shore, cross-shelf, eddies, fronts, filaments, blue water, etc.).

The NOAA Office of Marine and Aviation Operations (OMAO) allocated ship time for the 2016 cruise aboard the NOAA Ship *Nancy Foster* (NF-16-08) (http://www.moc.noaa.gov/nf/). The original project plan allowed for 14 days at sea, departing 5 October from Charleston, SC. The planned area of operations had been the Western Atlantic along the US Southeastern Coast and into Bahamian waters. These plans were altered in response to the passage of Hurricane Matthew (28 September through 9 October 2016), which passed eastward of Charleston necessitating a delay of several days. Actual executed cruise days were 13 October to 18 October 2016. With the shortened 6 day schedule and rough seas offshore, sampling was mostly confined to near shore waters in the vicinity of Charleston and Savannah except for the last day when seas calmed somewhat and the ship could venture offshore.

Twelve research groups participated in the cruise. Most of the principle investigators were funded partly through JPSS program. Table 1 lists the principal investigators, the associated institutions and abbreviations for the groups. These abbreviations will be used throughout this report. Thirteen scientists (Table 2), including three PhD students, sailed and conducted measurements with the support of officers and crew of the *Nancy Foster*. In addition, optical instruments were calibrated before and after the cruise in collaboration with the National Institute for Standards and Technology (NIST) at the NOAA/STAR optical laboratory in College Park, MD. The NOAA/STAR laboratory maintains an ongoing collaboration with NIST to validate the NOAA/STAR radiometric scales in support of cruise activities, and to provide traceable calibration services. NIST also provided a reference plaque currently in development (known as the "blue tile") which was used in the field for instrument inter-comparison exercises.

Any results shown in this report should be considered preliminary and are included here for the purpose of illustrating examples of measurements and observations. Post-processing and sample analyses are on-going. Results are expected to be published as peer-reviewed literature in scientific journals as work is completed. The cruise dataset will be formally archived through NOAA/NESDIS National Centers for Environmental Information (NCEI) as required by NOAA. Cruise data will also be available to the ocean community through NOAA CoastWatch/OceanWatch.

Table 1. Principal investigators (PIs), participating institutions and institution abbreviations.

PI Name (Last, First)	Participating Institutions	Research Group Abbreviation
Ondrusek, Michael*	NOAA/NESDIS/Center for Satellite Applications and Research	NOAA/STAR
Arnone, Robert	University of Southern Mississippi (USM) and Naval Research Center (NRL)	Stennis
Davis, Curtiss and Tufillaro, Nicholas	Oregon State University	OSU
Gilerson, Alex	City College of New York	CCNY
Goes, Joaquim	Lamont-Doherty Earth Observatory at Columbia University	LDEO
Hu, Chuanmin	University of South Florida	USF
Johnson, B. Carol	National Institute of Standards and Technology	NIST
Lee, ZhongPing	University of Massachusetts, Boston	UMB
Twardowski, Michael	Harbor Branch Oceanographic Institute at Florida Atlantic University	HBOI
Voss, Kenneth	University of Miami	U. Miami

*Chief Scientist

Table 2. List of science party personnel aboard the NOAA Ship *Nancy Foster* (alphabetical order).

Name (Last, First)	Title	Research Group/Home Institution*
Arnone, Robert	Research Professor	Stennis/USM
Goes, Joaquim	Professor	LDEO
Goode, Wesley	Researcher	Stennis/NRL
el Habashi, Ahmed	PhD Student	CCNY
Ladner, Sherwin	Researcher	Stennis/NRL
Lalovic, Ivan	Researcher	OSU
Lin, Junfang	Postdoctoral Researcher	UMB
Ondrusek, Michael	Chief Scientist	NOAA/STAR
Ottaviani, Matteo	Researcher	CCNY
Stengel, Eric	Researcher	NOAA/STAR
Stockley, Nicole	Researcher	HBOI
Sun, Shaojie	PhD Student	USF
Zoffoli, Laura	Postdoctoral Researcher	UMB

*See Table 1 for institution abbreviations.

2. Introduction

NOAA has been supporting satellite ocean color validation and calibration since the development and launch of the Coastal Zone Color Scanner (CZCS) [Gordon et al., 1980; Hovis et al., 1980] in the late 1970's and was instrumental in the development of the Marine Optical BuoY (MOBY) [Clark et al., 1997] in the Sea-viewing Wide Field-of-view Sensor (SeaWiFS) era [Gordon, 2010]. MOBY, now supported by NOAA, is the primary vicarious calibration reference standard for satellite ocean color sensors worldwide. In addition to high quality satellite sensor and vicarious calibrations, in situ radiometric measurements from a variety of ocean optical conditions are essential to the production of accurate remotely sensed ocean color products.

The JPSS VIIRS-SNPP satellite ocean color Cal/Val science plan calls for in situ observations for the purpose of developing and validating ocean color Environmental Data Records (EDRs) for global and coastal regions. Since 2014, the NOAA/STAR ocean color group has been conducting annual dedicated NOAA VIIRS Ocean Color Cal/Val Cruises [Ondrusek et al., 2016; Ondrusek et al., 2015] to validate VIIRS satellite ocean color data [Arnone et al., 2014; Arnone et al., 2012; Wang et al., 2014; Wang et al., 2013], quantify the variability of in situ measurements and study the optical signatures of oceanic processes.

To date, three dedicated VIIRS validation cruises have been conducted aboard the NOAA Ship *Nancy Foster* (referred to in this report as "*Foster*" or "ship") and were staged from the *Foster's* home port of Charleston, SC. The first (NF-14-09, formal NOAA/OMAO cruise identifier) took place in November 2014, generally along the US Mid-Atlantic Coast and across the Gulf Stream [Ondrusek et al., 2015]. The second (NF-15-13) was during December 2015 also along the US Mid-Atlantic Coast and across the Gulf Stream and included some stations in the Tongue of the Ocean (Bahamian waters) [Ondrusek et al., 2016]. The third (NF-16-08), during October 2016, is the subject of this report.

Due to Hurricane Matthew (28 September through 9 October 2016) which passed very near Charleston, SC, this 2016 cruise (NF-16-08) was delayed for a week to occur during 13-18 October and was reduced in duration to 6 days at sea from the originally planned 14 days. Figure 1 and Figure 2 are VIIRS SNPP true color images taken from NOAA/STAR Ocean Color team's monitoring tool, named "OCView". (https://www.star.nesdis.noaa.gov/sod/mecb/color/ocview/ocview.html).
Figure 2 shows a VIIRS SNPP true color image of the hurricane on 7 October 2016 as it neared Charleston and clear skies at the start of the cruise on 13 October 2016. Figure 2 shows the progression of the storm impact to coastal waters (before, shortly after and a few weeks after the hurricane). Rough seas offshore forced sampling to be mostly confined to near shore waters in the general vicinity of Charleston SC and Savannah GA. On the last day, however, calmer seas allowed for some offshore sampling. As is not unusual after the passage of a hurricane, the skies were generally clear so that 12 out of the 13 total stations had clear sky matchups with VIIRS overpasses, with 3 of those stations getting double orbits.

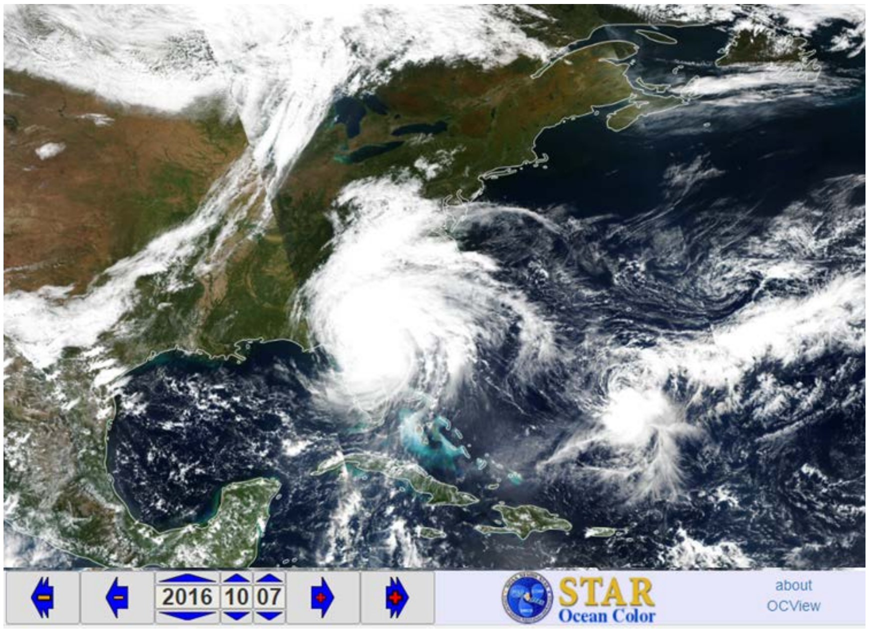

Figure 1. VIIRS SNPP true color image taken from NOAA/STAR Ocean Color OCView monitoring tool 7 October showing the approach of Hurricane Matthew toward the Charleston, SC area.

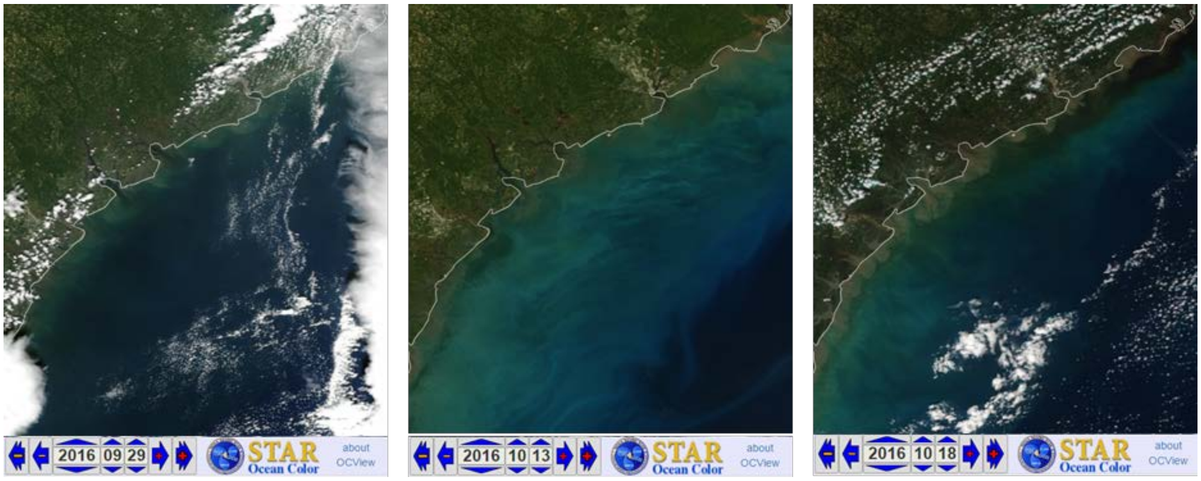

Figure 2. VIIRS SNPP true color images on clear days taken from NOAA/STAR Ocean Color OCView monitoring tool (left) 28 September, before Hurricane Matthew; (middle) 13 October, shortly after Hurricane Matthew; and (right) 18 October several weeks after Hurricane Matthew over US East Coast. The cruise began on 13 October and ended on 18 October. Note the progression of bright water (sediment plumes and chlorophyll) and dark water from coastal runoff.

At each station, simultaneous measurements were made with a suite of radiometric instruments to enable comparisons among the most widely utilized validation measurement techniques including in-water profiling and floating radiometers and hand-held above water radiometers. Optical properties were also surveyed continuously while underway by instruments plumbed into the ship's flow-through sea water system and mounted on masts at the bow of the ship. Additionally, water samples were collected at stations and from the flow-through sea water system for biogeochemical analyses of several environmental properties. More details regarding measurements follow in Section 6 and in the individual reports on each group's activities in Section 9.

3. Cruise Objectives

Shipboard observations of apparent optical properties (AOPs, i.e., radiances) and inherent optical properties (IOPs, e.g., absorption, beam attenuation and backscattering) as well as biogeochemical and biological measurements support three major objectives: 1) the validation of the VIIRS-SNPP ocean color satellite observations and derived products; 2) the characterization of the sources of uncertainty of in situ ocean color (remote sensing reflectance and IOPs) associated with nearly concurrent measurements by a variety of instruments and protocols; and 3) the characterization of optical properties of ocean variability (i.e., coastal, near-shore, cross-shelf, eddies, fronts, filaments, blue water) toward the future aim of using remotely sensed satellite ocean color data to monitor and study oceanographic processes. With the passing of Hurricane Matthew, a fourth objective was adopted to opportunistically observe potential impacts from the hurricane on ocean color parameters. Objectives are briefly discussed below, greater detail can be found in earlier cruise reports [Ondrusek et al., 2016; Ondrusek et al., 2015].

1) Validate VIIRS ocean color satellite remote sensing

Satellite sensor performance is evaluated, or validated, by matching up satellite observations with in situ observations, which are considered the "true" values for this purpose. The primary properties derived from ocean color satellite observations are AOPs including spectral normalized water-leaving radiance ($nL_w(\lambda)$) and spectral remote sensing reflectance ($R_{rs}(\lambda)$), where λ represents the specified nominal wavelength being measured. Therefore, in situ measurements for satellite validation are focused primarily on these AOP radiometric properties. By applying algorithms to $nL_w(\lambda)$s, other satellite ocean color remote sensing products can be estimated. Products including the concentration of chlorophyll-*a* (Chl-*a*) and IOPs such as coefficients of spectral absorption ($a(\lambda)$), scattering ($b(\lambda)$), backscattering ($bb(\lambda)$) and beam attenuation ($c(\lambda)$) were also validated by in situ measurements of these parameters. The sub-pixel variability of the IOP within VIIRS satellite pixels was examined using continuous flow-through measurements to validate satellite ocean color.

2) Characterize and quantify sources of uncertainty associated with in situ ocean color measurements
Sources of uncertainty for in situ measurements include errors associated with instruments, deployment and processing protocol differences and variances associated with the variability of the natural environment. Laboratory calibration of instruments (measurement conditions of repeatability [GUM, 1995]) and shipboard experiments (measurements conditions of reproducibility [GUM, 1995]) were conducted to quantify these differences [Johnson et al., 2014]. The following approaches, which represent conditions of reproducibility, were used to quantify measurement differences associated with: a) parallel observations from multiple instruments of the same or similar models deployed at the same time and in a small spatial range (within meters of each other); b) observations of the same in situ parameters by using different types of instruments (i.e., profiling in–water versus above-water versus hybrid floating instruments); c) different deployment protocols for sample collection; d) different post-processing methods for the in situ data; and e) observations in different environmental conditions (i.e., stations in different water masses and sky conditions).

3) Characterize the optical properties of dynamic ocean processes
The third objective of this cruise is to observe in situ optical characteristics of ocean variability related to dynamic processes in open and coastal waters for the purpose of exploring the utility of VIIRS ocean color satellite products in identifying and monitoring oceanographic processes from space. The cruise data will be used to evaluate and demonstrate the ability of VIIRS ocean color products to differentiate the variations of spectral features produced by physical and biological states and processes.

4. Cruise Track, Overall Conditions and Sampling Strategies

The 2016 cruise, conducted in the wake of Hurricane Matthew, concentrated on nearshore waters along the Southeast US Coast and into offshore waters of the Western Atlantic, across the Gulf Stream. Figure 3 shows the cruise track and station locations overlaid on VIIRS satellite chlorophyll 8-day merged data for the period of 12 October 2017 to 19 October 2017, after the passage of Hurricane Matthew. Stations were selected, within the limitations of sea state, to enable investigators to make in situ measurements in a variety of environmental conditions. Not unexpectedly after a storm, clear skies dominated and the number of match-ups between the VIIRS satellite data and in situ observations was favorable despite the shortened duration of the cruise period.

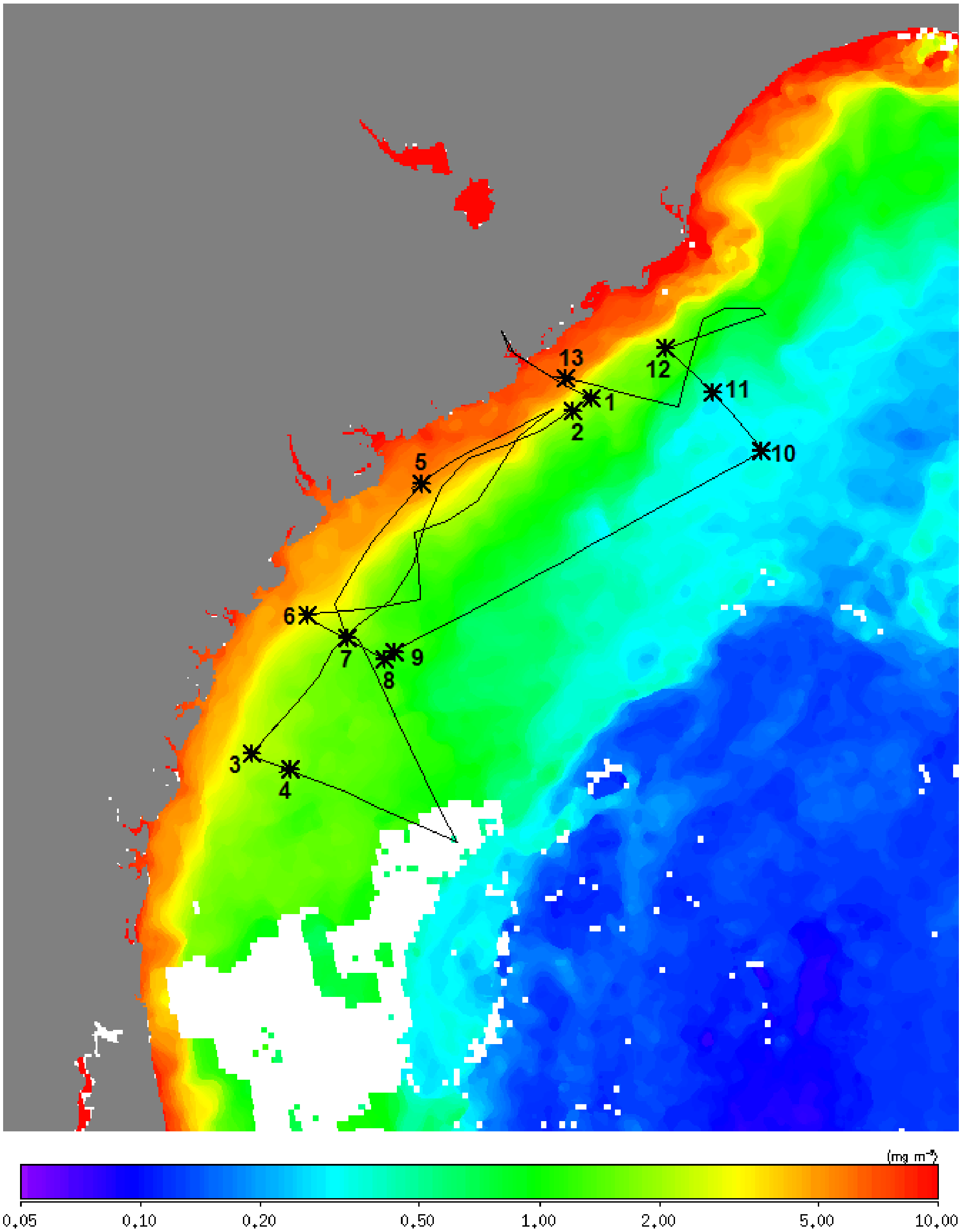

Figure 3. Cruise track and station locations overlaid onto an image of VIIRS MSL12 Science Quality Chl-*a* merged data covering the period 12 October 2017 to 19 October 2017. Units for colorbar are mg m^{-3}.

Measurements were made with a suite of instruments deployed both discretely at stations and continuously while plumbed into the ship's flow-through sea water system and mounted on masts at the bow of the ship. Additionally, water samples were collected at stations and from the flow-through sea water system for post-cruise laboratory analyses of several environmental properties.

Discrete Station Activities
Discrete stations, where the ship maintains a relatively stable location for the period of time it takes to execute measurements, were conducted daily, weather conditions permitting, during daylight hours between ≈0800 EST and ≈1730 EST local time (between ≈1300 UTC and ≈2230 UTC). A total of 13 stations were occupied over the course of the 6 days at sea. Twelve of those 13 resulted in match-ups with VIIRS satellite observations, and 3 stations had 2 VIIRS overpasses. Generally, several activities took place at each station, including:

- Profiling instrument packages - measured continuously and/or at discrete depths vertically through the water column, generally within the first 2 optical depths or to the physical mixed layer
- Floating instrument packages - configured to float at the water's surface
- Above water instruments - deployed by hand on deck
- Conductivity Temperature Depth (CTD)/Rosette package deployment - collected water samples into 12 Niskin bottles (5 L), usually from two discrete depths, nominally one near surface and a second near the chlorophyll maximum depth within the first optical depth (ranging from 12 m to 42 m). The CTD instruments collect profile data as well.
- Deck mounted instruments and instruments plumbed into ships flow-through system collected surface measurements continuously while on station.

Underway Flow-Through Sampling
A series of bio-optical and hydrographic instruments for continuous (underway and station keeping) sampling were plumbed into the ship's sea water flow-through system. The sea chest intake was at a depth of 3 m. Observational data were synchronized with time and location and were monitored in real time for determining station locations. The flow-through data will also be used for spatial variability analyses.

Underway Above Water (on deck) Sampling
AOPs were collected continuously from instruments mounted on the bow of the ship.

5. Observed effects of Hurricane Matthew
Evidence of the effects of Hurricane Matthew was seen in: 1) increased river discharge along the coast with increased turbid plumes, and 2) westward movement of offshore waters from the Gulf Stream and offshore eddies into coastal waters. The slow northwest movement of Matthew paralleling the coast brought strong and consistently onshore winds, which brought offshore waters onto the coast apparently due to increased undulations and changes in frontal eddies (i.e., shingles) in the Gulf Stream. Heavy rains and winds increased the surface water mixing which affected the sea surface temperature (SST) and also impacted the surface bio-optics and phytoplankton. These offshore waters mixed with the coastal river discharge waters and resulted in a complex surface water mass, which was visually observed during the cruise as varying plumes in the surface color. The coastal river discharge waters were observed in the VIIRS imagery with increased backscattering from the particles. The time sequence of VIIRS ocean color imagery shows the complex undulating Gulf Stream frontal eddies (shingles). It is noted that the VIIRS SST does not clearly delineate Gulf Stream features since the storm surface mixing impacted the surface temperature gradients. Following the storm passage, the SST characteristic Gulf Stream SST gradients reformed. These changes in the Gulf Stream and the eddy formation following the storm were identified by ocean circulation models and showed the interaction of the strong winds and offshore eddies on the flow field. The westward intrusion of the offshore Gulf Stream water brought a *Trichodesmium* bloom and patchiness into the coastal waters as far inshore as the entrance to Charleston and was visibly observed on the surface waters. These blooms strongly affected the ocean color properties with highly varying particles as observed at Station 1 off of Charleston, SC.

6. Parameters Measured

6.1 Introduction to Observations

Following is a concise accounting of the various parameters observed and instruments deployed or methods used to make these measurements. Table 3 shows observations made at each station and underway (continuous). Further details of instruments and deployment and processing protocols are provided in individual group sub-sections in Section 8 and Section 9 and an instrument list is consolidated in Table B2 of Appendix B. *Note that commercial equipment, instruments, or materials are identified in this report to foster understanding. Such identification does not imply recommendation or endorsement by NOAA, NIST or any of the participating institutions, nor does it imply that the materials or equipment identified are necessarily the best available for the purpose.*

6.2 Apparent Optical Properties

AOPs measured included downwelling irradiance (E_d), upwelling radiance (L_u) and incoming solar irradiance (E_s) spectrally (λ) across a range of wavelengths (e.g., ≈300 nm to 900 nm). These properties are used to determine in situ $nL_w(\lambda)$ and $R_{rs}(\lambda)$ (comparable with the satellite and $R_{rs}(\lambda)$ products).

- nL_w, R_{rs} – these parameters were measured using many different instruments deployed in a variety of ways:
  - On station
    - Water column profiles - 4 free-falling AOP profiling packages
      - Three hyperspectral profilers (NOAA/STAR, OSU and USF)
      - One multispectral profiler (deployed by NOAA/STAR, for NASA Goddard Space Flight Center (GSFC))
    - Sea surface, floating - 3 instrument packages with hyperspectral radiometric sensors configured to float at the sea surface (UMB; 2x Stennis)
  - Above surface, on deck
    - Seven handheld radiometers were deployed at stations with effort to make observations simultaneously under identical conditions (4 ASDs: NOAA/STAR, 2x Stennis, USF; 2 Spectral Evolutions: OSU, UMB; and a GER: CCNY).
    - Additionally, on-board experiments were conducted with subsets of handheld instruments, testing different locations on the ship, protocols and reference tiles
  - Continuous, on deck
    - An instrument package, HyperSAS-POL, mounted on a mast in the bow of the ship collected above water AOP measurements continuously. HyperSAS-POL measured both polarized and unpolarized AOPs (CCNY).

- Secchi depth (Stennis)
- Aerosol optical thickness (AOT; a component of atmospheric correction algorithms); handheld sun photometers were deployed at stations (NOAA, USF, CCNY)
- Radiance distribution of L_u (U. Miami)
- Daily solar E_d integrated from 400 nm to 700 nm, the photosynthetically active radiation (PAR) spectral region (USF)

6.3 Inherent Optical Properties

Several instrument packages measured IOPs. On stations, some profiled the water column, others floated at the water surface and some were plumbed into the underway, flow-through system. Instrument packages had unique combinations of sensors and are described in more detail within the specific group's sub section in Section 9.

6.3.1 Water Column – profiling (on station)

Measurements from dedicated IOP packages:

- Hyperspectral total absorption coefficient ($a(\lambda)$)
- Hyperspectral beam attenuation coefficient ($c(\lambda)$)
- Hyperspectral Chromophoric Dissolved Organic Material (CDOM) absorption coefficient (a_{CDOM})
- Backscatter coefficient (b_b)
- Fluorescence
- Volume scattering function (VSF)

IOPs included on AOP packages:

- Chlorophyll fluorescence
- CDOM fluorescence
- Phycoerythrin fluorescence
- Scattering (b; at 443 nm, 530 nm and 860 nm by NOAA/STAR and at 660 nm by USF).

IOPs on the *Foster's* CTD/Rosette package:

- Chlorophyll fluorescence (ship)

6.3.2 Continuous – near surface (underway flow-through)

- Hyperspectral $a(\lambda)$, $c(\lambda)$ and $a_{CDOM}(\lambda)$
- b_b at 470 nm, 572 nm and 670 nm
- Chlorophyll and UV fluorescence (ship)
- CDOM fluorescence
- Phycobilipigments fluorescence
- Phytoplankton functional types (PFTs; imaging)
- Phytoplankton photo-physiology from variable fluorescence

6.4 Discrete water sampling

These parameters were determined from analyses of discrete water samples collected from Niskin bottles on the CTD/Rosette or from the underway flow-through system:

- Extracted fluorometric Chl-*a* (fluorometry)
- Suspended Particulate Material (SPM; mass)
- Particle absorption by filter pad technique (FPT; spectrophotometry)
- CDOM (spectrophotometry)
- Phytoplankton pigments by high performance liquid chromatography (HPLC)
- Particulate organic carbon (POC) and particulate organic nitrogen (PON); (C H N combustion elemental analyzer)
- Nutrients; N (nitrate and nitrite), P and Si (colorimetry)
- Preserved samples for phytoplankton assemblage characterization (microscopy)
- Phytoplankton automated imagery

- Phytoplankton size
- Phycobilipigment types
- Photosynthetic efficiency

These parameters were observed by the standard instrumentation on the ship's CTD-rosette package.
- Salinity
- Sea surface temperature
- Dissolved O_2

These parameters were observed by other onboard instrumentation maintained by the ship.
  - Acoustic Doppler Current Profiler (ADCP)
  - Meteorology
    - o Wind speed
    - o Wind direction
    - o Sea state
    - o Air temperature

Table 3. Parameters observed by station number and underway (continuous from flow-through or above water on bow) measurements.

NF-16-08 Station ID#	**1**	**2**	**3**	**4**	**5**	**6**	**7**	**8**	**9**	**10**	**11**	**12**	**13**	**Under-way**
Date in October 2016	**13**	**13**	**14**	**14**	**15**	**16**	**16**	**16**	**16**	**17**	**17**	**17**	**18**	**13-18**
Day of Year	**287**	**287**	**288**	**288**	**289**	**290**	**290**	**290**	**290**	**291**	**291**	**291**	**292**	**287 to 292**
$L_u(\lambda)$, $R_{rs}(\lambda)$, $nL_w(\lambda)$ profiles	x	x	x	x		x	x	x	x	x	x	x	x	
$L_u(\lambda)$, $R_{rs}(\lambda)$, $nL_w(\lambda)$ surface polarized/unpolarized pairs	x	x	x	x	x	x	x	x	x	x	x	x	x	x
$L_u(\lambda)$, $R_{rs}(\lambda)$, $nL_w(\lambda)$ surface, in water floating	x	x	x	x				x		x	x	x	x	
$L_u(\lambda)$, $R_{rs}(\lambda)$, $nL_w(\lambda)$ surface, handheld	x	x	x	x	x	x	x	x	x	x	x	x	x	
$L_u(\lambda)$, $R_{rs}(\lambda)$, $nL_w(\lambda)$ blue tile					x						x			
Radiance distribution of L_u	x	x	x	x						x	x	x	x	
E_d(PAR)	x	x	x	x	x	x	x	x	x	x	x	x	x	x
$a_p(\lambda)$, $a_d(\lambda)$, $a_g(\lambda)$, from optical sensors	x	x	x	x		x	x	x	x	x	x	x	x	x
$c(\lambda)$	x	x	x	x		x	x	x	x	x	x	x	x	x
$a_{CDOM}(\lambda)$	x	x	x	x		x	x	x	x	x	x	x	x	x
$b_b(\lambda)$	x	x	x	x		x	x	x	x	x	x	x	x	x
$b(\lambda)$	x	x	x	x		x	x	x	x	x	x	x	x	x
CDOM fluorescence	x	x	x	x		x	x	x	x	x	x	x	x	x
VSF		x	x	x		x	x	x	x	x	x	x	x	
CDOM (spectrophotometry)	x	x	x	x		x	x	x	x	x	x	x	x	
$a_p(\lambda)$, $a_d(\lambda)$, $a_g(\lambda)$, from filter pad technique	x	x	x	x		x	x	x	x	x	x	x	x	
Chl-*a* and UV fluorescence	x	x	x	x	x	x	x	x	x	x	x	x	x	x
Chl-*a* extracted	x	x	x	x	x	x	x	x	x	x	x	x	x	
POC, PON	x	x	x	x	x	x	x	x	x	x	x	x	x	
SPM	x	x	x	x	x	x	x	x	x	x	x	x	x	
HPLC pigments	x	x	x	x	x	x	x	x	x	x	x	x	x	
Nutrient concentrations (N, P, Si)	x	x	x	x	x	x	x	x	x	x	x	x	x	
Microscopy	x	x	x	x	x	x	x	x	x	x	x	x	x	
Phycoerythrin fluorescence	x	x	x	x	x	x	x	x	x	x	x	x	x	x

NF-16-08 Station ID#	1	2	3	4	5	6	7	8	9	10	11	12	13	Under-way
Date in October 2016	**13**	**13**	**14**	**14**	**15**	**16**	**16**	**16**	**16**	**17**	**17**	**17**	**18**	**13-18**
Day of Year	**287**	**287**	**288**	**288**	**289**	**290**	**290**	**290**	**290**	**291**	**291**	**291**	**292**	**287 to 292**
***F_v/F_m* and σ_{PSII}**	x	x	x	x	x	x	x	x	x	x	x	x	x	x
Phycobiligment types (PE1, PE2, PE3)	x	x	x	x	x	x	x	x	x	x	x	x	x	x
Secchi depth	x	x	x	x		x	x	x		x	x	x	x	
AOT					x						x		x	
Currents	x	x	x	x	x	x	x	x	x	x	x	x	x	x
Wind speed and direction	x	x	x	x	x	x	x	x	x	x	x	x	x	x
Air temperature	x	x	x	x	x	x	x	x	x	x	x	x	x	x
Salinity	x	x	x	x	x	x	x	x	x	x	x	x	x	x
SST	x	x	x	x	x	x	x	x	x	x	x	x	x	x
Dissolved O2	x	x	x	x		x	x	x		x	x	x	x	
Water depth	x	x	x	x	x	x	x	x	x	x	x	x	x	
Cloud cover	x	x	x	x	x	x	x	x	x	x	x	x	x	
Sea state	x	x	x	x	x	x	x	x	x	x	x	x	x	

7. Laboratory Calibration of Radiometers

Pre- and/or post-cruise calibrations of several radiometers used in this cruise were conducted at the NOAA/STAR Optical Characterization Experiment Laboratory in College Park, Maryland using a NIST traceable type FEL 1000 W standard irradiance lamp (#39040C, serial #667) and an Optronic Laboratories OL-455-18 integrating sphere for radiance with values traceable to NIST (Figure 4). A discussion of the theoretical basis for radiometric instrument calibration was included in the 2014 cruise Technical Report [Ondrusek et al., 2015] as based on primary research by Zibordi and Voss [2014] and by Johnson et al. [2014] and others. Before the cruise, on 27 September 2016, and then again shortly after the cruise, on 2 November 2016, a total of 14 sensors were calibrated from several instrument packages:

- 3 Satlantic HyperPro Profiler IIs (i.e., HyperPro; NOAA/STAR, USF, OSU)
- Radiometer Incorporated Skylight Blocked Apparatus (RISBA; floating HyperPro modified by UMB).
- Biospherical Instruments C-OPS (deployed by NOAA/STAR on loan from NASA)

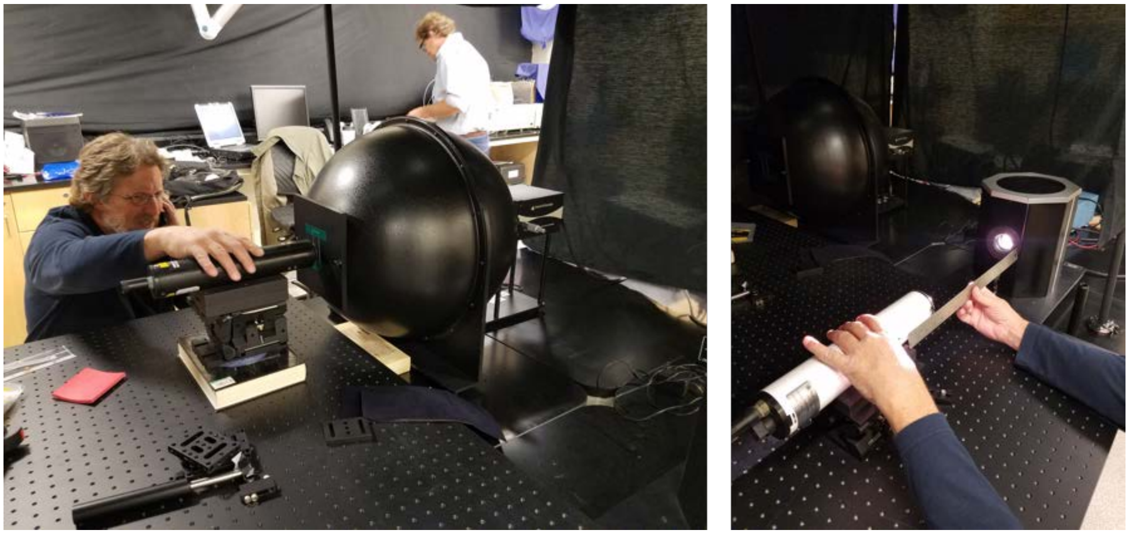

Figure 4. Calibration activities at the NOAA/STAR optical laboratory.

Figure 5 shows an example of the pre- and post-cruise measurement results for the NOAA/STAR L_u 206 radiance sensor along with the NIST calibration values for the spectral radiance of the sphere source, using the calibration coefficients from the current calibration. Figure 5 shows the percent difference between the sphere spectral radiance and that measured by the radiometers.

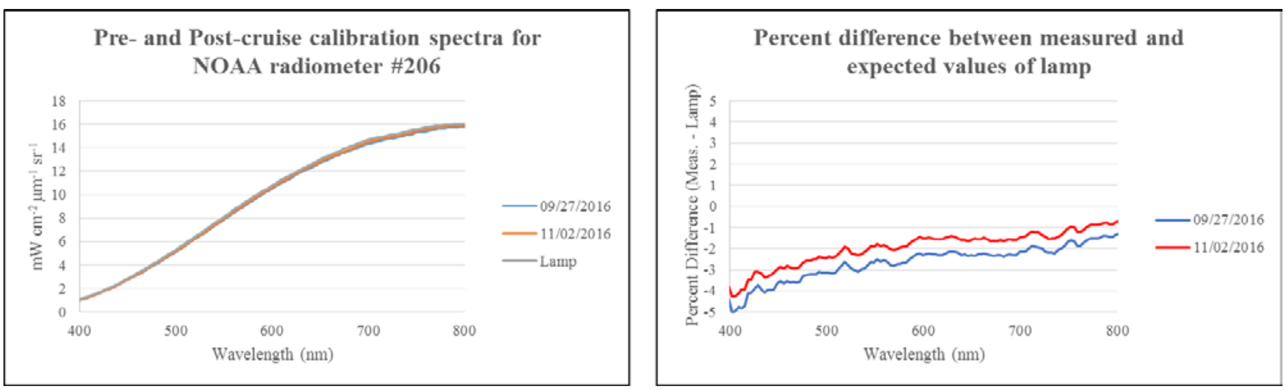

Figure 5. Example of the pre- and post-cruise calibration results for the NOAA/STAR L_u 206 radiance sensor (left) along with expected values for the lamp and (right) the percent difference between the expected lamp values and those measured by the radiometers.

8. Common Radiometric Measurements: Methods and Protocols

8.1 Overview of in situ radiometry methods

As light from the sun passes through seawater, its spectral shape and intensity are changed. Some of the light that enters the ocean is eventually re-emitted. This re-emitted light is part of the light that the ocean color satellite sensor “sees”. An in-water profiling radiometer is essentially a pair of spectrometers, one, upward looking, which measures downwelling irradiance ($E_d(\lambda)$), and another, downward looking, which measures upwelling radiance ($L_u(\lambda)$), that are dropped through the water column along with an above water reference sensor, which measures downwelling spectral irradiance ($E_s(\lambda)$). These measurements are used to calculate $nL_w(\lambda)$, which is the parameter observed by ocean color satellites. Above-water radiometers directly measure water leaving radiances to calculate $nL_w(\lambda)$. These $nL_w(\lambda)$ are used to validate satellite ocean color radiances and to derive other ocean color products such as Chl-*a* or SPM concentrations used in ecological studies [Ondrusek et al., 2012].

During this 2016 Cal/Val cruise, in situ observations were made using multiple spectroradiometric instruments that can be grouped by 4 distinct operational approaches: 1) in-water profiling, 2) surface floating, and 3) above water, handheld and 4) above water, mounted. Each approach has fundamental strengths and weaknesses. In-water profiling radiometers provide optical information about the water column and avoid light contamination above the surface. In order to calculate $nL_w(\lambda)$, values must be extrapolated, or modeled, from below the water's surface to above the water's surface. Sensors can be (and have been for this cruise) calibrated with NIST traceable reference source lamps. Deployment from the deck of a ship is not difficult, but requires dedicated ship activity and a complete series of measurements acquired (integrated) over a period of time during which varying sky conditions are to be avoided. Additional sensors (to simultaneously measure IOPs, for example) are often included with the instrument package. The floating radiometers are the same basic instrument as the profiling radiometers but are mounted with a buoyant collar so they remain in place near the sea surface. This arrangement allows for simultaneous above water E_d and below water L_u measurements very close to the actual sea surface, or, in the case of the SBA, both the E_d and the L_u sensors are just above the sea surface with the L_u sensor shielded to block sky light. The above water, handheld devices are relatively inexpensive, deployment logistics are relatively simple, and sampling time integration is relatively short, reducing risk of changes in sky conditions. The above water observations are more directly related to the satellite observation but are subject to multiple sources of light contamination (such as sun glint, sea foam, reflections from ship structure, etc.) and sampling variation. In theory, no instrument calibration is required for the handheld instrument because a reference plaque is measured. Note, that experiments were conducted on this and the two previous dedicated Cal/Val cruises, using a NIST blue tile reference being developed (see Section 9.6).

Multiple profiling radiometers and handheld spectrometers were deployed by groups using an agreed-upon set of protocols and common processing methods. These multi-instrument common deployments are described in the next 2 sections (8.2 and 8.3). Sometimes, individual researchers made additional handheld observations using different protocols to test the effects of protocol on measurements. The floating radiometers are discussed within their respective group's section (Stennis, Section 9.2 and UMB, Section 9.7).

8.2 In-water profiling radiometry

Four profiling radiometers were deployed simultaneously during this 2016 Cal/Val cruise in a similar fashion to the deployments of the 2014 and 2015 cruises [Ondrusek et al., 2016; Ondrusek et al., 2015] following recommended protocols [Satlantic, 2012, 2004], keeping them away from the ship and each other, and avoiding ship shadowing. At each station, the ship was positioned so that the sun was directly off the stern. The 4 profiling instruments, which were weighted to produce a descent rate of approximately 0.1 m s^{-1} to 0.3 m s^{-1}, were positioned evenly spaced at the stern (Figure 6) and lowered together to the sea surface. The ship steamed at approximately 1 knot as the cables were let out until the profilers were at least 20 m off the stern. After that, the ship maintained just enough headway to maintain the heading, to prevent the profilers from closing in on the ship and to prevent them from crossing cables while profiling. For each station, 3 to 5 multicast measurement sets were conducted. For each set, all four profilers were lowered to approximately 10 m to 15 m depth through the euphotic zone and raised together 3 to 5 times. If sky conditions changed significantly during the cast, the set was stopped and restarted when the conditions were favorable again.

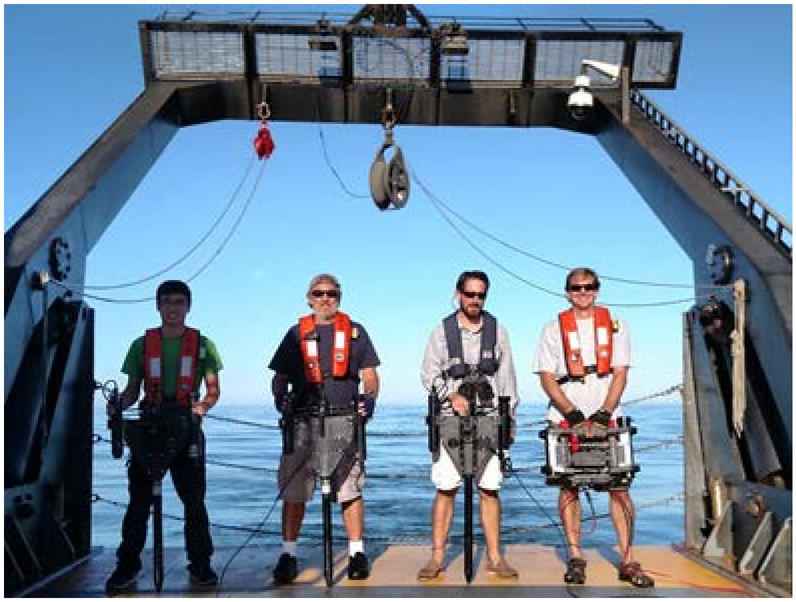

Figure 6. Four profiling radiometers were deployed simultaneously from the stern. The 3 HyperPro instruments are pictured on the left. The C-OPS is on the right.

Three of the four profiling radiometers were Satlantic HyperPro Profiler IIs (HyperPro; specifications and manuals can be found at http://www.satlantic.com). These HyperPros were deployed by research groups NOAA/STAR, USF and OSU. The fourth profiler was a Biospherical Instruments C-OPS system, provided by NASA Goddard Space Flight Center and operated on board by the NOAA/STAR group. All four profilers were deployed during 8 of the 13 stations occupied during the cruise. On 15 October, conditions were too rough to deploy any profilers. For the first two stations on 16 October, conditions were marginal and only one HyperPro profiler was deployed. For the third and fourth stations on 16 October only two HyperPros and the C-OPS were deployed. The profiling radiometers were calibrated before and after the cruise from 350 nm to 900 nm as described in Section 7.

The HyperPro system has a downward looking HyperOCR radiometer that measures $L_u(\lambda)$ and an upward looking HyperOCI irradiance sensor to measure $E_d(\lambda)$ in the water column. Each HyperOCR or HyperOCI has a 256 channel silicon photodiode array detector with 10 nm spectral resolution and spectral sampling of 3.3 nm pixel^{-1}. The HyperOCRs have dark signal corrections performed using shutter dark measurements collected every 5th scan. The C-OPS system has three radiometers each with a spectral range from 300 nm to 900 nm and 19 wavebands each (305 nm, 320 nm, 340 nm, 380 nm, 395 nm, 412 nm, 443 nm, 465 nm, 490 nm, 510 nm, 532 nm, 555 nm, 565 nm, 625 nm, 665 nm, 683 nm, 710 nm, 780 nm and 875 nm). The C-OPS L_u radiometer substitutes a broad natural chlorophyll fluorescence sensor (27 nm full width half maximum (FWHM), centered at 683nm) for the 875 nm sensor. All other wavelengths are 10 nm FWHM. The radiometers feature three gain stages, which provide 9 decades of dynamic range [Morrow et al., 2010]. The above water reference sensor was an upward looking HyperOCI irradiance sensor to measure $E_s(\lambda)$ used during data reduction. All of the E_s sensors (one for each instrument package) were mounted on a telescoping tower mounted on the 02 deck as pictured in Figure 7. Additional sensors incorporated into these profiling radiometer packages measure pressure, temperature, conductivity, and tilt. WETLabs ECO-Puck Triplet sensors for IOPs are also included in the profiling radiometer packages. Each group's ECO-Puck arrangements were unique and are described in the respective sub-sections of Section 9.

Figure 7. Telescoping tower pole for E_s sensors.

For consistency, the data processing for all of the profiling HyperPro systems followed multi-cast protocols established by Michael Ondrusek of NOAA/STAR using Satlantic ProSoft processing software version 8.1.6. The $nL_w(\lambda)$s are calculated using the equation:

$$nL_w(\lambda) = L_w(\lambda, 0^+) * F_0(\lambda)/E_s(\lambda) \quad (1)$$

where F_0 is the mean extraterrestrial solar irradiance and $E_s(\lambda)$ is the downwelling spectral irradiance just above the surface and is measured with the above water HyperOCR irradiance reference sensor. $L_w(\lambda)$ is the water-leaving radiance calculated just above the surface by:

$$L_w(0^+, \lambda) = L_u(0^-, \lambda) * [(1-\rho(\lambda, \theta))/n_w(\lambda)^2] \quad (2)$$

Here, $\rho(\lambda, \theta)$ is the sea surface Fresnel reflectance and is set as 0.021, and $n_w(\lambda)$ is the Fresnel refractive index of seawater and is set here as 1.345. $L_u(0^-, \lambda)$ is the calculated upwelling radiance just below the surface and is determined by using the diffuse attenuation coefficient ($K(L_u)$) calculated using a least squares regression fit from log transformed measured $L_u(\lambda)$ values and the intercept just below the surface.

8.3 Above water radiometry with handheld instruments

Above-water "handheld" radiometry measurements were conducted by the "Above Water Group" (AWG) using 7 handheld instruments at all 13 stations. The 7 instruments and associated groups are as follows:

- 4 x PANalytical FieldSpec Spectroradiometer HandHeld2 portable model (ASD; http://www.asdi.com/products/fieldspec-spectroradiometers/handheld-2-portable-spectroradiometer): measures radiance at <3 nm spectral resolution for wavelengths from ≈350 nm to >1000 nm operated by NOAA/STAR, USF and 2 by Stennis/NRL.

- 1 x GER 1500, Field Portable Spectroradiometer: measures wavelengths from 350 nm to 1050 nm at 3 nm FWHM resolution and uses a diffraction grating with a silicon diode array that has 512 discrete detectors and provides the capacity of reading 512 spectral bands, operated by CCNY.

- 2 x Spectral Evolution Spectroradiometer: 1) A model SE PSR-1100-F with a fiber input and 8-degree field-of-view (FOV) fore-optic was operated by OSU. This instrument measures radiance sampled every 1.5 nm, with a spectral resolution of 3.2 nm over the 320 nm to 1100 nm spectral range. However, due to the difficulty in calibrating the 99% Spectralon plaque below 360 nm and the low signal-to-noise ratio received from the water above 850 nm, generally only output spectra in the 360 nm to 850 nm range are used. 2) A model SR-1901 operated by UMB with 768 spectral bands (350 nm to1900 nm). The spectral resolution is 4 nm between 350 nm to 1000 nm and 10 nm between 1000 nm and 1900 nm.

At each station, the AWG met on deck with the assortment of instruments listed above and made near-coincident (within ≈30 min) measurements of the water reflectance. Six of the 7 instruments were deployed together using an agreed-upon standardized deployment protocol and the NRL 25 cm, 10% gray reference plaque (Reference #52301, 8/h NIST traceable, resurfaced and calibrated by Labsphere on 1 June 2016). This common deployment is described further, below. Most of the measurements made with the USF ASD instrument used the USF protocol rather than the NRL protocol. Major differences between NRL and USF deployments are noted below.

The common AWG instrument configurations, reference plaque and measurement angles are as follows:

- Integration time was optimized for each target prior to collection (i.e., integration time of sensor was changed based on relative brightness of the target and new dark counts were taken to correct for instrument noise). Integration times ranged from 68 ms to 4352 ms. USF protocol (for the ASD-HH2) uses a measurement series optimization, rather than optimization for each component of the R_{rs} estimate.
- The reflectance plaque, referred to here as the "NRL gray plaque," is a 10% gray Spectralon® card with a known directional/hemispherical reflectance and assumed to be a near-Lambertian surface. It is used to normalize the un-calibrated irradiance measurements for E_s. The NRL plaque was not used routinely by USF, though it was used for comparison at some stations.
- Instruments were positioned to make the reference measurement at between ≈30 cm and ≈60 cm above the NRL gray plaque.
- Fore-optic attachments with FOV angles unique to each instrument were used.
- Five consecutive radiometric spectral measurements were taken of each of the following targets: NRL gray plaque (S_g), water (S_{sfc}), and sky (S_{sky}).
- Most measurements were taken from the 01 deck on the ship. The exact location of sampling (port 01deck vs. starboard-03 deck) was dependent on the orientation of the ship relative to the sun to eliminate shadowing from the vessel and surface contamination. On the *Nancy Foster*, the stern is 1.5 m, 01 deck is 5m and the 03 deck is 8 m above the water surface.
- The optical sensor zenith angles for the NRL gray plaque (θ_g), water (θ_{sfc}) and sky (θsky) measurements were 135°, 135° and 45°, respectively. The relative azimuth angle of the sensor to the sun ($\Delta\varphi$) was 90° up to 135° depending on sea conditions and ship orientation. See Section 9.5 for sensor viewing angle used for USF measurements.

The collection of data at different deck heights and fore optics angles will be used to examine how the spot size affects the values of the R_{rs} retrieved.

Processing for AWG ASDs is being conducted using NRL-developed processing software that follows the guidelines of [Mueller et al., 2003] and utilizes 5 different processing models including: R_{rs} _sfc (no NIR reflectance correction), R_{rs}_fresnel (Fresnel correction omitted), R_{rs} [Carder and Steward, 1985], R_{rs} _ [Lee et al., 1997], and R_{rs} _ [Gould et al., 2001].

Reflectance, the sensor response signal, *S*, is obtained from averaging *n* readings (generally $n = 5$) from each target and normalized to the same integration time (1 s).

$$S = \frac{C * I_N}{n}, \int_{i=0}^{n} \frac{1}{I_i} \tag{3}$$

Here, *C* represents the dark-corrected output values from the instrument, I_i is the integration time used for that reading, I_N is the normalized integration time (standard $N = 1$ s), and *n* is the number of readings (3, 5, or 9 in practice depending on instrument protocol).

Following chapter 2 of the Optics Protocols [Mueller, 2003], one can express the water-leaving radiance, L_w, and incident spectral irradiance (E_S) in terms:

$$L_w = F_L \left[S_{sfc} - \rho S_{sky}\right] \text{ and } E_S = \frac{\pi F_L S_g}{R_g} \tag{4}$$

Here, F_L is the unknown instrument radiance response calibration factor (which will cancel when finding R_{rs}) and R_g is the gray plaque's bi-directional reflectance factor. The R_{rs} can be computed from the un-calibrated data using the following equation (correcting sky using Fresnel reflectance ρ of 0.025):

$$R_{rs}(\lambda) = \frac{S_{sfc}(\lambda) - \rho S_{sky}(\lambda)}{\pi S_g(\lambda)/R_g(\lambda)} \tag{5}$$

The computed R_{rs} should be "black" (≈ 0 sr^{-1}) at about 750 nm. If not zero, then it is assumed that the S_{sky} was not estimated correctly. Following the “quick and easy” algorithm of Carder and Steward [1985], it is further assumed that any error in the skylight reflection term is white (not wavelength dependent) and one may simply subtract the computed R_{rs} at 750 nm from the entire spectrum. In practice, this may lead to negative reflectance values R_{rs} near 750 nm. Therefore, the processing subtracts the smallest R_{rs} in the range from 700 nm to 825 nm.

$$R_{rs}(\lambda) = R_{rs}(\lambda) - MIN\left(R_{rs}(700 \text{ nm } to \text{ } 825 \text{ nm})\right) \tag{6}$$

To compare the in situ reflectance with satellite-derived reflectance, the mean reflectance is computed using the relative spectral response tables for each band of the satellite (VIIRS).

In addition to this common group activity, some AWG group members made additional measurements using their own established protocols with variations involving, for example, reference plaques, scan angles, number of scans, integration times and also post-processing methods. These variations are described within each of the collaborating groups’ sections.

8.4 Above Water Group measurements of NIST blue tile

To assess the effects of differences in measured R_{rs} due to different instruments, the AWG group measured the R_{rs} of the NIST blue reference tile (described in Section 9.6). AWG used a protocol as consistent as possible with that described earlier, along with the same NRL gray plaque but with the blue tile in place of the sea surface (Figure 8). Because blue tile measurements were made at different times from the water measurements, the solar azimuth angles differ. Blue tile experiments were conducted at Station 5 with ≈ 40% cloud cover and at Station 11 under mostly clear skies with only ≈5% cloud cover.

NRL processing was used to derive the relative reflectance of the blue tile (R_{tile}), however the equation is slightly modified. For the blue tile measurements, the derived reflectance is simply expressed as the ratio of the radiance (or net signal) for the test target (S_{tile}) to the standard gray target, as

$$R_{tile}(\lambda) = R_g(\lambda)\frac{S_{tile}(\lambda)}{S_g(\lambda)} \qquad (7)$$

In principle, the blue tile is a reference and the spectra should be the same. Preliminary results for two NRL ASD instruments were mixed. The NRL #1 ASD produced variable spectra between the two stations while NRL #2 ASD spectra were closely matched. Furthermore, spectral differences between stations were evident. All blue tile spectra (raw) were delivered to Carol Johnson (NIST) for reprocessing and further analysis.

Figure 8. Science team measuring the NIST blue tile with a handheld radiometer.

9. Participating Science Groups' Unique Activities, Methods and Protocols

9.1 NOAA/STAR – Michael Ondrusek and Eric Stengel

In-water radiometry

NOAA/STAR led the simultaneous deployment of the in-water radiometry instruments as described in Section 8.2. The NOAA/STAR HyperPro Profiler II package is equipped with depth, temperature, tilt and two WET Labs ECO-Puck Triplet sensors. One ECO-Puck sensor measures fluorescence to estimate concentrations of chlorophyll *a*, CDOM and phycoerythin. The second ECO-Puck sensor measures backscattering (b_b) at 443 nm, 530 nm, and 860 nm.

The Biospherical Instruments C-OPS system has three radiometers with a total spectral range from 300 nm to 900 nm, with 19 center wavelengths each as listed below. The upwelling radiance radiometer substitutes a broad natural chlorophyll fluorescence sensor (27 nm FWHM, centered at 683 nm) for the 875 nm sensor. All other wavelengths are 10 nm FWHM. The radiometers feature three gain stages, which provide 9 decades of dynamic range [Morrow et al., 2010].

List of 19 center wavelengths of the NASA's C-OPS profiling radiometer in nanometers:

305	320	340	380	395	412	443	465	490	510
532	555	565	625	665	683	710	780	875	

Figure 9 (left) shows preliminary results from NOAA MSL12 VIIRS *vs*. NOAA/STAR HyperPro comparisons from 14 October, 2016, Station 3. NOAA VIIRS data is averaged over 5 x 5 pixels centered at the location of the HyperPro cast.

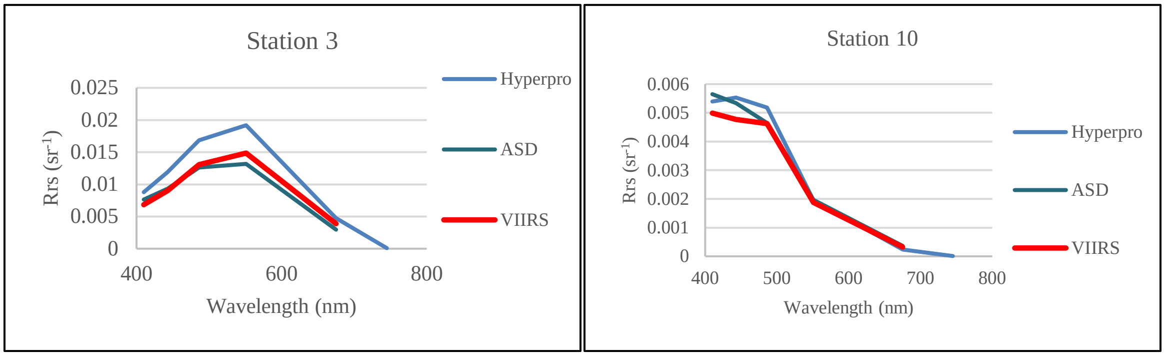

Figure 9. Preliminary results from 14 and 17 October, 2016, Station 3 (left) and Station 10 (right) comparisons with NOAA MSL12 VIIRS *vs*. NOAA/STAR HyperPro and ASD.

Above water radiometry
NOAA/STAR participated in the simultaneous deployment of above-water radiometry instruments as described in Section 8.3 with an ASD. Preliminary results of ASD comparison with VIIRS MSL12 is shown in Figure 9.

Extracted fluorometric Chl-*a*
Chl-*a* concentrations were measured using a Turner 10 AU Fluorometer [Welschmeyer, 1994]. Surface samples were collected in duplicate at each station from the Rosette Sampler and several times a day while underway from the flow-through system to calibrate the underway chlorophyll fluorometers. 100 mL to 400 mL of seawater was filtered on a 25 mm diameter, 0.7 µm glass microfiber filter (GF/F; Whatman). The filters were frozen in liquid nitrogen, then extracted in 90% acetone in a freezer for at least 48 h. The samples were vortexed then centrifuged for 5 min before being measured on the Turner 10 AU.

Suspended Particulate Matter (SPM)
SPM samples were collected in duplicate from the surface waters for each station. Up to 2 L of water were collected for each sample and processed according to techniques outlined by [Hunter, 2006]. Water samples were filtered on pre-weighed 47 mm diameter GF/F filters. The volume of filtrate was then measured with a graduated cylinder and recorded. Filters were rinsed 3 times with distilled water, placed in 47 mm diameter Petri dishes and oven dried at 60 °C for 12 h then stored in a desiccator until analysis. Filters were weighed on a Sartorius CPA 2250 balance (with a precision of 0.01 µg) and weighed at least three times until consecutive readings were less than 0.055% variable [EPA, 1971].

HPLC and POC/PON
Water from two hydrographic depths, one in the near-surface and the second near the chlorophyll maximum, were collected from each CTD rosette cast and sometimes from a bucket and from the underway flow-through system. Water collected from the CTD Niskin bottles was transferred to 10 L carboys which were covered with black plastic bags to prevent high light exposure while awaiting filtration. Single or duplicate samples for each parameter were filtered. For each sample, a known volume of water was filtered under gentle vacuum (≈127 mm Hg) onto a 25 mm diameter Whatman GF/F filter (nominal pore size ≈0.7 µm). For HPLC, filter samples were wrapped in aluminum foil and stored in liquid nitrogen onboard. For POC/PON, samples were filtered onto pre-combusted Whatman GF/F 25 mm filters. POC/PON filters were placed in pre-combusted foil pouches and flash frozen in liquid

nitrogen. In the laboratory, both HPLC and POC/PON samples are stored at -80°C until analysis. Samples will be analyzed at the NASA/GSFC Ocean Ecology Laboratory. The HPLC method is modified from Van Heukelem and Thomas [2001]. POC/PON samples are acidified by fuming with HCl, dried and then measured using an elemental analyzer.

AOT

AOT was measured at Stations 5, 11 and 13 using a Microtops sun photometer. The data are delivered for processing to NASA as part of the AERONET Marine Aerosol Network program.

9.2 Stennis - Robert Arnone (USM), Sherwin Ladner (NRL) and Wesley Goode (NRL)

Stennis participation and measurements on the VIIRS Cal/Val cruise included: coordination with NOAA for adaptive daily planning of the cruise track and sampling locations in coastal waters west of the Gulf Stream which included optimizing stations based on cloud cover and sea state. Measurements included 1) water leaving radiance with 2 (NRL, USM) floating HyperPros; 2) above water and NIST blue tile radiance with 2 (both NRL) ASDs at optimal station locations; and 3) underway IOPs. Goals included testing methods to develop collection and processing protocols to reduce uncertainty in in situ optical ocean measurements from multiple (identical and different) instruments collecting simultaneous observations for the purpose of satellite Cal/Val.

Floating HyperPro Measurements

The floating HyperPro is a hyperspectral profiling radiometer that simultaneously measures E_s, E_d and L_u on a tethered floating buoy platform and E_s onboard the ship from a sensor affixed to an elevated pole. From these measurements, in situ $nL_w(\lambda)$ and R_{rs} are calculated and used for validation of the VIIRS nL_w. On this cruise, the Stennis team utilized 2 floating HyperPros (USM and NRL) and collected measurements at 9 of the 13 stations. USM stations included 1, 2, 3, 4, 8, 10, 11, 12 and 13 and NRL stations included 2, 3, 4, 8, 10, 11, 12 and 13. The spectral range of both E_d and L_u sensors is from 350 nm to 805 nm with ≈3.5 nm resolution. These instruments were used with a molded floatation collar, enabling the observation of temporal variability (at the time scale of ≈10 min during deployment) of in-water surface measurements at a fixed depth just beneath the sea surface. The E_d sensor uses a cosine collector and is approximately 30 cm above the water surface. The L_u sensor is mounted approximately 30 cm below the water surface. The ship mounted E_s sensor also uses a cosine collector and was mounted on the 01 deck affixed to a pole which was elevated above the ships superstructure while on station (Figure 7). E_s from the ship mounted sensor was combined with L_u from floating HyperPro for computation of R_{rs}. Each participating group's E_s sensor was mounted on the elevated pole for consistency, except for the underway HyperSAS system from CCNY group which was mounted on the ships mast (see Section 9.3). Both the USM and NRL HyperPros were calibrated by NOAA/STAR in October 2015 [Ondrusek et al., 2016].

The floating HyperPro was deployed near the starboard and port quarters and allowed to float out about 20 m to 30 m from the ship, a sufficient distance to ensure no contamination from vessel-generated bubbles, ship shadowing or other potential disturbances. Once the instrument was satisfactorily placed, data were recorded for 10 minutes. Post processing of this dataset from level 1 to level 4 was done using Satlantic's ProSoft v8.1.4 with set protocols. The processing protocols for deriving R_{rs} from in water radiometry follow Mueller [2003]. R_{rs} is related to nL_w (computed as shown in Eqs. 4 and 5 above) as

$$R_{rs} = nL_w / F_0. \qquad (8)$$

A preliminary analysis revealed that 9 stations had limited or absent cloud cover where a direct comparison with VIIRS-retrieved nL_ws is possible. Data were filtered to remove spikes when the sensor tilted greater that 2° and then averaged over the collection time period (≈10 min). These protocols for processing the floating HyperPro for deriving *nLw/Rrs* are being tested and evaluated against the profiling HyperPro data and ASD observations. The USM and NRL E_s sensors gave results very similar to those of the other groups (Figure 10). The R_{rs} results from the USM and NRL floating HyperPros at the coincident stations are in good agreement (Figure 11).

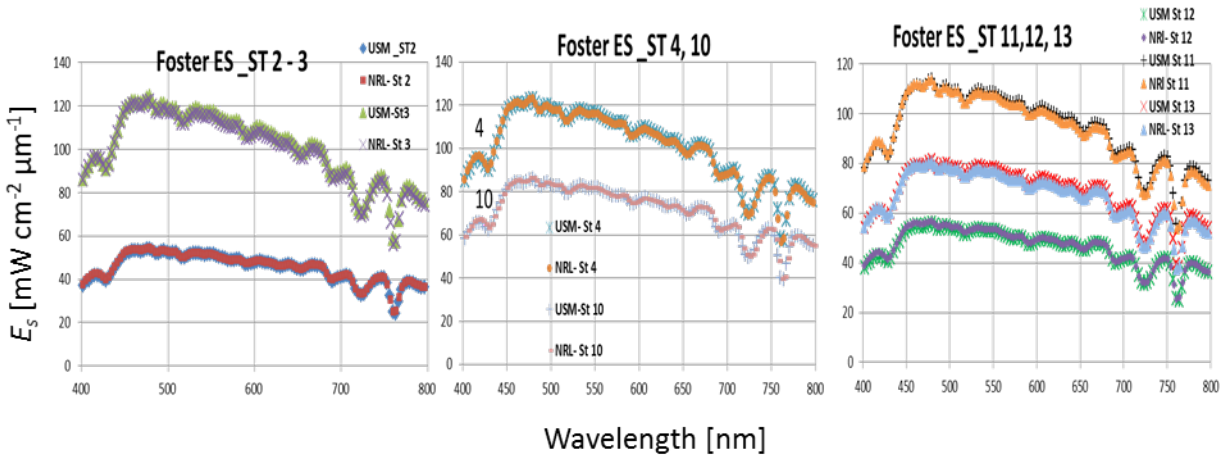

Figure 10. Preliminary results for multiple E_s sensors at several stations showing good agreement.

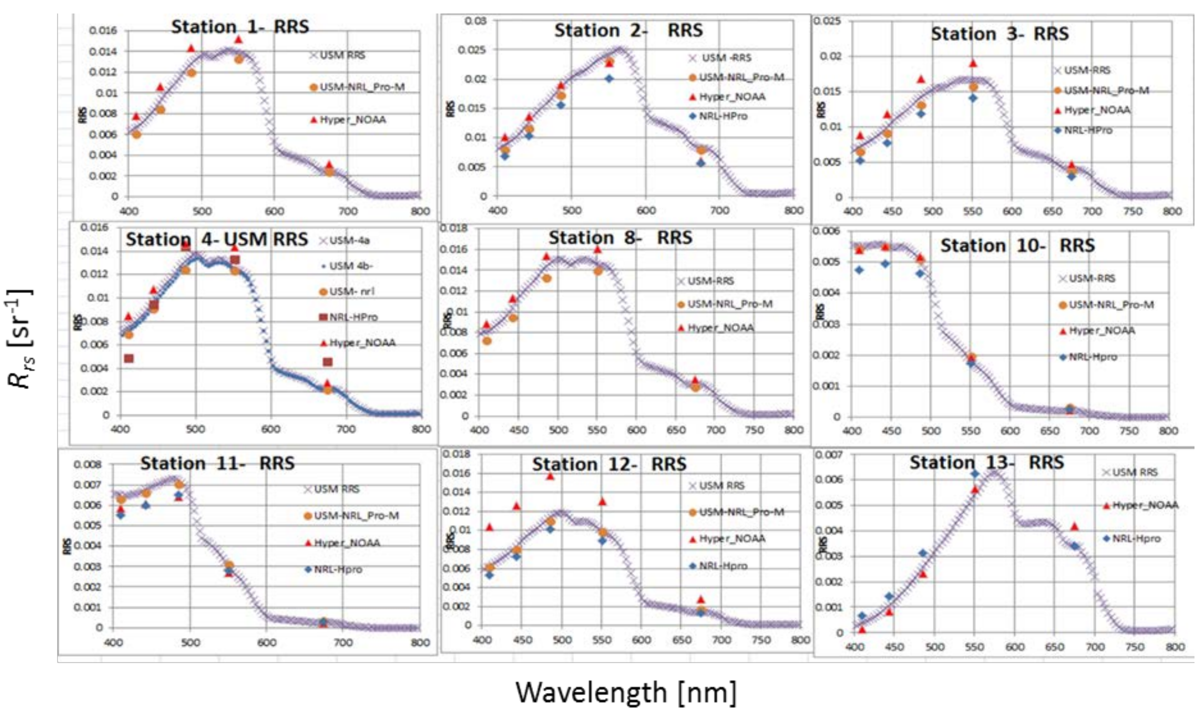

Figure 11. Preliminary comparisons of R_{rs} measured by Stennis floating HyperPro radiometers showing good agreement.

Inherent Optical Properties collected using underway flow-through system

IOPs were measured continuously while underway for real time monitoring of water mass characteristics. From these observations, spectral a, a_{CDOM}, particulate absorption (a_p), c and b and b_b can be determined and used to address several points related to overall cruise objectives:

a. Characterize the spatial variability of water's optical properties along the cruise track and how the variability impacts the uncertainty of in situ measurements at each station, which were used for VIIRS Cal/Val.
b. Validate IOPs derived from VIIRS.
c. Relate water mass optical characteristics of $a(\lambda)$ and $b(\lambda)$ to $nL_w(\lambda)$.
d. Define coastal/shelf frontal boundaries using thermal, biological and optical properties.
e. Define ocean processes and water mass types.

Two WETLabs absorption and beam attenuation instruments were connected to the ship's flow-through system which pumped water from a depth of ≈3 m. The hyperspectral instrument (ac-s), which covers the complete spectrum from 400 nm to 800 nm, measured the non-filtered water. The multispectral instrument (ac-9), which has nine wavelengths covering the visible to near infrared (412 nm, 440 nm, 488 nm, 510 nm, 532 nm, 555 nm, 650 nm, 676 nm, 715 nm), measured filtered water passed through a Cole Palmer 0.2 µm pore size filter. Both the ac-9 and ac-s instruments were placed in a controlled temperature water bath to dissipate heat and minimize electronic temperature instability in the instruments, which can impact the scattering and absorption measurements. The instruments were allowed to warm up and stabilize before measurements began for consistency with pure water laboratory calibration protocols. The ac-s and ac-9 and a backscattering sensor were interfaced with a WETLabs DH4 data logger with additional inputs from the ship's flow-through system needed for post-processing, including position, time, date, heading, water temperature, salinity, and uncalibrated fluorescence. The DH4 host software was used to combine data inputs and store them for later post processing. Sensor outputs were displayed real time using WetLab's WetView software to monitor system performance and ocean properties. The data sample rates were 6 Hz and 4 Hz for the ac-9 and ac-s respectively, which equates to a spatial resolution of ≈10 m at ship velocity of 5 knots. Data files from the DH4 were saved hourly for the entire cruise.

The ac-s and ac-9 instruments were calibrated 3 times: once prior to the cruise and twice during the cruise. Calibration of the ac meters included running Nanopure water through the systems (while the instruments remained in the controlled temperature water bath) using a gravity feed after the instruments were allowed to stabilize (≈5 min to ≈10 min) to reach a constant temperature. The calibration procedure included obtaining the clear water calibration before and after cleaning the absorption and scattering tubes. An update to instrument device files was applied in real-time if it was deemed that new corrections were necessary to assure good quality measurements.

The ac-s (non-filtered) was used to measure the "total" IOPs (combined effects of water, dissolved and particulate constituents of seawater). The filtered ac-9 was used to determine the IOPs associated with the dissolved constituents (i.e., gelbstoff which is primarily CDOM). The difference between the unfiltered (ac-s) and filtered (ac-9) measurements provides the IOPs associated with particles [Twardowski and Donaghay, 2001; Twardowski et al., 1999]. Post-processing of the ac-s and ac-9 data followed the "WET Labs, 2011" protocols [WETLabs, 2011]. The ac-9 data were processed using a scattering correction [Röttgers et al., 2013], adding back the pure water absorption (a_w) [Pope and Fry, 1997]. Additionally, corrections for temperature and salinity (using data from the CTD plumbed into the same flow-through system) were applied for ac-9 processing [Pegau et al., 1997; Sullivan et al., 2006]. This is required to account for the large changes between coastal and open ocean waters.

The standard order of post processing steps, all applied spectrally, include:

- Apply temperature and salinity corrections to in situ sample *a* and *c*.
- Apply temperature correction to pure water calibration *a* and *c*.
- Subtract the pure water calibration data from the in situ data.
- Omit the spikes in the data due to bubbles, etc., using a standard deviation filter and then interpolate.
- Apply the scatter correction [Zaneveld et al., 1994] to a_p.
- Add a_w [Pope and Fry, 1997] to $a_{(total\text{-}w)}$ to yield a_{total}.
- Compute scattering $b = c_{total} - a_{total}$.
- Compute omega = b/c.

These flow-through data will be used to assess the spatial coherence of the IOPs and to identify water mass changes while on stations and underway. For example, continuous monitoring of the IOPs from start to end while on stations can account for the changes in water masses during shipboard data collection due to ship drift. This can be significant, especially during stations at frontal boundaries with high variability. We will examine how the IOPs changed during the duration of the stations to help define how the IOP variability contributes to the uncertainty in the water-leaving radiance measurements from the HyperPro and the ASD, and also allow for better matchups between radiometric, IOPs and satellite measurements.

The flow-through system provided an extensive data set demonstrating the large variety of the water masses and ocean processes identified along the cruise track (Figure 12). The flow-through IOP products will be used to validate the VIIRS IOP products derived using the Quasi-Analytical Algorithm (QAA; [Lee et al., 2002]) (Figure 13) and provide an estimate of uncertainty due to different water masses including US coastal and shelf waters. Additionally, the high spatial resolution of the flow-through data can be used to characterize IOP spatial variability within a VIIRS 750 m pixel by defining the mean and variance of the in situ IOP measurements.

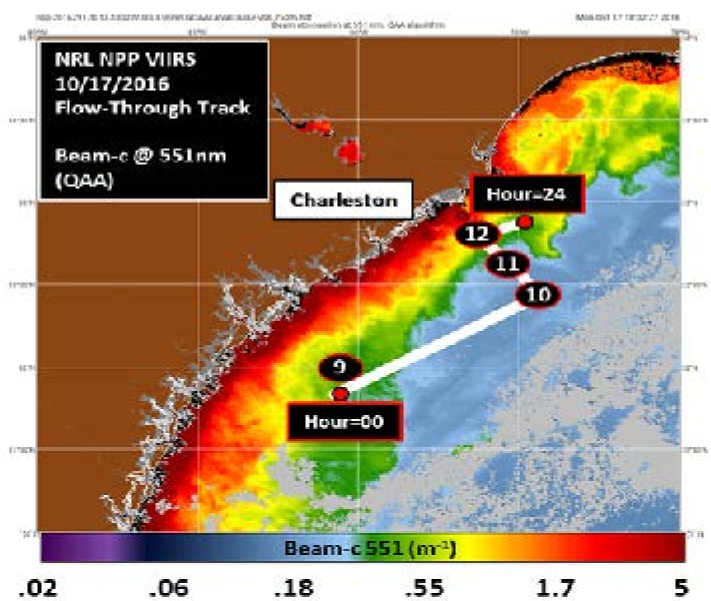

Figure 12. NPP VIIRS image for 17 October 2016 of beam-*c* showing the flow-through track for a 24 hour period along with the station locations and station numbers (black ovals) for that day.

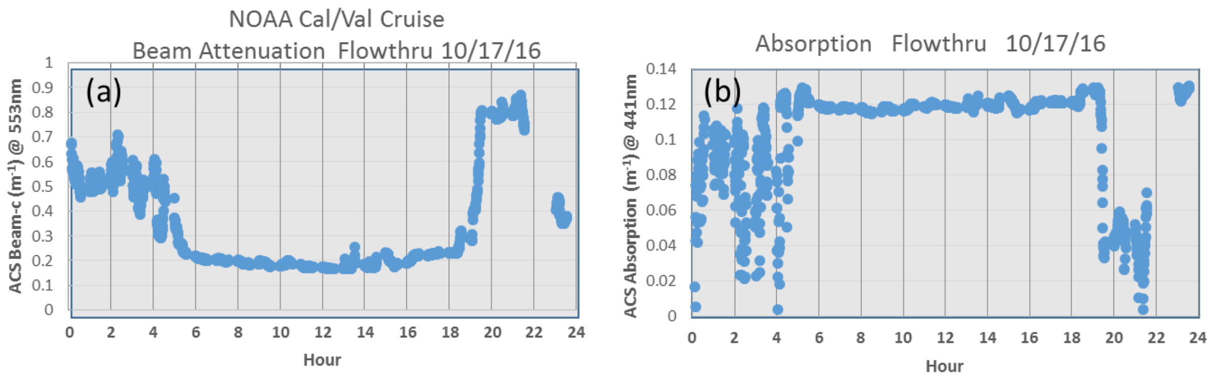

Figure 13. Flow-through post-processed ac-s data for 17 October 2016 (0-24 hours) for the track shown in Figure 12: a) beam-c(553); b) a_t(441). Hours 0-4 are in turbid coastal waters; hours 6-18 are in clearer shelf waters; hours 19-23 are back in turbid coastal waters. Note the daily/hourly variability.

Above water radiometry - ASD Measurements

The Stennis group deployed 2 ASDs with the AWG, measuring seawater and the NIST blue tile. Stennis/NRL processed data for all AWG measurements for consistency. See section 8.3 above for details on AWG activities and NRL processing. Figure 14 shows preliminary results for the Stennis/NRL ASD #2 which will be matched up with data from other above water, floating and profiling radiometers.

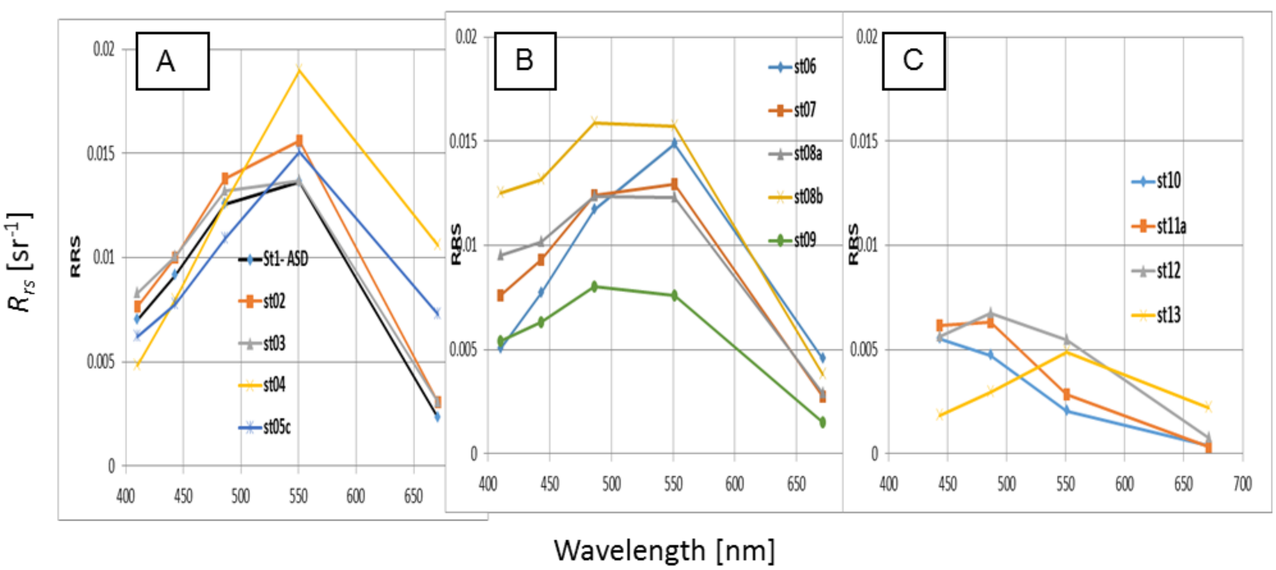

Figure 14. R_{rs} from Stennis/NRL ASD #1: A) Stations 1,2,3,4,5; B) Stations 6,7,8,9; C) Stations 10,11,12,13.

9.3 CCNY – Alex Gilerson, Sam Ahmed, Ahmed El-Habashi, Robert Foster and Matteo Ottaviani

Ahmed El-Habashi and Matteo Ottaviani sailed and Robert Foster participated in the installation of equipment. Alex Gilerson and Sam Ahmed are co-PIs for the CCNY VIIRS ocean color Cal/Val project. The CCNY group used two instruments for above water radiometric observations: GER, SpectraVista, NY and HyperSAS-POL, Satlantic, Canada, modified by CCNY.

GER 1500, Field Portable Spectroradiometer
CCNY deployed their GER 1500, Field Portable Spectroradiometer, a hand-held spectroradiometer designed to provide fast spectral measurements covering the UV, Visible and NIR wavelengths from 350 nm to 1050 nm at 3 nm FWHM resolution. The GER uses a diffraction grating with a silicon diode array that has 512 discrete detectors and provides the capacity of reading 512 spectral bands. A total of 482 spectral readings can be stored within its memory. Subsequent download and analysis is done using a personal computer with a standard RS232 serial port and the GER 1500 licensed operating software. The GER 1500 is equipped and operated with a standard lens with 4° nominal FOV for above water observations. The GER 1500 is used in the field to calculate R_{rs} by measuring the total radiance above the sea surface (L_t), the sky radiance (L_s) and downwelling radiance (L_d). The instrument has undergone radiometric and wavelength calibration in the optics mode (with the lens) at the manufacturer in 2013 but due to the nature of the measurement, calibration is not necessary.

In order to acquire L_t, the instrument was placed at the azimuth angle ≈90° from the sun and 40° viewing angle from the nadir and make 4 consecutive measurements. The L_s was measured by pointing the instrument at the sky at the same azimuth angle and 40° viewing angle from the zenith with 4 consecutive measurements. L_d was obtained by pointing the instrument at a Spectralon reference plaque at 40° viewing angle; also 4 consecutive measurements were made. Typically, a white reference plate was used with a known reflectance coefficient. In addition, at some stations the NRL gray plaque was used as well. All measurements were executed in target mode. $E_d = \pi * L_d/A$ where $A = 0.99$ is the reflectance factor of the white target according to the manufacturer calibration for the whole spectral range (Labsphere). Remote sensing reflectance is calculated by the following equation $R_{rs} = (L_t - r^* L_s)/ E_d$ where r is the sea surface reflectance factor. Typically, a value of $r = 0.028$ was used. For each station, the averages of all individual scans for L_t, L_s and L_d were used in R_{rs} calculations. Since most of the measurements were carried out in clear and light coastal waters R_{rs} (750) was subtracted for the entire R_{rs} spectrum to eliminate sunglint effects [Mobley, 1999]. Integration time is self-adjusted by the instrument and was typically 160 ms for water observations. CCNY participated in the AWG.

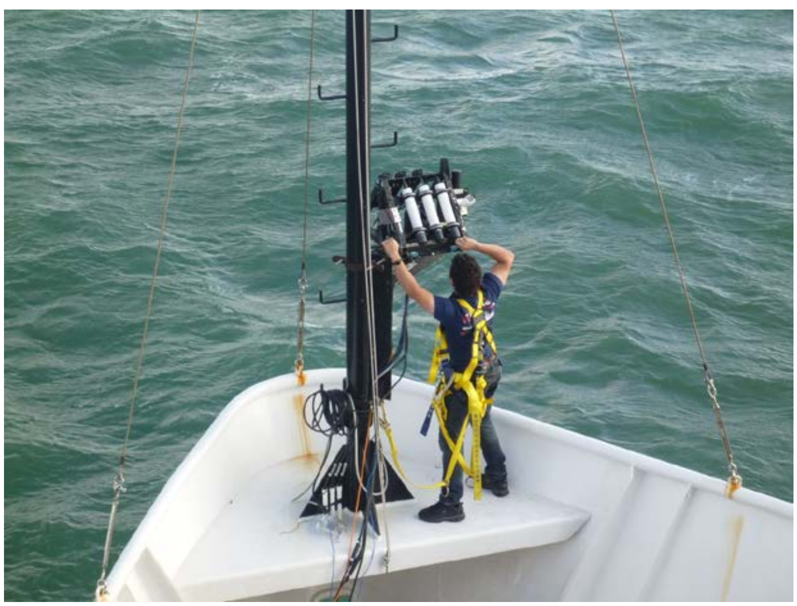

Figure 15. HyperSAS-POL on the mast at the bow of the ship.

HyperSAS-POL
The HyperSAS-POL instrument was operated from the bow of the ship. It has the software, electronics and communication systems for continuous (underway) positioning of the HyperSAS-POL at 90° or 135°

from the Sun (depending on ship orientation) in order to minimize sun glint. A tilt sensor was incorporated for exact knowledge of sensor geometry with respect to the ocean. The configuration and processing procedures were similar to those used on the 2015 cruise [Ondrusek et al., 2016]. The HyperSAS-POL mounted on the forward mast of the ship is shown in Figure 15. The instrument contains 3 Hyper OCR sensors (Satlantic, Canada) with 3° a FOV and looking at the water with a ≈40° viewing angle from nadir. One of the water-looking sensors is unpolarized, the second is horizontally polarized and the third has 45° polarization. Additionally, there are 3 sensors for the sky observations which are also unpolarized, horizontally polarized and 45° polarized as for the water looking sensors. One E_d irradiance sensor was positioned in the unobstructed area on the railing of the ship. The second E_d sensor was installed coincident to E_d sensors from other groups on top of a telescoping pole which was mounted to the deck of the ship (Figure 7). In the unpolarized mode the $R_{rs}(\lambda)$ were determined in a manner similar to the one described above for GER instrument with E_d irradiance used instead of $\pi * L_d / A$ from the plaque. Also, the r coefficient was not constant but was determined based on data from our recent simulations [Foster and Gilerson, 2016]. For the polarized mode, processing is very complex and currently under study. Integration time is self-adjusted by the instrument and was typically 2000 ms for water observations. Data were collected every 2 s during daytime. Multiple R_{rs} spectra collected for each station were averaged.

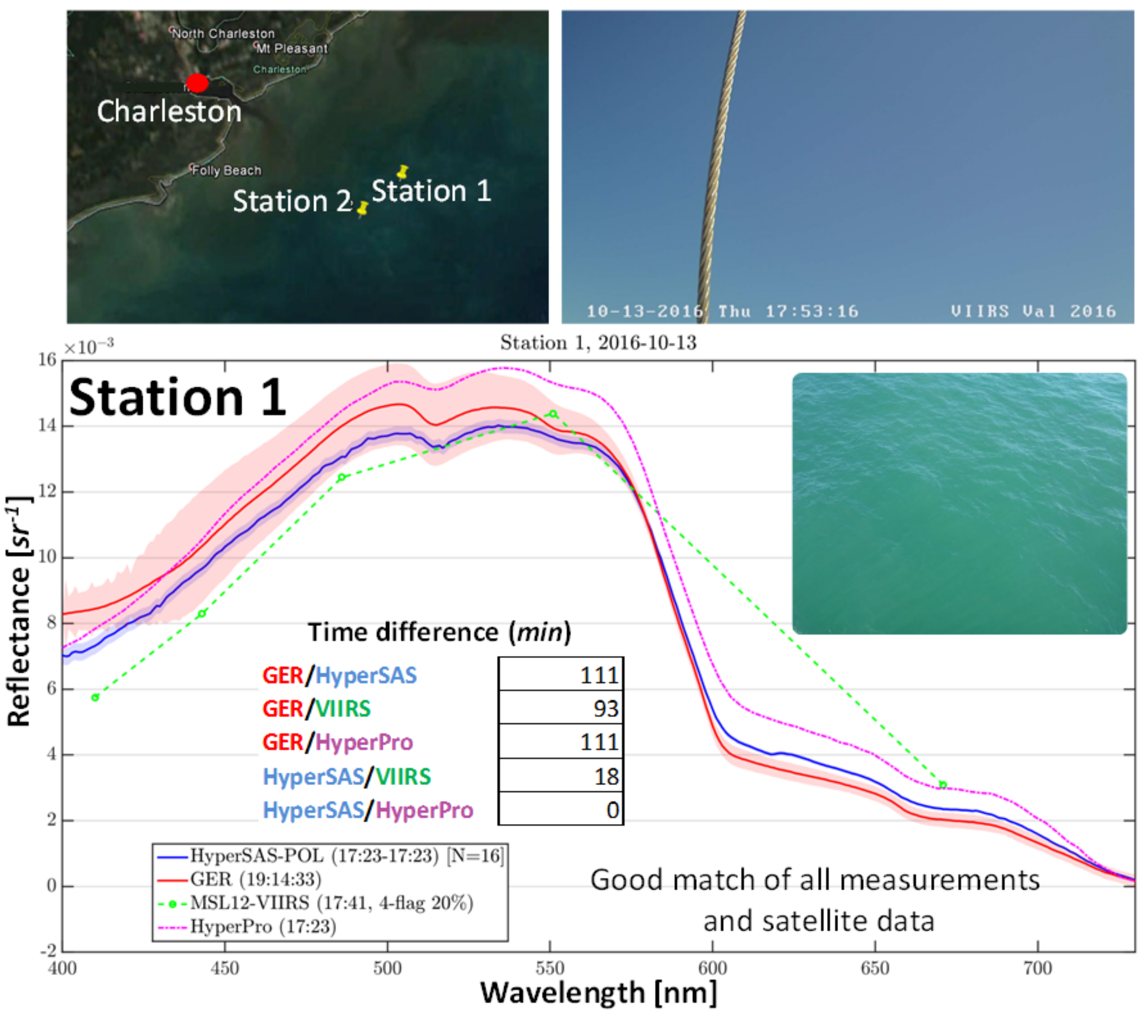

Figure 16. Station 1, coastal waters comparisons. Measured spectra by GER, HyperSAS-POL and HyperPro instruments are shown in comparison with VIIRS data. The top panel contains (top left): True

color satellite image with Station locations shown with yellow "pins"; (top right) photograph of sky; (inset photograph) photograph of water; and (main plot) R_{rs} versus wavelength for HyperSAS-POL (blue line), GER (red line); MSL12-VIIRS satellite data (green circles with dashed line) and HyperPro (purple dashed line). Also (inset table) time differences (in minutes) between various sets of measurements is included.

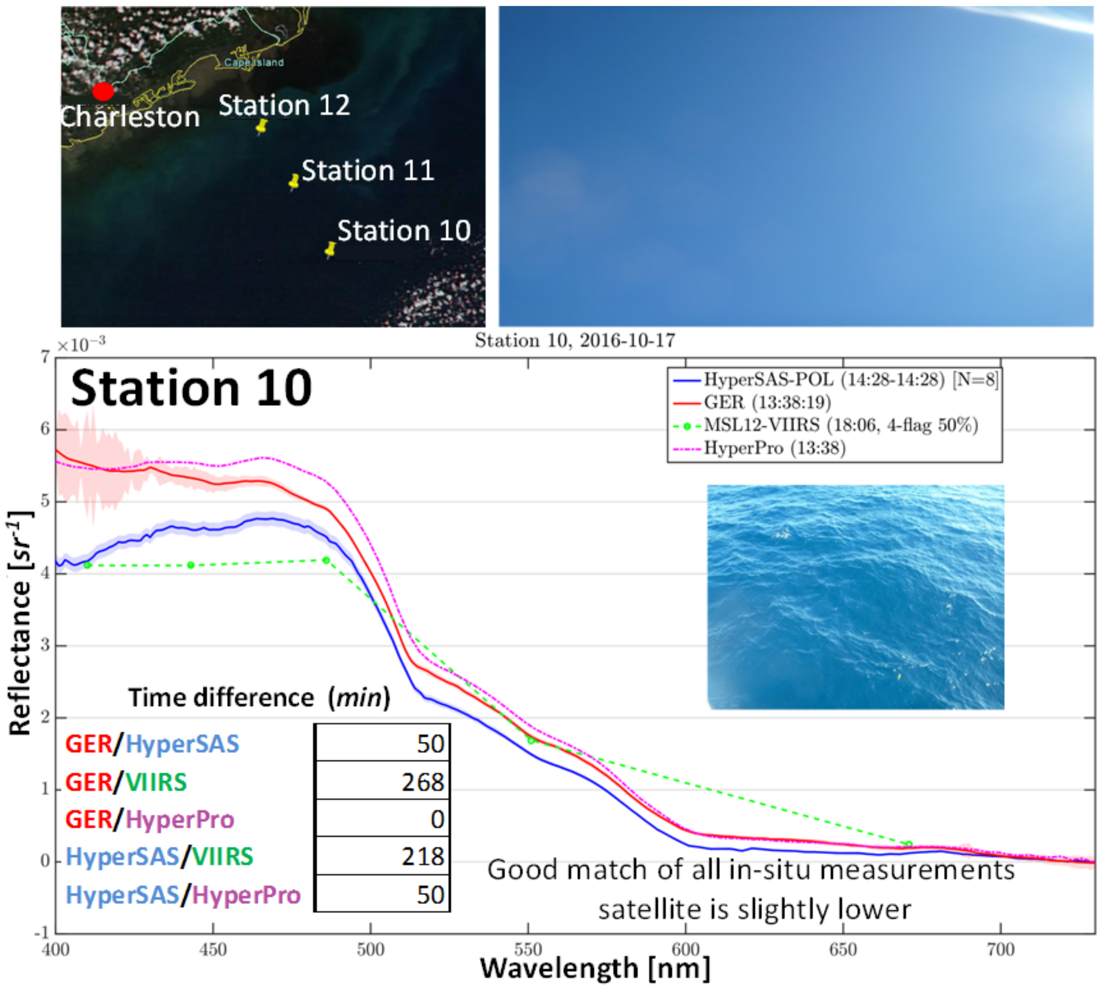

Figure 17. As for Figure 16 but for Station 10, open ocean comparisons.

Comparison of spectra measured by HyperSAS and GER with VIIRS satellite data for Station 1 (coastal water) and Station 10 (ocean water) are shown in Figure 16 and Figure 17, respectively, demonstrating the high potential of the HyperSAS instrument for accurate above water observations. Satellite data are from MSL12 VIIRS science quality as processed by Dr. M. Wang's group. True color images are at the top right corner of the figures. Sky images are from the camera installed on the HyperSAS.

A unique property of the HyperSAS is its capability of making measurements underway, thus substantially increasing the number of in-situ-satellite matchups. Example of such matchups are shown in Figure 18.

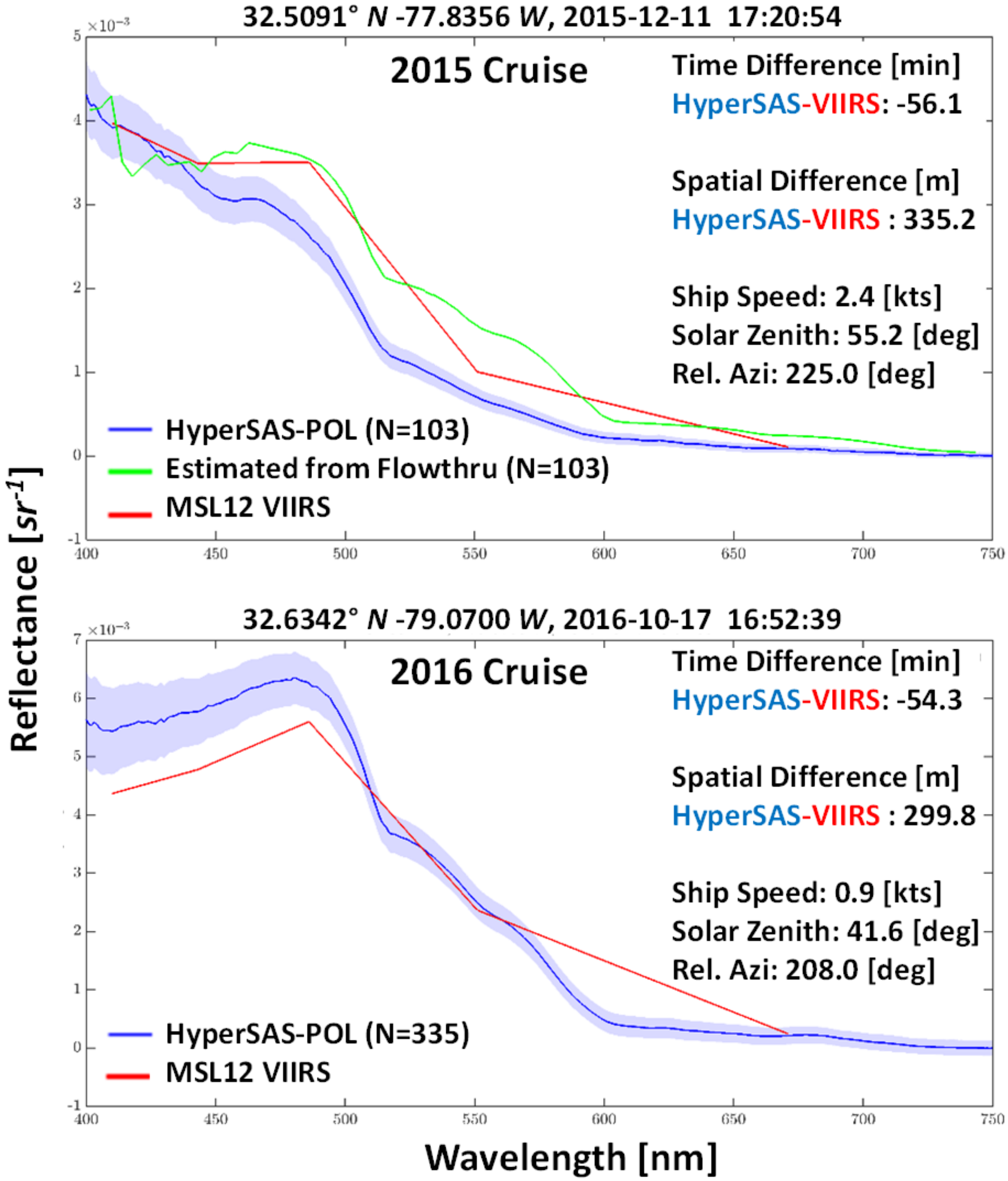

Figure 18. Example of VIIRS – HyperSAS matchup from underway measurements: (Top) 2015 cruise with additional flow-through data, near end of Station 20; (Bottom) 2016 cruise, near end of Station 11.

Microtops AOT

AOT was measured by Microtops sunphotometer (Solar Light, PA) at 5 wavelengths: 380 nm, 500 nm, 675 nm, 870 nm and 1020 nm.

9.4 LDEO - Joaquim I. Goes, Helga do Rosario Gomes, Kali McKee and Joo Won Kang

The LDEO group made high-resolution along track shipboard measurements of phytoplankton functional types, size classes and photosynthetic efficiency in support of VIIRS ocean color observations. Phytoplankton measurements and water samples collected for nutrient analyses were also made from discrete water samples at stations from the CTD rosette casts, providing additional information about the biogeochemical conditions in the water column.

Discrete Samples

Water samples were collected at a total of 13 stations along the cruise track. At each station aliquots of seawater samples from usually two, but sometimes three, depths (coincident with sampling for HPLC pigments, CDOM and absorption of phytoplankton normalized to chlorophyll (a^*_{ph} derived from a_p measured by the FPT method by the USF group) were collected for the following work:

i. Microscopic analysis of phytoplankton community composition and sizes.
ii. Counting, imaging and size estimations of phytoplankton and other detrital particles using a Fluid Imaging Technologies, Inc., FlowCAM.
iii. Estimates of phycobilipigments using a newly developed fluorescence technique developed at LDEO [in prep].
iv. Fluorescence based estimates of Chl-*a*, CDOM, phycobilipigments and variable fluorescence (F_v/F_m), a measure of phytoplankton photosynthetic efficiency, using a WET Labs Advanced Laser Fluorometer (ALF) [Chekalyuk et al., 2012; Chekalyuk and Hafez, 2008; Goes et al., 2014].
v. Measurements of F_v/F_m and the functional absorption cross-section of Photosystem II (σ_{PSII}) and Electron Transport Rates (*ETR*) in a mini-Fluorescence Induction and Relaxation (FIRe) Fast Repetition Rate Fluorometer (FRRF) [Gorbunov and Falkowski, 2004].

i. Microscopy based phytoplankton identification and cell counts

For microscopic identification and enumeration of phytoplankton, samples were collected in 100 mL screw top hard plastic bottles usually from 2 depths at each of the 13 stations (coincident with HPLC pigment analysis). Samples were fixed with 1% alkaline Lugol's iodine, preserved in 1.5% buffered formaldehyde solution and were stored in dark and cool conditions. Microscopic analysis is currently underway and includes overnight settling of 10 mL samples in an Ultermohl counting chamber and then counting the samples using a Nikon® inverted microscope at 200X and 400X magnifications. The smallest cells that can be enumerated by this method are ≈5 μm in diameter. Phytoplankton identifications are based on standard taxonomic keys [Tomas, 1997]. Cryptophytes are identified by epifluorescence microscopy using their yellow-orange fluorescence signatures [Booth, 1993; Goes et al., 2014; MacIssac and Stockner, 1993].

ii. FlowCAM based phytoplankton identification, cell counts and cell sizes

In addition to the microscopic analysis of phytoplankton, 2 x 25 mL aliquots of the preserved samples are being analyzed for phytoplankton community composition and size structure analysis using a FlowCAM particle imaging system equipped with a 4x objective (UPlan FLN, Olympus) and a 300 µm FOV flow cell. FOV flow cells ensure that the liquid passing through the flow cell is entirely encompassed within the camera's field of view. Phytoplankton cells within the preserved samples will be counted and imaged in auto-image mode with a peristaltic pump rate of approximately 0.32 mL min^{-1} to 0.44 mL min^{-1} as specified by the manufacturer. Cells will be classified to the genus level using the Visual Spreadsheet program (v. 2.2.2, Fluid Imaging). The instrument provides the total number of particles imaged, together with the dimensions of each particle allowing estimations of phytoplankton community structure, particle size distribution of both phytoplankton and of detrital particles.

iii. Phycobilipigment collection and analysis

Approximately 1 L to 2 L of seawater samples from 2 depths (coincident with the depths sampled for HPLC pigment analysis) were carefully filtered on to 4 x 25 mm Whatman GF/F filters for analysis of estimating phycoerythrin and phycourobilin pigments. Samples were immediately stored in liquid nitrogen for later analysis at LDEO using methods developed by us which rely on freezing, sonication and extraction of the phycobilipigments in phosphate buffer and analysis in a spectrofluorometer [Gomes et al., in prep].

iv. Automated Laser Fluorescence (ALF) measurements of phytoplankton groups

The ALF combines high-resolution spectral measurements of blue (405 nm) and green (532 nm) laser-stimulated fluorescence with spectral deconvolution techniques to quantify the following:

- fluorescence of Chl-*a* (peak at 679 nm),
- three phycobilipigment types: Phycoerythrin-1 (PE-1; peak at 565 nm), Phycoerythrin-2 (PE-2; peak 578 nm) and Phycoerythrin-3 (PE-3; peak at 590 nm),
- CDOM (peak at 508 nm)
- F_v/F_m

All fluorescence values obtained are normalized to the Raman spectra of seawater and generally expressed as relative fluorescence units (RFU), whereas F_v/F_m is unitless. PE-1 type pigments are associated with blue water or oligotrophic cyanobacteria with high phycourobilin/phycoerythrobilin (PUB/PEB) ratios, PE-2 type phytoplankton with low PUB/PEB ratios are generally associated with green water cyanobacteria that usually thrive in coastal mesohaline waters, and PE-3 attributable to eukaryotic photoautotrophic cryptophytes [Chekalyuk et al., 2012; Chekalyuk and Hafez, 2008; Goes et al., 2014]. RFU values for Chl-*a* can be converted into mg m^{-3} Chl-*a* values using least square regressions of acetone or HPLC measured Chl-*a* with RFU values for Chl-*a* measured in an ALF.

All samples for the ALF were collected directly from the Niskin samplers into 500 mL acid-washed amber glass bottles and stored for about 30 min in the dark at temperatures close to the average surface seawater temperature at each station. Dark adaptation allows all of the Photosystem II (PSII) reaction centers and electron acceptor molecules of phytoplankton to become fully oxidized and hence available for photochemistry thus minimizing the impacts of non-photochemical quenching before analysis.

v. Fluorescence Induction and Relaxation (FIRe) measurements of photosynthetic competency

The FIRe technique was developed to measure a comprehensive suite of photosynthetic and physiological characteristics of photosynthetic organisms [Bibby et al., 2008; Gorbunov and Falkowski, 2004]. This technique provides a set of parameters that characterize photosynthetic light-harvesting processes, photochemistry in PSII, and the photosynthetic electron transport down to carbon fixation. Because these processes are particularly sensitive to environmental factors, the FIRe technique can be utilized to provide a measure of natural (nutrient limitation, photoacclimation and photoinhibition, thermal and light stress, etc.) and anthropogenic stressors (such as pollution). One property that is unique and the most sensitive to environmental stressors is F_v/F_m. All optical measurements by the FIRe are sensitive, fast, non-destructive, and can be done in real time and in situ and can provide an instant measure of the photosynthetic efficiency of the cells.

vi. Nutrient analysis

At each of the stations, samples from discrete depths were collected directly from Niskin bottles attached to a Sea-Bird Electronics CTD rosette. The samples were pre-filtered using a syringe filter and then transferred into acid-washed 50 mL Falcon tubes, which were immediately frozen on board. Samples will be analyzed for inorganic nutrients (SiO_3, NO_3+NO_2 and PO_4) with a SEAL AA3 nutrient auto analyzer using the methods proposed by Knap et al. [1994].

Underway Flow-Through Measurements

Between stations, the ALF, the FlowCAM, the FIRe and a bbe Moldeanke AlgaeOnlineAnalyser [Richardson et al., 2010] were connected in parallel to the ship's seawater flow-through system, allowing for continuous in-water measurements of phytoplankton community composition, phytoplankton size, phycobilipigment types and photosynthetic efficiency. With the exception of a few breaks during stations and for reconditioning, all four instruments were operated over the entire cruise track, providing several thousand fluorescence based measurements of Chl-*a*, CDOM, PE-1, PE-2, PE-3, F_v/F_m and σ_{PSII} as well as continuous FlowCAM images that will allow high resolution measurements of phytoplankton composition and cell size distribution necessary for interpreting the optical measurements over the study area. The AlgaeOnlineAnalyser allows for continuous measurements of Chl-*a*, plus determination of cyanobacteria, green algae, brown algae (diatoms and dinoflagellates) and cryptophytes fluorescence using colored light emitting diodes. Preliminary data from the underway instruments is presented below in Figure 19 and Figure 20.

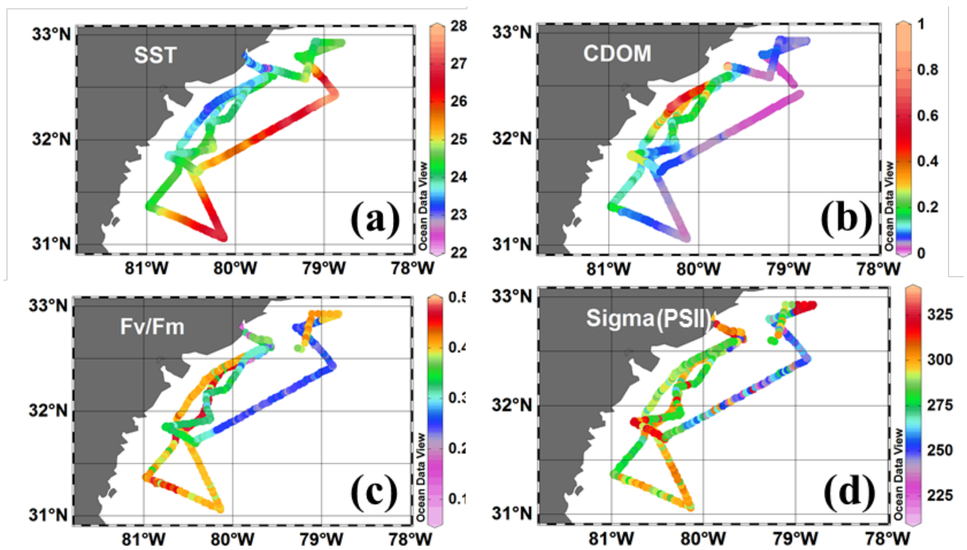

Figure 19. Distribution along cruise track of parameters: (a) SST in units of °C; (b) CDOM in relative fluorescence units; and photo-physiological properties of phytoplankton (c) F_v/F_m, a dimensionless ratio, the colorbar range is 0 to 0.5; and (d) σ_{PSII} in units of 0.1 nm^2 quanta^{-1}.

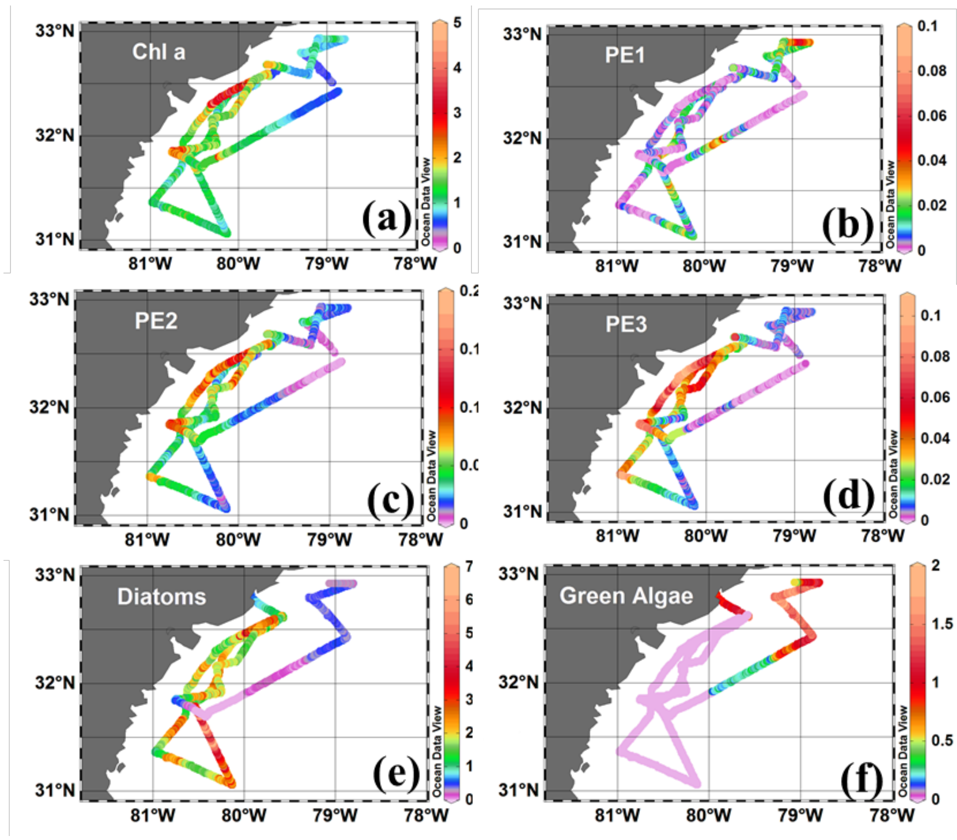

Figure 20. Distribution along the cruise track of parameters all in relative fluorescence units: (a) Chl-*a*; (b) PE1, open ocean cyanobacteria; (c) PE2, coastal water cyanobacteria; (d) PE3, cryptophytes; (e) diatoms and (f) green algae.

9.5 USF Optical Oceanography Laboratory – Chuanmin Hu, Jennifer Cannizzaro, Shaojie Sun and David English

Spectral absorption and pigment determinations

Understanding the variability in $a^*_{ph}(\lambda)$ is essential for primary production modeling, calculation of underwater light field characteristics, and development of remote sensing algorithms for estimating Chl-*a*. The spectral absorption of particles suspended in the water was assessed by filtering a water sample through a glass fiber filter and quantifying the spectral transmission of the filter relative to a wetted blank. The subsequent hot methanol extraction of the pigments from the particles captured by the filter, followed by re-measurement of both filters, allows for the $a_p(\lambda)$ to be separated into living (or pigmented, i.e., $a_p(\lambda)$) and non-living (or detrital, i.e., $a_d(\lambda)$) components [Kishino et al., 1985]. A custom-built 512-channel spectroradiometer ("Spectrix") is used for measuring spectral transmission of the filters. The extraction of pigments from the particles also enables Chl-*a* to be determined fluorometrically [Holm-Hansen and Riemann, 1978; Welschmeyer, 1994] from the same water sample that was used for $a_p(\lambda)$. The filtrate from particulate filtration undergoes additional filtration using a Nucleopore 0.2 µm membrane filter. A spectrophotometer subsequently measures the absorption spectra of this filtrate to determine $a_{CDOM}(\lambda)$, for the water sample.

During this cruise Chl-*a* and absorption data were computed from water samples collected from a bucket, the Niskin bottles of the CTD rosette, or from the flow-through seawater system (Table 4). At each station, water samples were collected from just below the water's surface and from a second and sometimes a third depth lower in the photic zone. The samples were used for assessment of the Chl-*a*, as well as the $a_p(\lambda)$ and $a_d(\lambda)$. Duplicate samples were collected at selected stations. Aliquots were filtered using low vacuum pressure (<100 mm Hg) to concentrate the particles for pigment and absorption determination onto a GF/F (Whatman) filter. These filters were placed into containers and quickly frozen using liquid nitrogen. Samples were kept frozen, stored at -80˚C until analysis with the filter pad technique described earlier. The filtrate from particulate filtration undergoes additional filtration using a 0.2 µm filter, and a portion of the subsequent filtrate is placed in 125 mL glass bottles and kept refrigerated (≈4°C) until analysis.

Table 4. Water samples collected during NF-16-08 (*n*=34). D: Duplicate filter pad samples collected.

Date (UTC)	10/13/16	10/13/16	10/14/16	10/14/16	10/15/16	10/16/16	10/16/16	10/16/16	10/16/16	10/17/16	10/17/16	10/17/16	10/18/16
Time (UTC)	19:00	21:38	12:40	22:17		12:17	16:14	19:02	21:56	0:12	17:18	20:58	12:05
Station ID	1	*2*	*3*	*4*	*5*	*6*	*7*	*8*	*9*	*10*	*11*	*12*	*13*
CTD Cast ID	1	*2*	*3*	*4*	-	*6*	*7*	*8*	*9*	*10*	*11*	*12*	*13*
Bucket (~0.5m)											X		
Flow-through (~3m)				20:19 UTC	17:48 UTC, 18:40 UTC							23:59 UTC	13:00 UTC
Niskin - Surface	X	X_D	X	X		X_D	X	X	X	X	X_D	X	X
Niskin - Chl_max	X	X	X	X		X	X	X	X	X	X	X	X
Niskin - Bottom										X			

Preliminary results show that the water sample from 70 m of Station 10 had the least Chl-*a* (0.12 mg m^{-3}) and a flow-through sample from Station 5 contained the greatest Chl-*a* (5.86 mg m^{-3}). Example a_p, a_d, a_{CDOM}, and a^*_{ph} spectra are shown in Figure 21.

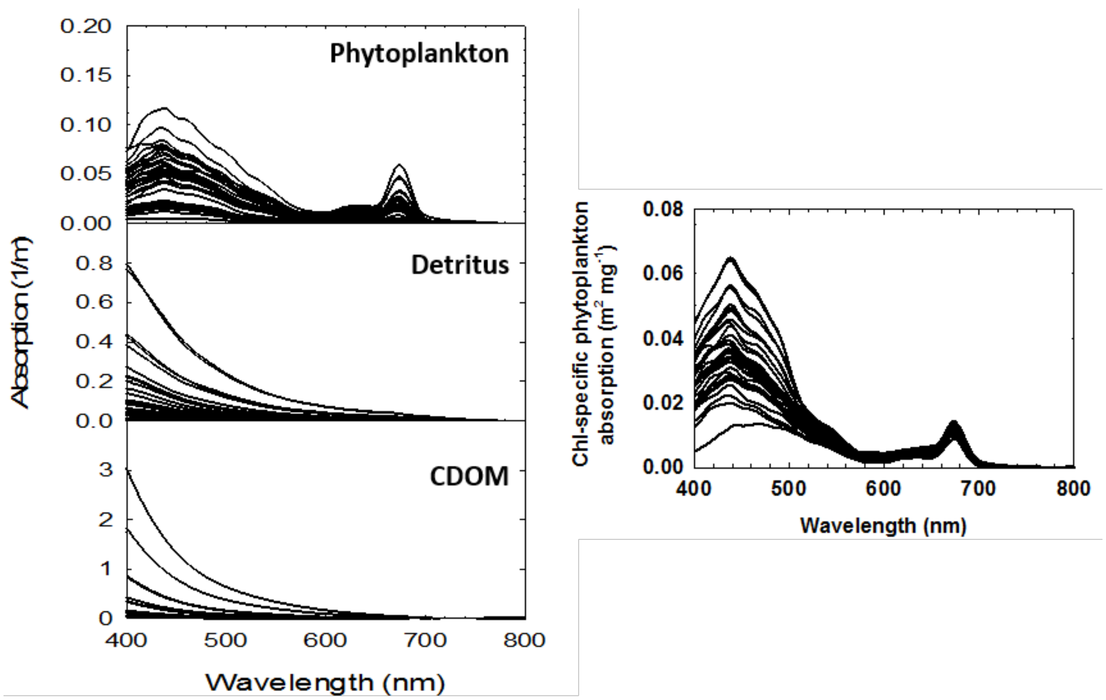

Figure 21. The measured a_p, a_d and a_{CDOM} spectra of water samples collected on this cruise. The figure to the right is the a^*_{ph} spectra derived from the water sample measurements.

In summary, the following parameters were determined from the water samples:

- $a_p(\lambda)$, $a_d(\lambda)$, $a_{ph}(\lambda)$
- $a_{CDOM}(\lambda)$
- Chl-*a*

Of these, Chl-*a* was determined by both acidification technique and non-acidification technique, with the following results:

- Range: 0.12 mg m^{-3} to 5.86 mg m^{-3} (Station 10, CTD cast 10, 70 m, and Station 5, flow-through ≈3 m, respectively)
- Mean: 1.74 ± 1.23 mg m^{-3}
- Median: 1.62 mg m^{-3}

The following provides a summary of the CDOM absorption measurements:

- Range: 0.036 m^{-1} to 3.05 m^{-1} (Station 10, CTD cast 10, 42 m, and Station 13, CTD cast 13, 2 m, respectively)
- Mean: 0.323 ± 0.592 m^{-1}
- Median: 0.142 m^{-1}

Above water remote sensing reflectance

Above water $R_{rs}(\lambda)$ estimates were made using USF's ASD Inc. HandHeld2-Pro spectroradiometer at 12 stations. The measurement protocol differed slightly from that described in Section 8.3. This instrument measures radiance at <3 nm spectral resolution for wavelengths from ≈350 nm to >1000 nm. For each $R_{rs}(\lambda)$ measurement, multiple spectra were collected of the radiance reflected from the sky, water surface, and a gray Spectralon reflectance target ("gray card") [Carder and Steward, 1985; Mueller et al., 2003]. Sea surface measurements were made while viewing the water with a ≈30° zenith angle and at an azimuth angle between 90-135° relative to the sun. Sky measurements were made at a complimentary zenith angle for the sea surface measurement, at the same azimuth orientation. The HandHeld2-Pro was held level at >30 cm above either the USF or the NRL gray plaque during the reference measurement. The instrument's FOV was constrained to ≈7.5°, and its integration time was kept constant throughout the series of gray, water, and sky measurements. $R_{rs}(\lambda)$ estimates for the waters sampled during this cruise are shown in Figure 22. Additional measurements of the NIST blue reference plaque were made at Station 5 and Station 11.

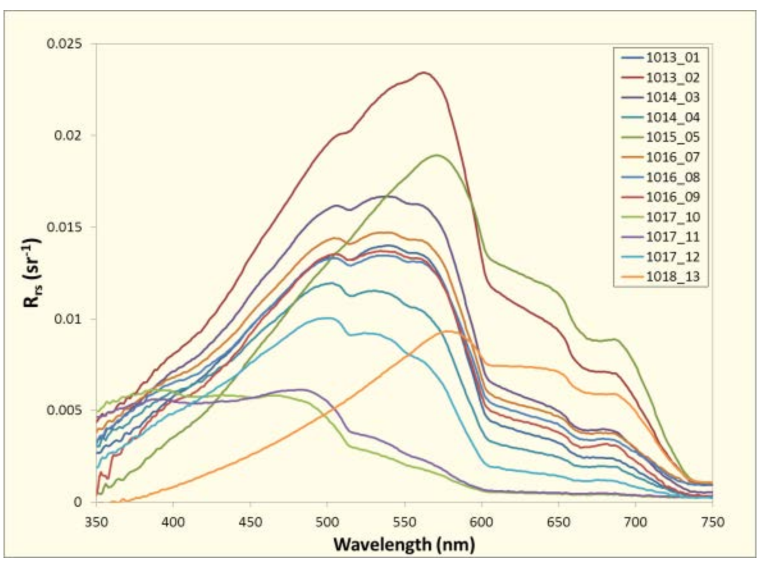

Figure 22. Preliminary *$R_{rs}(\lambda)$* estimates from shipboard (above-water) remote sensing reflectance measurements made at 12 stations on NF-16-08.

The USF group made handheld observations at a slightly different time from the observations made by the AWG due to participation in the profiling radiometer activities which were often conducted at the same time as the AWG handheld activities. The data were processed at USF (due to use of a slightly different measurement protocol than described in Section 7.3) consistent with accepted remote sensing practices [Carder and Steward, 1985; Mueller et al., 2003].

Near-surface light field profiling

Vertical profiles of the light available in the near-surface waters were collected using a Satlantic HyperPro-II, as described in Section 8.2. The USF hyperPro-II is equipped with two hyperspectral radiometers, one facing upward and the other downward. The sensors incorporated into this instrument system include pressure, temperature, conductivity, and tilt sensors, in addition to a WETLabs ECO-Puck Triplet (chl-*a* & CDOM fluorescence and $b_b(660)$) and an above-water hyperspectral radiometer.

USF's HyperPro system was deployed with the profiling HyperPro group (see Section 8.2) at most of the sampling stations using the manufacturer's multi-cast protocol [Satlantic, 2012, 2004]. The data from this instrument and the other HyperPro systems were processed by Michael Ondrusek of NOAA/STAR for consistency.

Evaluation of VIIRS performance using field data

Preliminary results were obtained by comparing $R_{rs}(\lambda)$ from shipboard above-water measurements and VIIRS-derived $R_{rs}(\lambda)$. Figure 23 shows the $R_{rs}(\lambda)$ comparisons for 4 of the NF-16-08 stations.

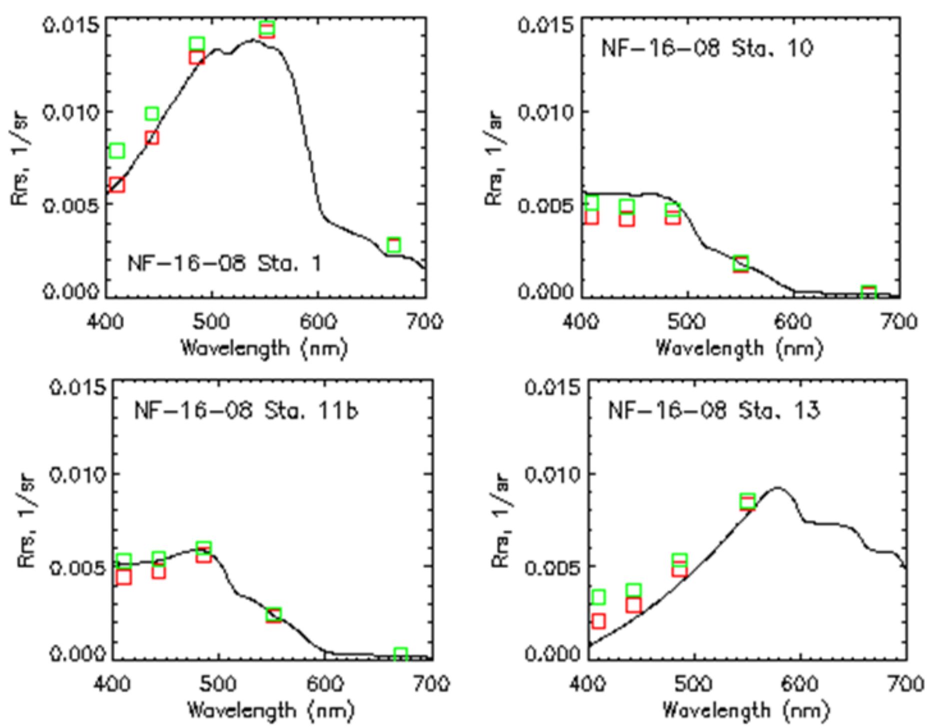

Figure 23. Comparisons between field $R_{rs}(\lambda)$ (solid line) and VIIRS $R_{rs}(\lambda)$ processed before (red squares) and after (green squares) the MSL12 routine was updated and the VIIRS SDR was improved in early 2017. These improvements included correction of the blue-band polarization effects.

9.6 NIST—B. Carol Johnson

NIST Blue Tile

The NIST blue tile is a reflectance target made from two pieces of 3.8 mm-thick, 16.51 cm square, F65 plate glass. The configuration of the blue tile target was identical to the 2015 cruise [Ondrusek et al., 2016]. Briefly, the surfaces of one of the glass plates was roughened by sandblasting to create a diffuse surface. Then the two plates were stacked together, with the diffuse glass on the top, and held in a 30.48 cm-square by 2 cm thick-black plastic mounting cell. The glass plates are mounted in a 7.6 cm-deep square area centered in the black plastic cell. This results in the ground optical surface of the blue tile flush with the top of the black plate, see Figure 24. A wooden storage container with a cutout on the inside of the top lid holds the blue tile and prevents anything touching the optical surface during storage or shipment. The bottom half of the storage container has two cutouts for ease of removal of the blue tile assembly from the storage container. Alignment indicators, labeled "point to Sun" and "90° azimuth" were placed on the surface of the mounting cell prior to the 2015 VIIRS Cal/Val cruise (blue tape in Figure 24).

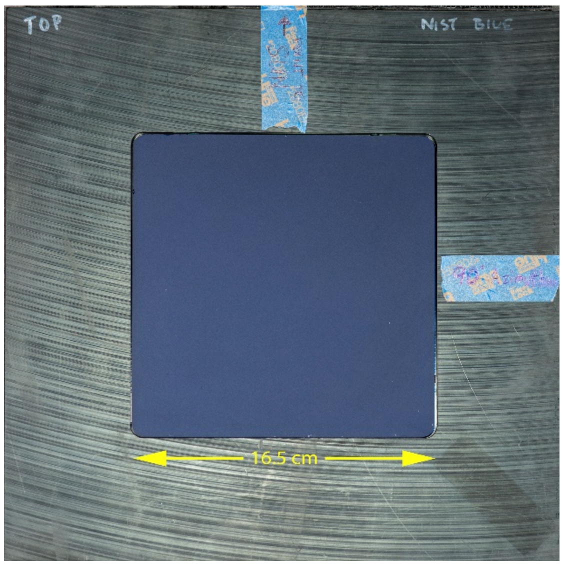

Figure 24. Photograph of the NIST blue tile in its black plastic mounting cell.

As described earlier, a portion of the activities during the October 2016 cruise involved derivation of R_{rs} using in-air, hand-held, radiometers and a white or gray diffuse reflectance standard to establish traceability to the SI. This protocol is described in [Mobley, 2015, 1999; Mueller et al., 2003]. NIST first developed the blue tile in support of the Long Island Workshop that took place in August 2010 [Johnson et al., 2012]. It has been deployed as an experimental validation standard in November 2014 [Ondrusek et al., 2015] and December 2015 [Ondrusek et al., 2016], aboard the NOAA ship *Nancy Foster*.

The concept is simple: if the reflectance of the blue target is stable in time, all researchers should derive the same reflectance values for this faux water target when using their white or gray reflectance standard as the reference. With the reflectance scales of the various instruments thus compared to a common reference, the blue tile measurements could then be used to determine the sensitivity to other measurement conditions. Of course, an independent white or gray reflectance target could also be used for this purpose, but having a blue reflectance target for testing increases the parameter space to include the instrument sensitivity to stray light, which is exacerbated by differences between the spectral distribution of the calibration source (sunlight) and the unknown source (sky and water). More details are given in previous VIIRS Cal/Val cruise reports [Ondrusek et al., 2016; Ondrusek et al., 2015].

The white or gray reflectance standards can be procured from companies such as Labsphere, Inc. (North Sutton, NH) or Avian Technologies LLC (New London, NH), who provide reflectance values, typically directional-hemispherical reflectance factors $R(8; h; \lambda)$ (e.g. 8° incident angle, collection over the entire hemisphere above the sample) to customers for these standards. For the blue tile, preliminary measurements of $R(0; 45; \lambda)$ (e.g. 0° incident angle, 45° reflected angle) by comparison to a NIST Spectralon standard were done prior to the 2010 Long Island Workshop. The NIST blue tile was measured for $R(0; 45; \lambda)$ by the NIST Spectral tri-function automated reference reflectometer (STARR) [Proctor and Barnes, 1996] in October 2014 and February 2015; these measurements showed the reflectance of the blue tile was stable in time. The uncertainties in these bi-directional reflectance factors were between 5% and 8.6% ($k = 2$) between 280 nm to 440 nm. The peak reflectance was observed at about 415 nm, see Figure 25. The STARR measurements are in-plane. Because the plastic mounting cell was too large to be mounted in the STARR facility, the two glass pieces were removed and measured for $R(0; 45; \lambda)$ with nothing behind the back surface.

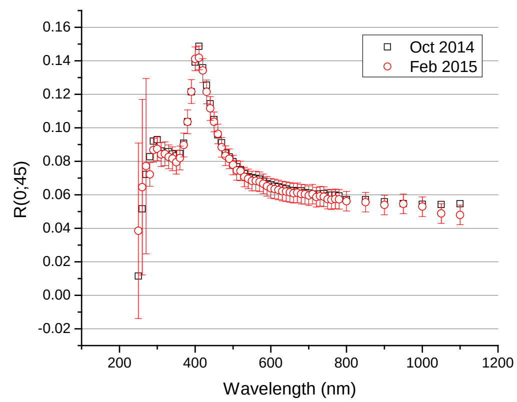

Figure 25. NIST STARR bi-directional reflectance values for the blue glass assembly.

Because the blue tile is used outdoors under conditions of hemispherical illumination, it is important to quantify the BRDF for out-of-plane angles. Georgi Georgiev of NASA/GSFC performed a series of measurements of the blue tile mounted in the black plastic cell in November 2015 using the Diffuser Calibration Laboratory described in Schiff et al. [1993] and Georgiev and Butler [2008]. The BRDF was measured at 350 nm, 410 nm, and 900 nm at 0° angle of incidence with θ_r = 15°, 30°, 45°, and 60° and ϕ_r = 0° to 315° in 45° steps, (where θ is the polar angle, ϕ is the azimuth angle and subscript "r" indicates "reflected"). The BRDF was also measured at 410 nm for θ_i = 30°, 45°, and 60°, ϕ_i = 0° for θ_r = 15°, 30°, 45°, and 60°, ϕ_r = 0° to 180° in 90° steps, where θ and ϕ are as above and subscript "i' indicates "incident"). Figure 26 illustrates variation in bi-directional reflectance factor for a scatter azimuth of 90° (ϕ_r = 90°) from the plane of incidence as a function of incident and reflected (view) zenith angles.

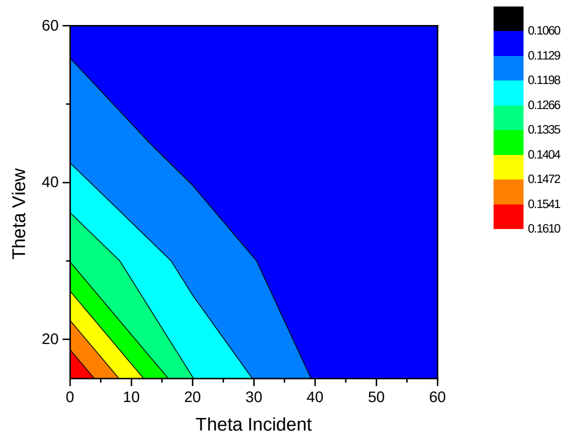

Figure 26. Blue tile bi-directional reflectance factor dependence on incident and reflected zenith angles at 90° to the plane of incidence and at 410 nm.

From Figure 26, we see the blue tile is not Lambertian – the maximum variation is 50% for this subset of the data. However, for the solar zenith angles during the cruise in October 2016, and a view angle of 40° to 60°, the variation in bi-directional reflectance is reduced. Spectralon is also not Lambertian; in-plane measurements of the BRDF for four incident angles (0° to 60°) and a range of view angles (0° to ±60°) of a 99% sample showed variations of up to 25% at large angles of incidence [Early et al., 2000]. It has also been established for Spectralon that $R(0; 45; \lambda) \approx 1.028R(8; h; \lambda)$ (see Appendix B in Johnson et al. [1996]); not equal as would be the case if Spectralon were an ideal Lambertian diffuser. The non-Lambertian behavior of the blue tile reduces its effectiveness as a test standard because of the sky contribution, and we expect to see the least variability in its derived reflectance for the cloud free stations, stable atmospheres, short time durations, and no interference in the light field from adjacent objects such as the ship's structure.

Measurements of the blue tile and Spectralon targets not used for the reflectance calibration will be analyzed as described in the 2014 cruise report [Ondrusek et al., 2015]. Comparisons will be made among the different instruments and stations as well as to the laboratory measurements. The NIST BRDF measurements will be repeated with the blue glass mounted in a smaller black plastic cell, in order to compare more accurately with the NASA/GSFC results.

9.7 UMB - Zhongping Lee, Laura Zoffoli and Junfang Lin

Our objectives for this cruise included: 1) to obtain R_{rs} with a Radiometer Incorporated Skylight Blocked Apparatus (RISBA) for instrumental inter-comparison and validation of the NOAA VIIRS ocean color data; 2) to measure IOPs including the non-water absorption coefficient (a_{pg}) and particle backscattering coefficient (bb_p) to evaluate VIIRS ocean color products; and 3) to measure phytoplankton assemblage using an Imaging Flow Cytometry system in order to understand the primary contributors to photosynthesis.

Instruments and Deployments

Figure 27. Instruments used on the 2016 VIIRS cruise: (a) Radiometer incorporating the Skylight-Blocked Apparatus (RISBA), (b) Spectral Evolution SR-1901, (c) IOP package including ac-s and BB9, and (d) Imaging Flow Cytobot.

Radiometer Incorporating the Skylight-Blocked Apparatus (RISBA)

To characterize the water optical properties, we measured L_w with a hyperspectral radiometer incorporating the skylight-blocked apparatus [Lee et al., 2013]. The RISBA system is equipped with one hyperspectral irradiance sensor (HyperOCI, Satlantic Inc.) measuring E_s and one hyperspectral radiance sensor (HyperOCR, Satlantic Inc) which simultaneously records the L_{w0+} by blocking off the surface-reflected skylight (Figure 27a).

The Satlantic's hyperspectral radiometers are fully digital optical packages. HyperOCR has a half angle FOV of 11.5° in air (8.5° in water). The radiance can be measured at about 3 nm increments from ultraviolet (≈350 nm) to near-infrared (≈800 nm) wavelengths with a wavelength accuracy of ±0.1 nm. Each spectral band is approximately 10 nm wide. HyperOCI has a cosine response collector and has an accuracy of ideal cosine response within ±3% for sun angle 0° to 60° and ±10% for sun angle 60° to 85°.

Both radiometers were calibrated by the manufacturer and further validated at the NOAA/STAR radiometric calibration facilities (see Section 7). During deployment, the instrument package was always kept >20 m away from the ship to avoid shadows or reflections of the ship hull. For the measured E_s and L_{w0+} data pairs, only those with an inclination less than 5° were used for further analysis. The E_s was interpolated spectrally so as to match up with the wavelengths of the L_w sensor. The instantaneous remote sensing reflectance was first determined as the ratio of instantaneous L_{w0+} to the corresponding E_s.

$$R_{rs}(\lambda,t)=\frac{L_w(0^+,\lambda,t)}{E_s(\lambda,t)} \qquad (9)$$

The first mode of the $R_{rs}(698, t)$ data sequence was then located from its probability density function. Further, all those measurements $R_{rs}(698, t)$ beyond ±15% of the model were filtered out. This procedure was designed to eliminate those potentially contaminated measurements by sea surface reflection and/or immersed sensor head at high sea conditions. The remaining $R_{rs}(\lambda, t)$ spectra were used to derive the median $R_{rs}(\lambda)$ spectrum at each station.

Above-water handheld radiometer

UMB participated in the AWG handheld radiometer activities (Section 8.3). The SR-1901 spectra-radiometer (Spectral Evolution, Inc; Figure 27b) measured the L_{sky} and the total of surface-reflected sky radiance and water-leaving radiance (L_{ref}+L_w), and E_s. The measurements were recorded at 768 spectral bands (350 nm to1900 nm). The spectral resolution is 4 nm between 350 nm to 1000 nm and 10 nm between 1000 nm and 1900 nm. When measuring L_{sky} and L_{ref}+L_w, the radiometer was pointed to the target at 135° azimuth direction relative to the Sun and 40° zenith/nadir angle. UMB did not participate in the blue tile comparisons.

IOP package

The IOP package (Figure 27c) was integrated with one ac-s (WetLabs Inc.) and one backscattering meter (BB7FL2, WetLabs Inc.) to measure the water inherent optical properties.

The ac-s measures *a* and *c* at 80 plus wavelengths from 400 nm to 732 nm. Pure water calibration was carried out before the cruise using Milli-Q water. The BB7FL2 measures the b_b at seven wavelengths (412 nm, 440 nm, 488 nm, 532 nm, 595 nm, 695 nm and 715 nm) and the CDOM and chlorophyll fluorescence at two wavelengths. Dark currents were measured in situ by covering the sensor heads with black electric tape. A new calibration was performed on this instrument immediately before the cruise by WetLabs Inc.

Imaging Flow Cytobot

The Imaging FlowCytobot (IFCB) (Figure 27d) uses a combination of video and flow cytometric technology to capture images of organisms for identification and to measure chlorophyll fluorescence associated with each image. The IFCB has sufficient resolution (≈1 μm) to image nano- and microplankton (≈10 μm to >100 μm). Phytoplankton in this size range can be especially important in coastal phytoplankton blooms, and microzooplankton is critical to the diets of many grazers.

The images can be automatically processed and classified following the approach described by Sosik and Olson [2007]. The approach relies on a supervised machine learning algorithm where the training will be based on example images collected in situ and categorized by manual inspection. Unfortunately, the IFCB encountered some significant vibration or rough handling during the shipping. There was damage to the pump mounts as well as two lengths of sheath tubing. This created a leak condition that allowed air into the system that would inhibit efficient flow of the sheath fluid. This, in turn, caused poor flushing of the flow-cell where significant bio-fouling was evident. As a consequence, the IFCB data collected on this cruise are not useable.

Some Preliminary Results

Satellite and in situ data matchups

In situ measurements of R_{rs} were made at a total of 13 stations during 6 days. We found that 7 stations had valid match-ups between in situ and VIIRS satellite measurements. VIIRS R_{rs} data were calculated as follows: values were retrieved from a box of 3×3 pixels surrounding the station location; 3 quality flags were applied (high solar zenith angle, sensor zenith angle and sun glint); if the number of valid pixels in the box was more than 50% of all pixels (i.e., at least 5 out of 9 pixels had valid values), the valid pixel values were averaged.

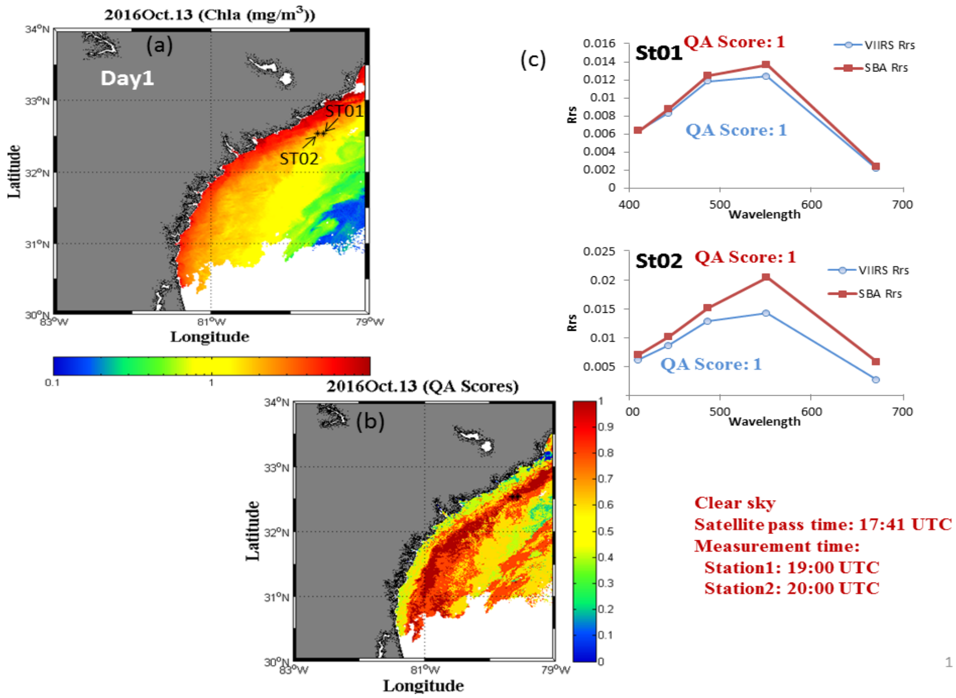

Figure 28. (a) VIIRS Chl-*a* on the first day of 2016 VIIRS cruise with locations of Stations 1 and 2 marked; (b) QA score images for the same day generated following the method developed by Wei et al. [2016]; (c) RISBA R_{rs} and match-up VIIRS level 2 R_{rs}. R_{rs} is shown in units of sr^{-1}.

Figure 28c compares VIIRS R_{rs} with in situ R_{rs} for the first two stations on the first day (Stations 1 and 2). The distributions of VIIRS Chl-*a* and a quality assurance (QA) are also shown in Figure 28a and Figure 28b, respectively. The QA is a metric of the quality for R_{rs}, based on empirical in situ observations and detailed by Wei et al. [2016]. The QA score ranges from 0 to 1 where a high QA value indicates a high quality of R_{rs}. The in situ R_{rs} were collected under a clear sky. High QA scores were observed for both VIIRS and in situ R_{rs} (Figure 28b), and VIIRS R_{rs} agrees very well with in situ measurements (Figure 28c).

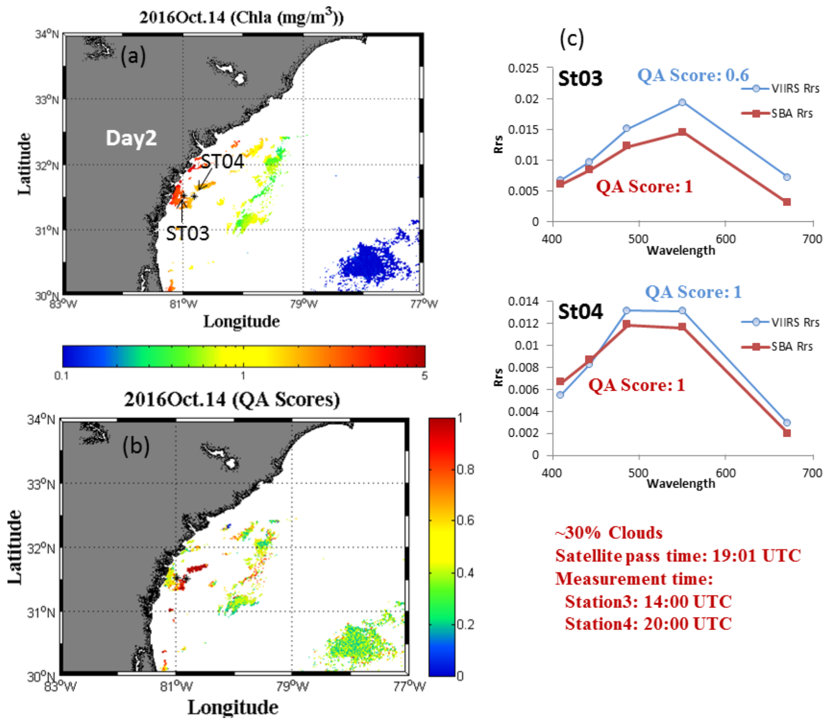

Figure 29. As Figure 28 but for the second day of the 2016 VIIRS cruise.

On the second day of the cruise, the in situ R_{rs} at two stations (Stations 3 and 4) were collected under a partially cloudy sky (≈ 30% clouds). Generally, the in situ R_{rs} agrees with VIIRS R_{rs} very well (Figure 29c). Very good quality of the in situ R_{rs} was obtained (for both stations, the QA scores are 1, Figure 29c). For VIIRS R_{rs}, high QA score (QA = 1) was also obtained for Station 4, but lower QA score (QA = 0.6) for Station 3.

For the third and fourth days of the cruise, there were no matchups between in situ and satellite data using our exclusion criteria for high cloud coverage.

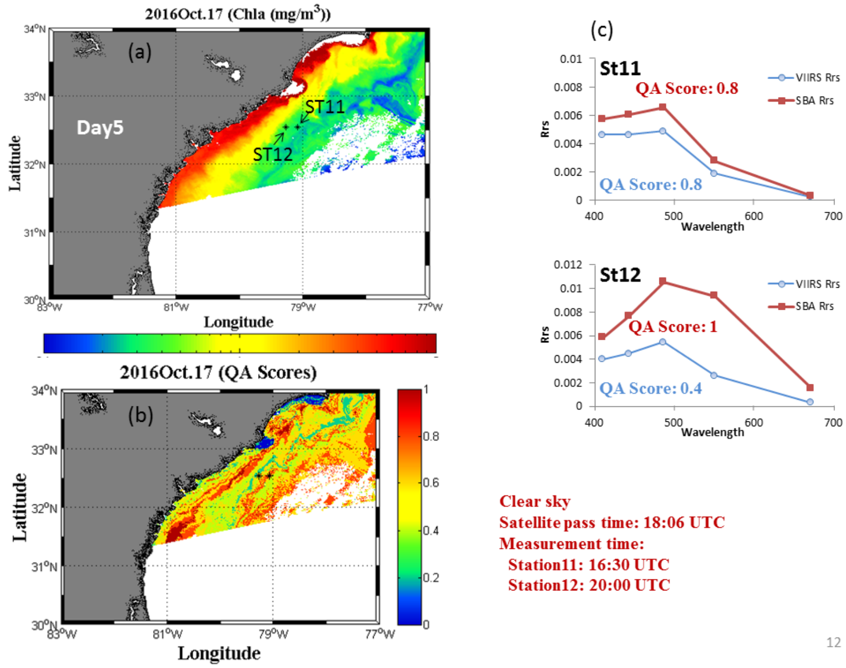

Figure 30. As Figure 28 but for the fifth day of the 2016 VIIRS cruise.

On the fifth day, there were two matchup stations (Stations 11 and 12). The in situ measurements were collected under a very clear sky. The validation results are shown in Figure 30. For Station 11, the VIIRS R_{rs} agrees very well with in situ R_{rs}, but for Station 12, the VIIRS R_{rs} was much lower than in situ R_{rs} (Figure 30c) due to the high spatial variability of water properties in this region.

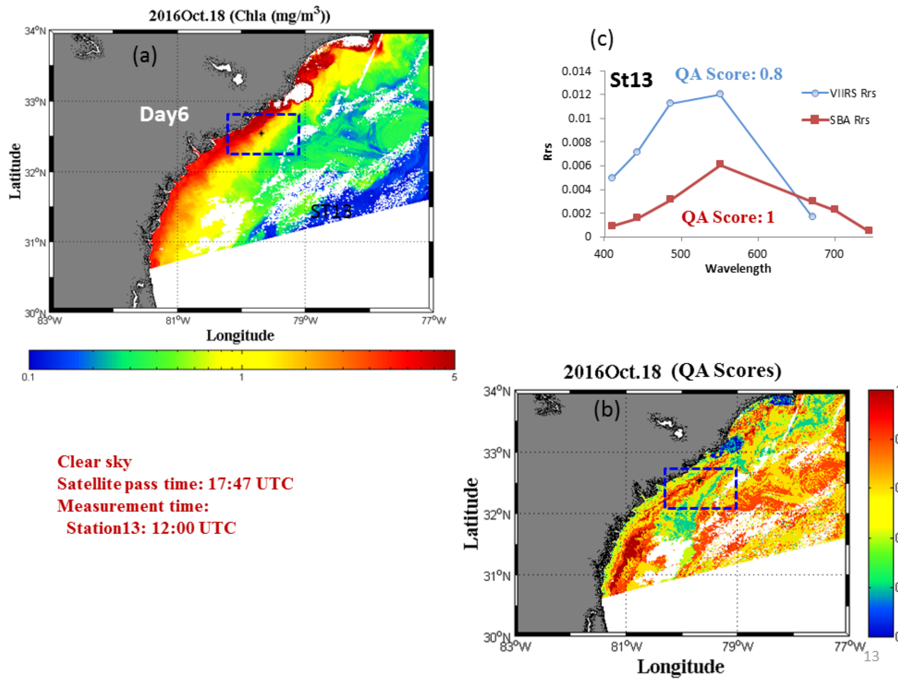

Figure 31. As Figure 28 but for the last day of 2016 VIIRS cruise.

On the last day of the cruise, there was only one matchup station. For both in situ and VIIRS R_{rs}, the QA scores are relatively high (QA ≥ 0.8), but large differences between VIIRS and in situ R_{rs} were obtained (Figure 31). This result was also due to the highly spatial variability of the water properties and large temporal difference between sampling and overpass times.

9.8 OSU - Nicholas Tufillaro and Ivan Lalovic

OSU operated a Satlantic Free Falling Optical Profiler (aka HyperPro; http://satlantic.com/profiler) (Figure 6, third from left) for in water radiance measurements and a Spectral Evolution Field Spectrometer PSR-1100-F (http://www.spectralevolution.com/lightweight_portable_battery_operated_spectrometer.html) (Figure 32) for handheld above water radiance and reflectivity measurements. The HyperPro is also equipped with a WETLabs ECO-Puck with scattering at 470 nm and 700 nm, and chlorophyll fluorescence with 470 nm excitation/695 nm emission (http://wetlabs.com/eco-puck).

Figure 32. Mounting bracketand sensor head for Spectral Evolution spectrometer; (inset) typical operation of above water radiometer.

Protocols: Satlantic HyperPro

The HyperPro deployment was from the stern of the NOAA Ship *Nancy Foster* as part of the profiling radiometery group under the direction of Michael Ondrusek of NOAA/STAR (see Section 7). The deployment and processing protocols used 'yoyo' multi-casts. Satlantic ProSoft processing are described in "OMEL HyperPro Processing Instructions" http://meris.coas.oregonstate.edu/tmp/OSU_NOAA_CRUISE_REPORT_2015_12/OSU_4_REPORT_APPENDIX_C_HyperPro_Processing_Instructions_v8.1.3_20150831_PDF.pdf [Ondrusek et al., 2016].

Protocols: Spectral Evolution, PSR-1100-F

The Spectral Evolution spectrometer was first used during the 2015 NOAA VIIRS Cal/Val cruise and is a handheld instrument deployed on deck in a similar manner as the ASD. The measurement protocols are detailed in "Methods for measuring R_{rs}" documented here: http://meris.coas.oregonstate.edu/tmp/OSU_NOAA_CRUISE_REPORT_2015_12/OSU_3_REPORT_APPENDIX_B_Methods%20for%20measuring%20Rrs_2016-02-16_90%20deg8FOV_WORD.doc [Ondrusek et al., 2016].

OSU participated in the AWG activities (see Section 8.3). A sequence of three measurements were made of (1) a standard reflectance plaque, (2) the water reflectance, and (3) the sky radiance. From these, R_{rs} is estimated (refer to Section 8.3). OSU measured the NRL gray reference plaque and a white Spectralon plaque. OSU also participated in measuring the NIST blue tile.

As part of our NOAA supported work, this year we developed an automated program to do both quality control and the computation of R_{rs} for the Spectral Evolution radiance data. Figure 33 shows the screen displays from the software. The standalone program automatically removes 'outliers' after setting threshold variance levels for rejection (typically 2 σ), and then computes R_{rs} using the remaining data. An optical 'red end' base-line subtraction is also included as a rough correction for any surface reflectance issues such as glint.

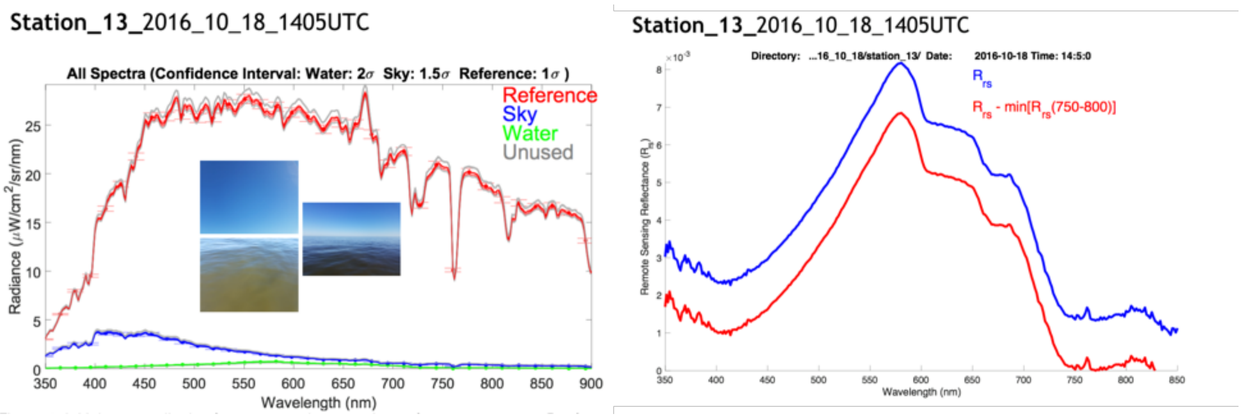

Figure 33. (Left) Initial screen display for automated processing software to compute R_{rs} for the Spectral Evolution spectrometer. The red line is the reference 99% reflectance plaque, the blue line is sky L_{sky}, the green line is *Lw*. The gray line are spectra that fall outside a 2 sigma variance window and are not used in final calculations. (Right) Station 13 computed R_{rs} after automated removal of outliers (blue line) and after adjusting the baseline at 750 nm to 0 (red line).

Data

Summaries of HyperPro and Spectral Evolution measurements of R_{rs} from all stations during the cruise is shown in Figure 34. The open ocean spectra look relatively clear after the passing of Hurricane Matthew. As Figure 34 shows, at Station 10 (approximately 80 km east of Charleston) the R_{rs} generally decreases in the blue end of the spectrum to a value of ≈ 0.005 sr^{-1} with reasonable agreement between the in situ and VIIRS estimated spectra. The station log indicates clear skies, sandbar sharks, and *Aurelia aurita* ("moon jellies") in the water.

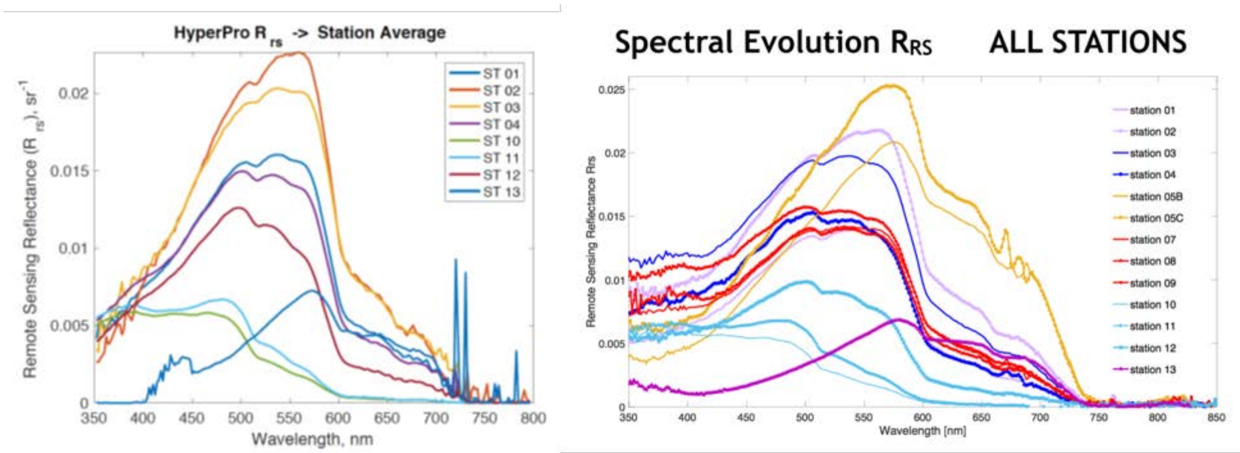

Figure 34. R_{rs} spectra from all stations (left) collected with HyperPro and (right) collected with Spectral Evolution. Stations 10 and 11 show relatively clear open water about 80 km east of Charleston.

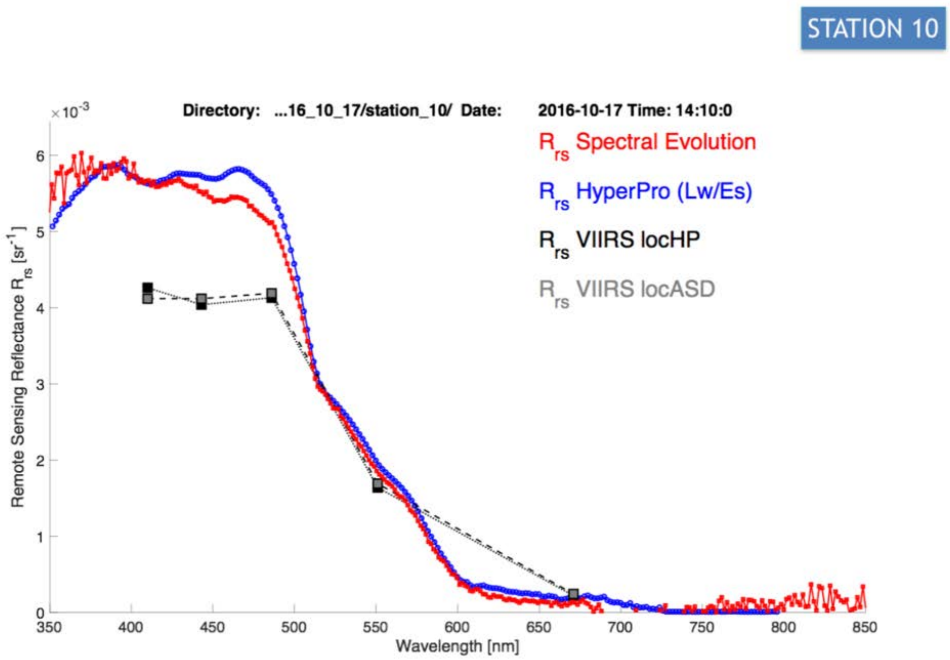

Figure 35. Comparison of in situ and VIIRS R_{rs} spectra at Station 10, clear open ocean 80 km east of Charleston

Plaque Comparisons

The above water reflectance measurements can use different instruments and protocols. In particular, OSU uses a ‘white’ 99% reflectance plaque, while NRL uses the NRL gray 10% reflectance plaque (Figure 36). A comparison of the reflectances was estimated in a typical in situ measurement sequence which appears to indicate some systematic differences between the plaques (Figure 36). Not unexpectedly, the variance in the signals from the white plaque typically were two times less than those from the gray plaque. Because lab measurements show that reflectance can vary as much as 10% over the full spectral range (Figure 37), it is recommended to use a spectrally dependent reflectance.

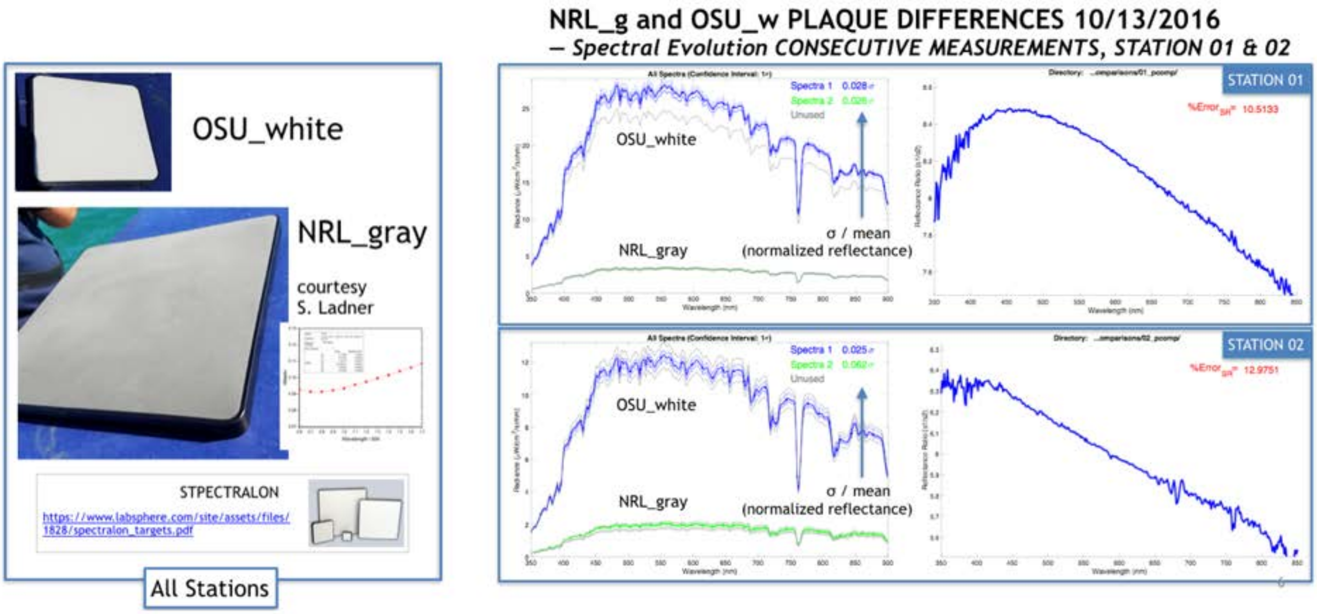

Figure 36. Comparisons of plaque reflectance using typical in situ measurement protocol. The small plot on the left is shown enlarged in Figure 37. The horizontal axis in each of the 4 plots shown in the right hand panels is wavelength from 300 nm to 900 nm. The 2 plots in the center have vertical axes of radiance. The top, center plot radiance axis ranges from 0 µW cm^{-2} sr^{-1} nm^{-1} to 30 µW cm^{-2} sr^{-1} nm^{-1}. The bottom, center plot radiance axis ranges from 0 µW cm^{-2} sr^{-1} nm^{-1} to 13 µW cm^{-2} sr^{-1} nm^{-1}. The 2 plots at the right have vertical axes of spectral error calculated as [(s1 – s2)/(s1 + s2)], where s1 and s2 are the spectra 1 (blue) and spectra 2 (green), respectively, in the center plot. The top, right spectral error axis ranges from ≈0.75 to ≈0.80 (dimensionless) and the bottom, right spectral error axis ranges from ≈0.685 to ≈0.745 (dimensionless).

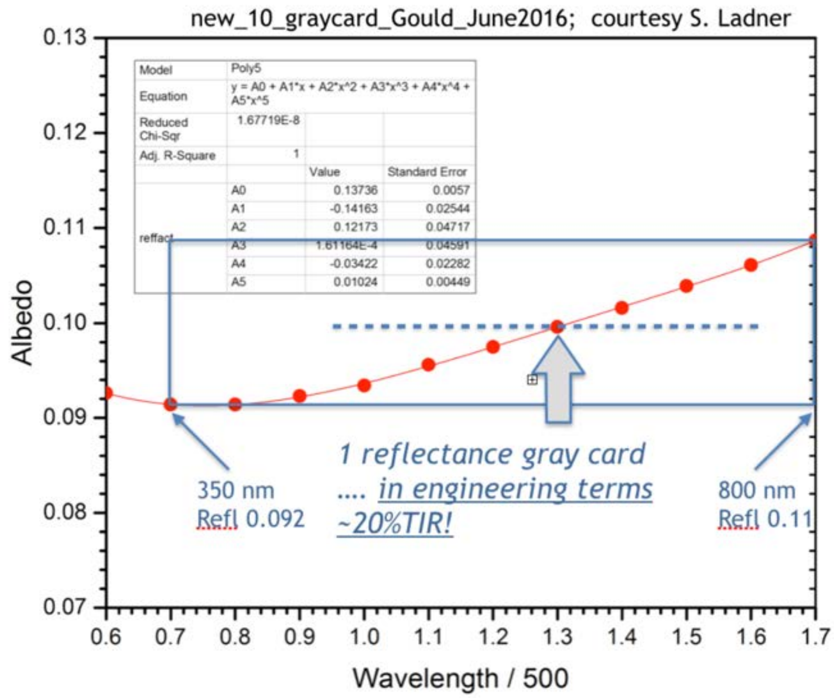

Figure 37. Measurement of NRL gray plaque across full bandwidth shows wavelength dependence in reflectance. Albedo is the dimensionless ratio of reflectance from a black body (=0) to a white body (=1).

Summary

R_{rs} was obtained for all stations with good matches between HyperPro and Spectral Evolution over most stations. Quantitative differences between OSU, NRL and NIST blue plaque were measured during typical in situ measurements with typical errors of 2% to 5%. Overall experimental uncertainty, though, needs better quantification which can be achieved by more carefully noting measurement conditions (e.g., noting potential reflectance from the hull), as well as creating a comprehensive error budget of instruments, plaques, and measurement and processing protocols. Lastly, we are also testing different base line correction procedures to account for factors such as glint, and these will be added to our automated processing routines for R_{rs}. Additional data summaries and reports are provided in the following link: http://meris.coas.oregonstate.edu/tmp/OSU_NOAA_CRUISE_REPORT_2016_12/.

9.9 HBOI – Michael Twardowski and Nicole Stockley

In situ profiles of inherent optical properties

HBOI deployed an instrument package to measure the IOPs of the water column at each station (Figure 38). The package included multiple instruments to measure *a*, *b* and *c* and was designed to allow for simultaneous replicate measurements to differentiate instrument variability from environmental and temporal variability.

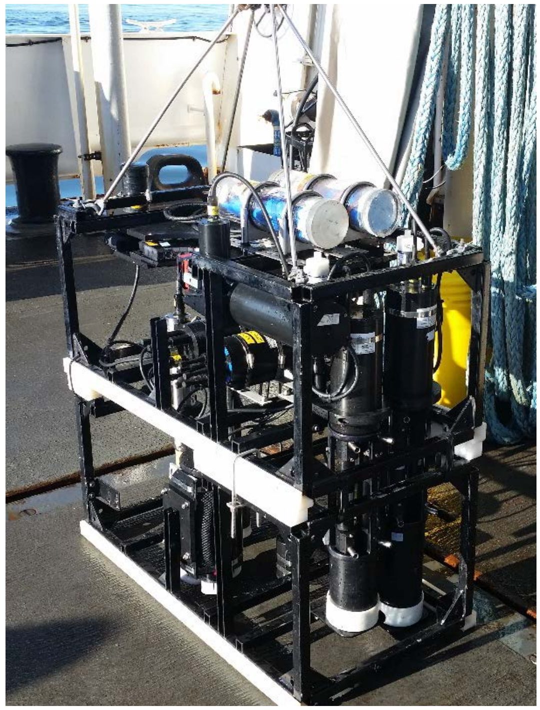

Figure 38. HBOI in situ IOP instrument package.

Measurements of *a* and *c* were made with a WETLabs ac-9 (25 cm path; 412 nm, 440 nm, 488 nm, 510 nm, 532 nm, 555 nm, 650 nm, 676 nm, 715 nm) and a WETLabs ac-s (25 cm path; 400nm to 725 nm, ≈4 nm resolution). At each station, a profile was completed with both instruments measuring a_{pg} and c_{pg}. At 4 of 11 stations when sufficient time was available for a replicate cast, both units were equipped with a 0.2 μm Pall Maxi Capsule filter on both the *a* and *c* sides to measure a_{CDOM} and c_{CDOM}. A WETLabs C-Star (25 cm path; 532 nm) was also included to provide an additional measurement of c_{pg}.

To measure $b(\lambda)$, a WETLabs ECO BB9 (124°; 403 nm, 443 nm, 487 nm, 506 nm, 525 nm, 594 nm, 657 nm, 680 nm, 720 nm) and two WETLabs ECO BB3 units (124°; 469 nm, 529 nm, 652 nm and 470 nm, 532 nm, 660 nm) were located in the same plane on the bottom of the package. The VSF was measured by the WETLabs Multi-Angle Scattering Optical Tool (MASCOT) [Twardowski et al., 2012], which uses a 650 nm laser and 17 detectors ranging from 10° to 170° from the source with a single 1 mL sample volume located 20 cm from each detector. The MASCOT was also equipped with a polarization filter wheel which measured the cross- and co-polarized VSF in addition to the unpolarized VSF throughout the vertical profile.

A WETLabs FL3 fluorometer was included to measure chlorophyll fluorescence at two excitation/emission pairs (440 nm/680 nm and 510 nm/680 nm) and CDOM fluorescence (370 nm/470 nm). A Satlantic OCR507 radiometer (411.6 nm, 442.6 nm, 490.7 nm, 531.9 nm, 554.5 nm, 664.8 nm, 683.3 nm) was included to measure E_d. The package was equipped with a Sea-Bird SBE 49 CTD. Power for the system was provided by Sartek lithium ion battery packs. Two WETLabs DH4s were used to record data and distribute power. The CTD data stream was recorded on both DH4s which allowed the data recorded on the secondary DH4 to be consistently time-stamped to the data recorded on the primary DH4.

Both the ac-s and the ac-9 units were calibrated once during the cruise with purified water produced by equipment aboard the ship. Calibrations were also performed at HBOI before and after the cruise with laboratory water. The MASCOT and the three ECO BB units were calibrated at HBOI following the procedure in Sullivan et al. [2013]. The MASCOT, BB9, and one BB3 were calibrated in December 2016, while the second BB3 was calibrated in April 2016. A third BB3 owned by HBOI that was included in the shipboard flow-through system was also calibrated in April 2016.

Full processing of this dataset is underway. When a thorough quality control analysis has been completed, data will be made available to cruise participants and will be prepared for submission to NOAA and to NASA SeaWiFS Bio-optical Archive and Storage System (SeaBASS).

9.10 U. Miami – Kenneth J. Voss

NuRads measurements of the BRDF or Radiance Distribution

NuRads measures the spectral upwelling radiance distribution [Voss and Chapin, 2005]. The upwelling light field from the same water type in the ocean varies with the illumination geometry and the measurement geometry. Almost all in situ measurements of the upwelling radiance used for satellite validation/calibration are made in the nadir direction (instrument looking straight down, light coming straight up), however the satellite views the ocean at different angles, depending on where the specific pixel is in the satellite scan line. To relate the measurement made on the ground to what the satellite is viewing requires information on the variation of the radiance with direction, which is the radiance distribution. The shape of the radiance distribution also changes spectrally, so the spectral variation of the radiance distribution must also be determined. This is exactly the parameter that NuRads measures.

The model currently used in the data reduction process of satellite data is provided in Morel et al., 2002. This model has been validated several times [Gleason et al., 2012; Voss et al., 2007; Voss and Morel, 2005], but the model is aimed at Case I waters (i.e., open ocean, oligotrophic; water parameters determined by a statistical relationship with Chl-*a*), and breaks down in coastal waters. While we have taken a considerable amount of open ocean radiance distribution data, and some coastal radiance distribution data, because of the variability of the water properties in the coastal area it is reasonable to expand the data set and to take radiance distribution data along with other validation data when doing experiments such as this.

The NuRads instrument was calibrated following previously published protocols [Voss and Chapin, 2005; Voss and Zibordi, 1989]. During the October 2016 cruise, NuRads was deployed by NOAA personnel. When deployed, floats are attached to the instrument and it is floated 20 m to 50 m away from the ship, at the surface (measurement depth is 0.75 m). When deployed, the instrument measures the upwelling radiance continuously, cycling through the 6 different wavelengths and associated dark measurements. NuRads measurements were made at 6 stations (1, 2, 3, 11, 12 and 13). The data have been reduced and processed and quality control is currently being conducted.

10. Conclusion

An abundance of clear skies following in the wake of Hurricane Matthew provided many opportunities for potential match-ups with VIIRS (6 to 9 stations covering 3 to 5 separate days) during the 2016 dedicated VIIRS Cal/Val cruise aboard the NOAA Ship *Nancy Foster*. Rough seas limited the region of sampling relatively close to the US southeast coast for most of the cruise. In situ AOP radiometry and IOP optical measurements were made with multiple instruments deployed in several modes (e.g., profiling, flow-through, etc.) and water samples were collected for later processing to provide measurements of additional ocean properties. Uncertainties in the in situ and satellite validation measurements will be estimated by utilizing pre- and post-cruise calibrations of instruments, simultaneous measurements of parameters utilizing multiple techniques and instruments and evaluation of data processing techniques.

Furthermore, the cruise presented the opportunity to document and quantify the influence of Hurricane Matthew on the water properties along the US coastal region. Oceanic processes will be investigated using multiple platform techniques, which include near-real time satellite measurements, in situ flow-through, profiling, and above water data. Spatial gradients will be studied using in situ data and compared with VIIRS data to assess the ability of VIIRS to capture the scales and magnitude of naturally occurring variability in dynamic coastal waters.

In summary, observations from this cruise along with those from the two previous dedicated VIIRS Cal/Val cruises [Ondrusek et al., 2016; Ondrusek et al., 2015] have added a significant number of validation-quality in situ match-ups for a comprehensive evaluation of VIIRS performance validation techniques and various ocean color applications. Coming in the wake of Hurricane Matthew, this cruise also will contribute to the knowledge base and analysis of the effect of the storm on coastal waters.

11. Cruise Data Access

All data collected on this cruise will be formally archived with NOAA/NCEI according to their guidelines and will also be publicly accessible through NOAA CoastWatch/OceanWatch. Data users are strongly urged to communicate with cruise investigators for appropriate collaborations and citations. Data for standard measurements taken routinely aboard the NOAA Ship *Nancy Foster* can be found here: http://coastwatch.pfeg.noaa.gov/erddap/tabledap/fsuNoaaShipWTER.htmlTable?cruise_id%2Cexpocode%2Cfacility%2CID%2CIMO%2Cplatform%2Cplatform_version%2Csite%2Ctime%2Clatitude%2Clongitude%2CairPressure%2CairTemperature%2Cconductivity%2CrelativeHumidity%2Csalinity%2CseaTemperature%2CseaTemperature2%2CwindDirection%2CwindSpeed%2CplatformCourse%2CplatformHeading%2CplatformSpeed%2CplatformWindDirection%2CplatformWindSpeed%2Cflag&time%3E=2016-10-12T23%3A59%3A00Z&time%3C=2016-10-18T23%3A59%3A00Z&flag=~%22ZZZ.*%22. Some data from this cruise have been or will be submitted to the NASA SeaBASS archive.

12. Acknowledgments

Funding for this project was provided as follows: NOAA OMAO for ship time and crew support; JPSS VIIRS Ocean Color Cal/Val funding supported some science group participation; investigator groups external to the JPSS VIIRS Ocean Color Cal/Val provided their own support. We thank the crew of the NOAA Ship *Nancy Foster* for their support in making data collection possible. NASA/GSFC contributed the use of instruments for onboard measurements and performed laboratory analyses on discrete water samples for some parameters. We are grateful to Georgi Georgiev of NASA/GSFC and Catherine Cooksey of NIST for BRDF measurements of the blue tile. The views, opinions, and findings contained in this report are those of the authors and should not be construed as an official NOAA or US Government position, policy, or decision.

13. References Cited

Arnone, R., M. Fargion, P. Martinolich, S. Ladner and e. al. (2012), Validation of the VIIRS Ocean color, *Proc. SPIE 8372, Ocean Sensing and Monitoring IV, 83720G*, doi: http://dx.doi.org/10.1117/12.922949.

Arnone, R., R.A. Vandermeulen, S. Ladner, J. Bowers, P. Martinolich, M. Fargion and M. Ondrusek (2014), Sensitivity of calibration "gains" to ocean color processing in coastal and open waters using ensembles members for NPP- VIIRS, *Proc. SPIE 9111, Ocean Sensing and Monitoring VI, 911105.* , doi: http://dx.doi.org/10.1117/12.2053409.

Bibby, T.S., M.Y. Gorbunov, K.W. Wyman and P.G. Falkowski (2008), Photosynthetic community responses to upwelling in mesoscale eddies in the subtropical North Atlantic and Pacific Oceans, *Deep Sea Research Part II: Topical Studies in Oceanography*, *55*(10–13), 1310-1320, doi: 10.1016/j.dsr2.2008.01.014.

Booth, B.C. (1993), *Estimating cell concentration and biomass of autotrophic plankton using microscopy.*, Lewis Publishers, Boca Raton, Florida, USA.

Carder, K.L. and R.G. Steward (1985), A remote-sensing reflectance model of a red-tide dinoflagellate off west Florida, *Limnology and Oceanography*, *30*(2), 286-298.

Chekalyuk, A. and M.A. Hafez (2008), Advanced laser fluorometry of natural aquatic environments, *Limnology and oceanography, methods*, *6*, 591.

Chekalyuk, A.M., M.R. Landry, R. Goericke, A.G. Taylor and M.A. Hafez (2012), Laser fluorescence analysis of phytoplankton across a frontal zone in the California Current ecosystem, *J. Plankton Res.*, *34*(9), 761-777, doi: 10.1093/plankt/fbs034.

Clark, D.K., H.R. Gordon, K.J. Voss, Y. Ge, W. Broenkow and C. Trees (1997), Validation of atmospheric correction over the oceans, *J. Geophys. Res.-Atmos.*, *102*(D14), 17209-17217, doi: 10.1029/96jd03345.

Early, E.A., P.Y. Barnes, B.C. Johnson, J.J. Butler, C.J. Bruegge, S.F. Biggar, P.R. Spyak and M. Pavlov (2000), Bidirectional reflectance round-robin in support of the Earth Observing System Program, *J. Atmos. and Oceanic Tech.*, *17*, 1077 - 1091.

EPA (1971), Methods for chemical analysis of water and wastes, EPA-NERL: 160.2, US Environmental Protection Agency.

Foster, R. and A. Gilerson (2016), Polarized transfer functions of the ocean surface for above-surface determination of the vector submarine light field, *Appl. Optics*, *55*, 9476-9494.

Georgiev, G.T. and J.J. Butler (2008), Laboratory-based bidirectional reflectance distribution functions of radiometric tarps, *Appl. Optics*, *47*(18), 3313 - 3323.

Gleason, A.C.R., K.J. Voss, H.R. Gordon, M. Twardowski, J. Sullivan, C. Trees, A. Weidemann, J.F. Berthon, D. Clark and Z.P. Lee (2012), Detailed validation of the bidirectional effect in various Case I and Case II waters, *Optics Express*, *20*(7), 7630-7645, doi: 10.1364/oe.20.007630.

Goes, J.I., H.d.R. Gomes, E.M. Haugen, K.T. McKee, E.J. D'Sa, A.M. Chekalyuk, D.K. Stoecker, P.J. Stabeno, S.-I. Saitoh and R.N. Sambrotto (2014), Fluorescence, pigment and microscopic characterization of Bering Sea phytoplankton community structure and photosynthetic competency in the presence of a Cold Pool during summer, *Deep Sea Research Part II: Topical Studies in Oceanography*, *109*(0), 84-99, doi: 10.1016/j.dsr2.2013.12.004.

Gomes, H.d.R., K. McKee and J.I. Goes (in prep), Improved methods for determination of phycoerythin and phycocyanin in natural seawater samples.

Gorbunov, M.Y. and P.G. Falkowski (2004), Fluorescence induction and relaxation (FIRe) technique and instrumentation for monitoring photosynthetic processes and primary production in aquatic ecosystems, (ed.), *Proceedings of Photosynthesis: Fundamental Aspects to Global Perspectives"- Proc. 13th International Congress of Photosynthesis, Montreal, Aug*.

Gordon, H.R. (2010), Some reflections on thirty-five years of ocean-color remote sensing, in *Oceanography from Space: Revisited*, Edited by Barale, V., Gower, J.F.R. and Alberotanza, L., 289-305, Springer Netherlands.

Gordon, H.R., D.K. Clark, J.L. Mueller and W.A. Hovis (1980), Phytoplankton Pigments from the Nimbus-7 Coastal Zone Color Scanner: Comparisons with Surface Measurements, *Science*, *210*(4465), 63-66, doi: 10.2307/1684604.

Gould, R.W., R.A. Arnone and M. Sydor (2001), Absorption, scattering; and remote-sensing reflectance relationships in coastal waters: Testing a new inversion algorithm, *J. Coast. Res.*, *17*(2), 328-341.

GUM (1995), Evaluation of measurement data - Guide to the expression of uncertainty in measurement.(ed.), http://www.bipm.org/en/publications/guides/gum.html.

Holm-Hansen, O. and B. Riemann (1978), Chlorophyll a determination: improvements in methodology, *Oikos*, *30*, 438-447.

Hovis, W.A., D.K. Clark, F. Anderson, R.W. Austin, W.H. Wilson, E.T. Baker, D. Ball, H.R. Gordon, J.L. Mueller, S.Z. El-Sayed, B. Sturm, R.C. Wrigley and C.S. Yentsch (1980), Nimbus-7 Coastal Zone Color Scanner: System Description and Initial Imagery, *Science*, *210*(4465), 60-63, doi: 10.2307/1684603.

Hunter, C. (2006), Particulate organic carbon, nitrogen and total suspended matter. Methodologies, protocols and analyses used in the development of ocean color product algorithms., Technical Publication 06–1(ed.), Moss Landing Marine Laboratories.

Johnson, B.C., G.S. Fargion, R.D. Saunders and M. Ondrusek (2012), Comparisons of reflectance targets at the Above Water Radiometry Workshop on Long Island Sound, August 4 - 6, 2010, in *2010 American Geophysical Union Fall Meeting*, edited, pp. A33M-0330, San Francisco, CA.

Johnson, B.C., J. Rice, H. Yoon and A. Parr (2014), Principles of optical radiometry, in *Optical radiometry for ocean climate measurements*, edited by Zibordi, G., Donlon, C. and Parr, A., pp. 13-67, Academic Press, Waltham, MA.

Johnson, B.C., S.S. Bruce, E.A. Early, J.M. Houston, T.R. O'Brian, A. Thompson, S.B. Hooker and J.L. Mueller (1996), *The Fourth SeaWiFS Intercalibration Round-Robin Experiment (SIRREX-4), May 1995*, 65 pp., NASA Goddard Space Flight Center, Greenbelt, Maryland.

Kishino, M., M. Takahashi, N. Okami and S. Ichimura (1985), Estimation of the spectral absorption coefficients of phytoplankton in the sea, *Bulletin of Marine Science*, *37*(2), 634-642.

Knap, A., A. Michaels, A. Close, H. Ducklow and A. Dickson (1994), Protocols for the Joint Global Ocean Flux Study (JGOFS) Core Measurements. JGOFS Report,(ed.) 170 pp.

Lee, Z.P., K.L. Carder and R.A. Arnone (2002), Deriving inherent optical properties from water color: a multiband quasi-analytical algorithm for optically deep waters, *Appl. Optics*, *41*(27), 5755-5772, doi: 10.1364/ao.41.005755.

Lee, Z.P., N. Pahlevan, Y.-H. Ahn, S. Greb and D. O'Donnell (2013), Robust approach to directly measuring water-leaving radiance in the field, *Appl. Optics*, *52*(8), 1693-1701.

Lee, Z.P., K.L. Carder, R.G. Steward, T.G. Peacock, C.O. Davis and J.L. Mueller (1997), *Remote-sensing reflectance and inherent optical properties of oceanic waters derived from above-water measurements*, 160-166 pp., Spie - Int Soc Optical Engineering, Bellingham, doi: 10.1117/12.266436.

MacIssac, E.A. and J.G. Stockner (1993), Enumeration of phototrophic picoplankton by autofluorescence microscopy., in *Handbook of Methodology in Aquatic Microbial Ecology*, Edited by Kemp.P.F., Sherr, B.F., Sherr, E.B. and J., C.J., 187-197, Lewis Publishers, Boca Raton, Florida, USA.

Mobley, C.D. (1999), Estimation of the remote-sensing reflectance from above-surface measurements, *Appl. Optics*, *38*(36), 7442-7455, doi: 10.1364/ao.38.007442.

Mobley, C.D. (2015), Polarized reflectance and transmittance properties of windblown sea surfaces, *Appl. Opt.*, *54*(15), 4828 - 4849.

Morel, A., D. Antoine and B. Gentili (2002), Bidirectional reflectance of oceanic waters: accounting for Raman emission and varying particle scattering phase function, *Appl. Optics*, *41*(30), 6289-6306, doi: 10.1364/ao.41.006289.

Morrow, J.H., C.R. Booth, R.N. Lind and S.B. Hooker (2010), The Compact Optical Profiling System (C-OPS). Advances in Measuring the Apparent Optical Properties (AOPs) of Optically Complex Waters, NASA Tech. Memo. 2010–215856, Morrow, J.H., Hooker, S.B., Booth, C.R., Bernhard, G., Lind, R.N. and J.W., B. (ed.) 42–50 pp, NASA Goddard Space Flight Center, Greenbelt, Maryland.

Mueller, J.L. (2003), In-Water Radiometric Profile Measurements and Data Analysis Protocols, in *Ocean Optics Protocols For Satellite Ocean Color Sensor Validation, Revison 4, Volume III: Radiometric Measurements and Data Analysis Protocols*, Edited by Mueller, J.L., Fargion, G.S. and Mcclain, C., NASA/TM-2003-21621/Rev4-Vol III, p.^pp. 7 - 20, Goddard Space Flight Center, National Aeronautics and Space Administration, Greenbelt, Maryland.

Mueller, J.L., C.O. Davis, R. Arnone, R. Frouin, K. Carder, Z.P. Lee, R.G. Steward, S.B. Hooker, C.D. Mobley and S. McLean (2003), Above-water radiance and remote sensing reflectance measurement and analysis protocols, in *Ocean Optics Protocols For Satellite Ocean Color Sensor Validation, Revison 4, Volume III: Radiometric Measurements and Data Analysis Protocols*, Edited by Mueller, J.L., Fargion, G.S. and Mcclain, C., NASA/TM-2003-21621/Rev4-Vol III, p.^pp. 21 - 31, Goddard Space Flight Center, National Aeronautics and Space Administration, Greenbelt, Maryland.

Ondrusek, M., E. Stengel, C.S. Kinkade, R.L. Vogel, P. Keegstra, C. Hunter and C. Kim (2012), The development of a new optical total suspended matter algorithm for the Chesapeake Bay, *Remote Sensing of Environment*, *119*, 243-254, doi: 10.1016/j.rse.2011.12.018.

Ondrusek, M., E. Stengel, V.P. Lance, M. Wang, K. Voss, G. Zibordi, M. Talone, Z. Lee, J. Wei, J. Lin, et al. (2015), Report for Dedicated JPSS VIIRS Ocean Color Calibration/Validation Cruise. NOAA/NESDIS Technical Report, Lance, V.P. (ed.) 60 pp, National Oceanic and Atmospheric Administration, US Department of Commerce, Washington, DC.

Ondrusek, M., V.P. Lance, E. Stengel, M. Wang, R. Arnone, S. Ladner, W. Goode, R. Vandermeulen, S. Freeman, C.J. E., et al. (2016), Report for Dedicated JPSS VIIRS Ocean Color Calibration/Validation Cruise December 2015 NOAA/NESDIS Technical Report, Lance, V.P. (ed.) 66 pp, National Oceanic and Atmospheric Administration, US Department of Commerce, Washington, DC.

Pegau, W.S., D. Gray and J.R.V. Zaneveld (1997), Absorption and attenuation of visible and near-infrared light in water: dependence on temperature and salinity, *Appl. Optics*, *36*(24), 6035-6046, doi: 10.1364/ao.36.006035.

Pope, R.M. and E.S. Fry (1997), Absorption spectrum (380-700 nm) of pure water .2. Integrating cavity measurements, *Appl. Optics*, *36*(33), 8710-8723, doi: 10.1364/ao.36.008710.

Proctor, J.E. and P.Y. Barnes (1996), NIST high accuracy reference reflectometer-spectrophotometer, *J. Res. NIST*, *101*(5), 619 - 627.

Richardson, T.L., E. Lawrenz, J.L. Pinckney, R.C. Guajardo, E.A. Walker, H.W. Paerl and H.L. MacIntyre (2010), Spectral fluorometric characterization of phytoplankton community composition using the Algae Online Analyser®, *Water Res*, *44*(8), 2461-2472.

Röttgers, R., D. McKee and S.B. Woźniak (2013), Evaluation of scatter corrections for ac-9 absorption measurements in coastal waters, *Methods in Oceanography*, *7*, 21-39, doi: http://dx.doi.org/10.1016/j.mio.2013.11.001.

Satlantic (2004), SatView Data Logging / Display Program Users Guide; Version 2.8.(ed.), Satlantic Incorporated, Halifax, Nova Scotia.

Satlantic (2012), Operation Manual for Profiler II.(ed.), Satlantic Incorporated, Halifax, Nova Scotia.

Schiff, T.F., M.W. Knighton, D.J. Wilson, F.M. Cady, J.C. Stover and J.J. Butler (1993), Design review of a high accuracy UV to near IR scatterometer, *Proc. SPIE*, *1995*, 121 - 130.

Sosik, H.M. and R.J. Olson (2007), Automated taxonomic classification of phytoplankton sampled with imaging-in-flow cytometry, *Limnology and Oceanography: Methods*, *5*(6), 204-216.

Sullivan, J.M., M.S. Twardowski and J.R.V. Zaneveld (2013), Measuring optical backscattering in water, in *Light Scattering Reviews 7*, Edited by Kokhanovsky, A.A., Springer-Praxis Books.

Sullivan, J.M., M.S. Twardowski, J.R.V. Zaneveld, C.M. Moore, A.H. Barnard, P.L. Donaghay and B. Rhoades (2006), Hyperspectral temperature and salt dependencies of absorption by water and heavy water in the 400-750 nm spectral range, *Appl. Optics*, *45*(21), 5294-5309.

Tomas, C.R. (1997), *Identifying marine phytoplankton*, Academic press.
Twardowski, M., X.D. Zhang, S. Vagle, J. Sullivan, S. Freeman, H. Czerski, Y. You, L. Bi and G. Kattawar (2012), The optical volume scattering function in a surf zone inverted to derive sediment and bubble particle subpopulations, *J. Geophys. Res.-Oceans*, *117*, doi: 10.1029/2011jc007347.
Twardowski, M.S. and P.L. Donaghay (2001), Separating in situ and terrigenous sources of absorption by dissolved materials in coastal waters, *J. Geophys. Res.-Oceans*, *106*(C2), 2545-2560, doi: 10.1029/1999jc000039.
Twardowski, M.S., J.M. Sullivan, P.L. Donaghay and J.R.V. Zaneveld (1999), Microscale quantification of the absorption by dissolved and particulate material in coastal waters with an ac-9, *J. Atmos. Oceanic Technol.*, *16*, 691–707.
Van Heukelem, L. and C.S. Thomas (2001), Computer-assisted high-performance liquid chromatography method development with applications to the isolation and analysis of phytoplankton pigments, *Journal of Chromatography A*, *910*(1), 31-49, doi: 10.1016/s0378-4347(00)00603-4.
Voss, K.J. and G. Zibordi (1989), Radiometric and geometric calibration of a spectral electro-optic “fisheye" camera radiance distribution system, *J. Atmosph. and Ocean. Techn.*, *6*, 652-662.
Voss, K.J. and A.L. Chapin (2005), Upwelling radiance distribution camera system, NURADS, *Optics Express*, *13*(11), 4250-4262, doi: 10.1364/opex.13.004250.
Voss, K.J. and A. Morel (2005), Bidirectional reflectance function for oceanic waters with varying chlorophyll concentrations: Measurements versus predictions, *Limnol. Oceanogr.*, *50*(2), 698-705.
Voss, K.J., A. Morel and D. Antoine (2007), Detailed validation of the bidirectional effect in various Case 1 waters for application to ocean color imagery, *Biogeosciences*, *4*(5), 781-789.
Wang, M., X. Liu, L. Jiang and S. Son (2017), The VIIRS Ocean Color Product Algorithm Theoretical Basis Document, National Oceanic and Atmospheric Administration, National Environmental Satellite and Data Information Service, 68 pp., doi: TBD.
Wang, M., X. Liu, L. Tan, L. Jiang, S. Son, W. Shi, K. Rausch and K. Voss (2013), Impact of VIIRS SDR performance on ocean color products, *J. Geophys. Res. Atmos.*, *118*, 10347–10360, doi: doi:10.1002/jgrd.50793.
Wang, M., X. Liu, L. Jiang, S. Son, J. Sun, W. Shi, L. Tan, P. Naik, K. Mikelsons, X. Wang and V. Lance (2014), Evaluation of VIIRS Ocean Color Products, *Proc. SPIE 9261*, *92610E*, doi: 10.1117/12.2069251.
Wei, J.W., Z.P. Lee and S.L. Shang (2016), A system to measure the data quality of spectral remote-sensing reflectance of aquatic environments, *J. Geophys. Res.-Oceans*, *121*(11), 8189-8207, doi: 10.1002/2016jc012126.
Welschmeyer, N.A. (1994), Fluorometric analysis of chlorophyll-*a* in the presence of chlorophyll-*b* and pheopigments, *Limnol. Oceanogr.*, *39*(8), 1985-1992, <Go to ISI>://A1994QG41300020.
WETLabs (2011), ac meter protocol document. ac meter protocol (acprot); Revision Q 20 April 2011(ed.).
Zaneveld, J.R.V., J.C. Kitchen and C.C. Moore (1994), Scattering error correction of reflecting-tube absorption meters, (ed.), *Proceedings*, doi: 10.1117/12.190095.
Zibordi, G. and K.J. Voss (2014), In situ Optical Radiometry in the Visible and Near Infrared, *Experimental Methods in the Physical Sciences*, *47*, 247-304.

Appendix A – Station Information Tables

Table A1. Station identification, dates, starting and ending times and locations, and drift.

NF-16-08 Station ID#	Date in Oct-ober 2016	Day of Year	Start Time [hh:mm UTC]	Start Latitude [decimal degrees N]	Start Longitude [decimal degrees E]	End Time [hh:mm UTC]	End Latitude [decimal degrees N]	End Longitude [decimal degrees E]	Station Drift Estimate [nautical miles]
1	13	287	17:00	32.618	-79.571	19:34	32.602	-79.611	n/a
2	13	287	20:10	32.573	-79.650	21:50	32.578	-79.652	n/a
3	14	288	12:40	31.372	-80.972	16:20	31.366	-80.981	n/a
4	14	288	17:48	31.318	-80.814	20:59	31.319	-80.816	4 to 5
5	15	289	18:17	32.311	-80.282	18:50	32.310	-80.295	2
6	16	290	12:24	31.857	-80.746	14:00	31.847	-80.758	2
7	16	290	16:00	31.779	-80.579	16:40	31.769	-80.566	<1
8	16	290	17:55	31.702	-80.427	19:40	31.696	-80.424	<1
9	16	290	20:40	31.726	-80.384	21:10	31.728	-80.386	<1
10	17	291	12:10	32.431	-78.876	14:45	32.440	-78.877	<1
11	17	291	16:35	32.636	-79.074	18:30	32.635	-79.085	<1
12	17	291	20:10	32.790	-79.266	21:36	32.796	-79.295	> 1.5
13	18	292	12:00	32.685	-79.682	14:30	32.681	-79.688	<1

Table A2. Cloud cover, wind, sea state, water depth, secchi depth and station notes from on board log.

NF-16-08 Station ID#	Cloud Cover (%)	Wind Direction [degrees]	Wind Speed [kt]*	Sea State [feet]*	Water Depth [m]	Secchi Depth [m]	Station Notes
1	0	50	10	3	14	4	Off Charleston, SC entrance, 8 nm.
2	0	60	9	2-3	16	3.5	Off Charleston Harbor buoy south; *Trichodesmium* in water surface sample
3	10; built to 25	64	9	3	18	3.5	Off Savannah GA T3, 17 miles off coast; no vertical structure; Station interrupted by drill 13:50 to 15:10; returned to Station 3 for HyperPro casts.
4	50	56	15	4-6	9	6	Cut NURADS wire, divers in water; drifted South for floats and CTD; Station took 34 h.
5	40	64	15	5	15	n/a	Just off coast, rough seas. Above-water and flow-through only.
6	25 to 50	70	15-20	5	14	2.5	Close to land near Savannah, GA; too rough for floats.
7	50	65	15-20	5-6	25	3.5	Move offshore transect; too rough for floats
8	40; patchy	55	19	4-5	18	4	Offshore track from Savannah
9	20	57	5	5	19	n/a	No floats allowed; video of water; high seas.
10	5	65	10	3	92	24	Outer station offshore blue water, north of Charleston; great conditions, clear sky; some *Sargassum*.
11	5	60	9.9	2	27	15	Eddy. No current model; time of VIIRS overpass; *Trichodesmium* from Gulf Stream; great conditions.
12	0	70	8	2-3	35	5	North of Charleston, 3rd station of the day, good late afternoon sky.
13	0	70	4	1-2	14	3.5	Entrance to Charleston; 7 nm inshore of Station 1; Early Morning, calm; had to leave Station by 10:30 am local time to be in by noon local time.

*These values are reported here in units as they were recorded on the ship rather than converting them to SI units. One knot is a nautical mile per hour, or 0.5144 meter per second. One foot is 0.3048 meters.

Table A3. Times and locations for deployment of profiling and floating radiometers and Secchi Disk.

	Profiling Radiometer Deployment*			Floating HyperPros and NuRads Deployment**		
NF-16-08 Station ID#	**Time [UTC hh:mm]**	**Latitude [decimal degrees N]**	**Longitude [decimal degrees E]**	**Time [UTC hh:mm]**	**Latitude [decimal degrees N]**	**Longitude [decimal degrees E]**
1	17:20	32.539	-79.572	17:43	32.622	-79.580
2	20:10	32.573	-79.650	20:46	32.574	-79.647
3	15:25	31.371	-80.973	16:00	31.366	-80.981
4	17:53	31.318	-80.814	18:25-18:40 No NURADS	31.330	-80.833
5	no deployments					
6	14:45	31.855	-80.755	no deployments		
7	16:25 NOAA only	31.775	-80.574	no deployments		
8	18:03	31.702	-80.427	18:30 USM only	31.695	-80.424
9	20:40	31.728	-80.386	no deployments		
10	13:41	32.432	-78.877	14:20 No NURADS	32.432	-78.884
11	17:33	32.632	-79.077	18:00	32.632	-79.084
12	20:15	32.791	-79.266	20:45	32.795	-79.272
13	13:41	32.655	-79.681	14:20	32.682	-79.688

*Four profiling radiometers were deployed simultaneously by NOAA/STAR (HyperPro and a C-OPS), OSU and USF (HyperPros).

**The NuRads (U. Miami) and 3 floating HyperPros (UMB, Stennis/USM and Stennis/NRL) were deployed simultaneously.

Table A4. Times and locations of handheld spectroradiometer deployments along with record of HyperSAS status at each station.

Handheld Spectroradiometer* Nominal Deployment					
NF-16-08 Station ID#	**Time [UTC hh:mm]**	**Deck [#]**	**Latitude [decimal degrees N]**	**Longitude [decimal degrees E]**	**HyperSAS-POL at Bow Status**
1	18:43	01	32.624	-79.577	on
2	20:18	03	32.573	-79.650	on
3	13:55	01	31.367	-80.969	on
4	17:53	03	31.318	-80.812	on
5	18:17 Blue Tile; 18:43 regular protocol	01	32.308	-80.299	on
6	14:15 ASDs & GER	01	31.859	-80.748	on
7	16:00	bow glint; 03	31.778	-80.578	on
8	18:03	01	31.702	-80.426	on
9	20:54	01	31.726	-80.385	on
10	13:40	01	32.431	-78.877	on
11	17:33 regular protocol; 17:46 with Blue Tile	clear sky; 01	32.632	-79.078	on
12	20:15	01	32.793	-79.267	on
13	13:40	01	32.685	-79.684	on

*Seven handheld radiometers deployed: 4x ASD (NOAA/STAR, USF, and 2x Stennis NRL); 2x Spectral Evolution (UMB and OSU); and 1x GER (CCNY). Refer to individual datasets for precise metadata regarding deployment times and locations.

Table A5. Times, locations and bottle depths for CTD/Rosette cast.

Ship's Rosette Package Deployment				
NF-16-08 Station ID#	**Time [UTC hh:mm]**	**Latitude [decimal degrees N]**	**Longitude [decimal degrees E]**	**Nominal Water Sampling* Depths [m]**
1	17:53	32.622	-79.580	2, 16 a_p @ 2 only
2	21:50	32.578	-79.652	2, 15
3	12:40	31.372	-80.972	2, 15
4	20:50	31.319	-80.816	2, 15
5		No deployment		Sampled from flow-through system, ≈2
6	12:24	31.857	-80.747	Bucket, 2.5, 12
7	16:15	31.774	-80.572	2, 15
8	19:02	31.696	-80.424	2, 15
9	20:12	31.728	-80.386	2, 18
10	12:10	32.431	-78.876	2, 42,70
11	17:12	32.631	-79.076	2, 17
12	20:52	32.796	-79.275	2, 13
13	12:00	32.685	-79.682	Surface

*Measurements made from discrete water samples include:

<u>*USF*</u>

- Filter pad absorption
- CDOM
- Extracted Chl-*a*

<u>*NOAA/STAR*</u>

- Extracted Chl-*a*
- SPM
- HPLC pigments
- POC, PON
- CDOM

<u>*LDEO*</u>

- Nutrients (SiO_3, NO_3+NO_2 and PO_4)
- Microscopy (preserved)
- Cell imagery (FlowCAM)
- Phycobilipigments
- F_v/F_m and σ_{PSII}
- Fluorescence of Chl-*a*, CDOM, PE-1, PE-2, PE-3

Table A6. Times and locations for profiling IOP sampling packages.

	HBOI* and UMB**		
NF-16-08 Station ID#	**Time [UTC hh:mm]**	**Latitude [decimal degrees N]**	**Longitude [decimal degrees E]**
1	18:20	32.625	-79.577
2	21:50	32.579	-79.650
3	13:42	31.371	-80.972
4	20:50	31.319	-80.816
5	No profiling IOP deployments		
6	13:20	31.859	-80.746
7	16:10	31.776	-80.574
8	19:25	31.695	-80.424
9	21:37	31.726	-80.393
10	13:10	32.430	-78.875
11	17:03	32.633	-79:074
12	21:23	32.796	-79.288
13	20:00	32.476	-79.160

*<u>*HBOI*</u> profiling IOP package includes:

- ac-9, *a* and *c*, 25 cm path; 412 nm, 440 nm, 488 nm, 510 nm, 532 nm, 555 nm, 650 nm, 676 nm, 715 nm
- ac-s, *a* and *c*, 25 cm path; 400 nm to 725 nm, ≈4 nm resolution
- C-Star, *c*, 25 cm path; 532 nm
- ECO BB9, b_b, 124°; 403 nm, 443 nm, 487 nm, 506 nm, 525 nm, 594 nm, 657 nm, 680 nm, 720 nm
- ECO BB3 (1), b_b, 124°; 469 nm, 529 nm, 652 nm
- ECO BB3 (2), b_b, 124°; 470 nm, 532 nm, 660 nm
- MASCOT, *vsf*, 650 nm laser; 17 detectors 10° to 170° and polarization filter wheel
- FL3, Chl and CDOM fluorescence, ex/em: 440 nm/680 nm and 510 nm/680 nm (Chl) and 370 nm/470 nm (CDOM)
- OCR507, E_d, 411.6 nm, 442.6 nm, 490.7 nm, 531.9 nm, 554.5 nm, 664.8 nm, 683.3 nm)
- SBE 49, CTD

**<u>*UMB*</u> profiling IOP package includes:

- ac-s, *a* and *c*, at 80+ wavelengths from 400 nm to 732 nm;
- BB7FL2, b_b, at 412 nm, 440 nm, 488 nm, 532 nm, 595 nm, 695 nm and 715 nm; and CDOM and chlorophyll fluorescence

Table A7. Nominal conditions recorded at stations as measured from instruments plumbed into the ship's flow-through system. Temperature, salinity and fluorescence were measured by the ship's standard equipment. IOPs and phytoplankton characterization instruments were supplied by the science teams.

	Ship Flowthrough*			Cal/Val Flowthrough		
NF-16-08 Station ID#	**Temperature [°C]**	**Salinity [psu]**	**Fluorescence Chl and UV [volts]**	**IOP absorption and beam attenuation [m^{-1}]****	**IOP backscatter and volume scattering function*****	**PAR**
1	24.1	35.89	Chl=2.16	*a*(440)=0.06 *c*(440)=2.3	yes	yes
2	24.0	35.74	Chl=1.2	yes	yes	yes
3	24.1	35.24	Chl=1.2	*a*(440)=0.74 *c*(440)=3.1	yes	yes
4	24.9	35.75	n/a	*a*(440)=0.53 *c*(440)=2.04	yes	yes
5	23.1	32.67	Chl=4.78 UV=5.57	*a*(440)=2.5 *c*(440)=10.5	yes	yes
6	23.6	34.07		*a*(440)=1.4 *c*(440)=5.0	yes	yes
7	24.2	35.39	Chl=4.7 UV=1.5	yes	yes	yes
8	24.8	35.78	Chl=4.78 UV=1.29	*a*(440)=0.6 *c*(440)=2.0	yes	yes
9	24.9	35.89	Chl=4.78 UV=1.257	n/a	yes	yes
10	27.5	36.14	Chl=4.78 UV=0.989	*a*(440)=0.055 *c*(440)=0.159	yes	yes
11	25.8	36.22	n/a	*a*(440)=0.07 *c*(440)=0.22	yes	yes
12	24.2	35.73	Chl=3.13 UV=1.59	*a*(440)=0.27 *c*(440)=1.0	yes	yes
13	23.4	34.27	Chl=3.56 UV=5.39	*a*(440)=1.27 *c*(440)=3.38	yes	n/a

* SBE-49: temperature, salinity, pressure
**ac-s-103: 74 wavelengths: from ≈400 nm to 745 nm, unfiltered and ac-9-156: 9 wavelengths: 412 nm, 440 nm, 488 nm, 510 nm, 555 nm, 630 nm, 650 nm, 676 nm, 715 nm, used with 0.2 µm filter (Stennis).
***Backscatter at 470 nm, 532 nm, 670 nm
NOTE: in between stations phytoplankton characterization instruments were plumbed into flow-through system to measure cell imagery (FlowCAM), F_v/F_m and $\sigma_{PSII,}$ fluorescence of Chl-*a*, CDOM, PE-1, PE-2, PE-3.s

Appendix B – Abbreviations, Units and Acronyms

Table B1. Notations, descriptions and units if applicable.

Abbreviation	Description	Typical Units (if applicable)
a	Absorption coefficient	m^{-1}
a_{CDOM}	Absorption coefficient due to CDOM	m^{-1}
a_d	Absorption coefficient of detrital matter	m^{-1}
AOP	Apparent optical property	
a_p	Absorption due to particles	m^{-1}
a_{pg}	Absorption due to particles plus gelbstoff (detrital matter)	m^{-1}
a_{ph}	Phytoplankton pigment absorption coefficient	m^{-1}
a^*_{ph}	Chlorophyll-specific phytoplankton absorption coefficient	$m^2\ mg^{-1}$
a_t	Total absorption (all components)	m^{-1}
b	Scattering coefficient (in any/all directions)	m^{-1}
b_b	Backscattering (scattering in the backwards direction)	m^{-1}
BRDF	Bi-directional reflectance distribution function	
c	Attenuation coefficient	m^{-1}
Cal/Val	Calibration and Validation	
CCNY	City College of New York	
CDOM	Chromophoric dissolved organic material	ppb
CEOS	Committee on Earth Observation Satellites	
Chl-*a*	Chlorophyll *a* concentration	$mg\ m^{-3}$
CZCS	Coastal Zone Color Scanner instrument aboard the NIMBUS-7 satellite	
E_d	Downwelling irradiance	$mW\ cm^{-2}\ \mu m^{-1}$
EDIS	Environmental Data Information Service	
EDR	Environmental Data Record	
EDS	Environmental Data Service	
EPA	US Environmental Protection Agency	
E_s	Downwelling irradiance from above water reference sensor	$mW\ cm^{-2}\ \mu m^{-1}$
ESSA	Environmental Science Services Administration	
EST	Eastern Standard Time	
FAFOV	Full Angle Field of View	
FEL	Lamp type designation assigned by the American National Standards Institute (not an acronym)	
F_L	Unknown spectral response calibration factor	
F_0	Mean extraterrestrial solar irradiance	$mW\ cm^{-2}\ \mu m^{-1}$
FOV	Field of view	
FPT	Filter Pad Technique	
F_v/F_m	Photosynthetic efficiency	dimensionless
FWHM	Full width half maximum	
GCOM-C	Global Climate Observation Mission-Climate	
GUM	Guide to Uncertainty in Measurement	
HPLC	High Pressure Liquid Chromatography	
IFCB	Imaging Flow CytoBot instrument (see Table B2)	
I_f	Immersion factor accounting for the change in responsivity of the sensor when immersed in water with respect to air	
I_i	integration time used for that reading	s
I_N	normalized integration time	s
INSITU-OCR	International Network for Sensor Inter-comparison and Uncertainty assessment for Ocean Color Radiometry	
IOCCG	International Ocean Colour Coordinating Group	
IOP	Inherent Optical Property	
JPSS	Joint Polar Satellite System (program)	
JPSS-1; JPSS-2	Joint Polar Satellite System -1 -2 (future satellite missions)	
K_d	Downwelling diffuse attenuation coefficient	m^{-1}
K_{Lu}	Upwelling radiance diffuse attenuation coefficient	m^{-1}
L	Radiance	$mW\ cm^{-2}\ \mu m^{-1}\ sr^{-1}$
L_d	Downwelling radiance	$mW\ cm^{-2}\ \mu m^{-1}\ sr^{-1}$
LDEO	Lamont-Doherty Earth Observatory at Columbia University	
LISCO	Long Island Sound Coastal Observatory	
L_{ref}	Radiance of reference	$mW\ cm^{-2}\ \mu m^{-1}\ sr^{-1}$
L_{sky}	Radiance of sky	$mW\ cm^{-2}\ \mu m^{-1}\ sr^{-1}$
L_t	Total radiance	$mW\ cm^{-2}\ \mu m^{-1}\ sr^{-1}$
L_u	Upwelling radiance	$mW\ cm^{-2}\ \mu m^{-1}\ sr^{-1}$
$L_u(0^-, \lambda)$	Spectral upwelling radiance just below water surface	$mW\ cm^{-2}\ \mu m^{-1}\ sr^{-1}$
L_w	Water-leaving radiance	$mW\ cm^{-2}\ \mu m^{-1}\ sr^{-1}$
MIN	Minimum	
MOBY	Marine Optical BuoY	

Abbreviation	Description	Typical Units (if applicable)
MSL12	Multi-Sensor Level-1 to Level-2 processing system	
n	number of readings	
n/a	Not available	
NASA	National Aeronautics and Space Agency	
NASA/GSFC	NASA/Goddard Space Flight Center	
NCEI	National Centers for Environmental Information	
NESC	National Environmental Satellite Center	
NESDIS	National Environmental Satellite, Data, and Information Service	
NESS	National Environmental Satellite Service	
NIR	Near infrared	
NIST	National Institute of Standards and Technology	
nL_w	Normalized water-leaving radiance	mW cm^{-2} μm^{-1} sr^{-1}
NOAA	National Oceanic and Atmospheric Administration	
NOAA/STAR	NOAA/Center for Science tech, algorithm, research	
NRL	Naval Research Laboratory	
NURADS	New Upwelling Radiance Distribution camera System	
n_w	Refractive index of seawater	
OCR-VC	Ocean Colour Radiometry Virtual Constellation	
OLCI	Ocean and Land Colour Instrument	
OMAO	Office of Marine and Air Operations	
OSU	Oregon State University	
PAR	Photosynthetically Active Radiation	
PI	Principal Investigator	
POC	Particulate Organic Carbon	mmol C m^{-3}
PON	Particulate Organic Nitrogen	mmol N m^{-3}
PSU	Practical salinity unit	
R_g	Bi-directional reflectance of gray plaque	
R_{rs}	Remote sensing reflectance	sr^{-1}
R_{tile}	Relative reflectance of the NIST blue tile	
s	Seconds	
s/n	Serial number	
S	Radiometric spectrum measurement	
SeaBASS	SeaWiFS Bio-optical Archive and Storage System	
SeaWiFS	Sea-viewing Wide Field-of-view Sensor	
S_g	Radiometric spectrum measurement of gray plaque	
SGLI	Second Generation Global Imager	
SNPP	Suomi National Polar-orbiting Partnership	
S_{sfc}	Radiometric spectrum measurement of surface water	
S_{sky}	Radiometric spectrum measurement of sky	
SST	Sea surface temperature	°C
STARR	NIST Spectral tri-function automated reference reflectometer	
S_{tile}	Radiometric spectrum measurement of the NIST blue tile	
SPM	Suspended Particulate Material	mg L^{-1}
t	Time	s
U. Miami	University of Miami	
UMB	University of Massachusetts – Boston	
USF	University of South Florida	
USM	University of Southern Mississippi	
UTC	Coordinated Universal Time	
UV	Ultraviolet	
VIIRS	Visible Infrared Imaging Radiometer Suite	
$\Delta\phi$	Relative azimuth between the sun and the instrument viewing direction	°
λ	Wavelength	nm
ϕ_i	Scatter azimuth, incident	°
ϕ_r	Scatter azimuth, reflective	°
φ	Relative azimuth of the sensor to the sun	°
ρ	Reflectance	
$\rho(\lambda, \theta)$	Fresnel reflectance factor of seawater	
θ	Angle	°
θ_g	Sensor zenith angle for gray plaque	°
θ_i	Sensor zenith angle, incident	°
θ_r	Sensor zenith angle, reflective	°
θ_{sfc}	Sensor zenith angle for water surface	°
θ_{sky}	Sensor zenith angle for sky	°
σ_{PSII}	functional absorption cross-section of Photosystem II	0.1 nm^2 $quanta^{-1}$

Table B2. Instrument shorthand, description and manufacturer with modifications when applicable.

Instrument Shorthand	Full Identification/Purpose	Manufacturer or Citation
ac-9	In situ spectrophotometer - 9 channel resolution	WET Labs
ac-s	In situ spectrophotometer – high spectral resolution	WET Labs
ADCP	Acoustic Doppler Current Profiler	Teledyne RD Instruments
ALF	Advanced Laser Fluorometer	WET Labs
AlgaeOnlineAnalyser	Spectral fluorometer	bbe Moldeanke
ASD	Analytical Spectral Device; HandHeld2-Pro visible and near infrared spectrophotometer	PANalytical
BB-3	Backscatter – 3 channels	
BB7FL2	Backscatter – 7 channels, Fluorescence – 2 channels	WET Labs
C-OPS	compact hyperspectral optical profiling system	Biospherical Instruments, Inc.
CTD	Conductivity, Temperature, Depth	Generic, various manufacturers
ECO BB9	Backscatter – 9 channels	WET Labs
ECO-Puck Triplet Fluorometer	Fluorescence at 3 channels for determining chlorophyll, CDOM and phycoerythrin	WET Labs
ECO-Puck Triplet Scatterometer	Scatter – 3 channels (443, 550, 860)	WET Labs
FIRe	Variable fluorescence	Satlantic
FlowCam	Dynamic imaging particle analysis for species composition and size measurements	Fluid Imaging Technologies, Inc.
FRRF	Fast Repetition Rate Fluorometer	Generic
GER	Field portable spectroradiometer	Spectra Vista Corporation
HyperOCI	Hyperspectral irradiance sensor	Satlantic LP
HyperOCR	Hyperspectral radiance sensor	Satlantic LP
HyperPro, HyperPro-II	Free-falling hyperspectral optical profiler	Satlantic LP
HyperSAS-POL	Above water optical system with sky polarimeter	Satlantic LP with modifications by CCNY
HyperTSRB	Hyperspectral radiometer configured to float on the sea surface	Satlantic LP
Imaging Flow CytoBot (IFCB)	Automated microscopic imaging instrument	McLane Research Labs
MASCOT	Multi-Angle Scattering Optical Tool	WET Labs
Microtops	Handheld sun photometer (atmospheric aerosols and optical depth)	Solar Light Company
NuRads	Upwelling Radiance Distribution Camera System	Voss and Chapin, 2005
RISBA	Radiometer Incorporating the Sky Blocking Approach	Lee et al. 2013
Sartorius CPA 2250	Balance	Sartorius
SBE 49	Conductivity, Temperature, Depth	SeaBird Scientific
SR1900 (Spectral Evolution)	Spectroradiometer, handheld	Spectral Evolution, Inc.
VSF-9	Volume scattering function – 9 channels	WET Labs